2008

Novel Complex Adaptive Signal Processing Techniques Employing Optimally Derived Time-varying Convergence Factors With Applicatio

Raghuram Ranganathan
University of Central Florida

NOVEL COMPLEX ADAPTIVE SIGNAL PROCESSING TECHNIQUES EMPLOYING OPTIMALLY DERIVED TIME-VARYING CONVERGENCE FACTORS WITH APPLICATIONS IN DIGITAL SIGNAL PROCESSING AND WIRELESS COMMUNICATIONS

by

RAGHURAM RANGANATHAN
B.S. R.V College of Engineering, India, 2001
M.S. University of Central Florida, 2004

A dissertation submitted in partial fulfillment of the requirements
for the degree of Doctor of Philosophy
in the School of Electrical Engineering and Computer Science
in the College of Engineering and Computer Science
at the University of Central Florida
Orlando, Florida

Fall Term
2008

Major Professor: Wasfy B Mikhael

ABSTRACT

In digital signal processing in general, and wireless communications in particular, the increased usage of complex signal representations, and spectrally efficient complex modulation schemes such as QPSK and QAM has necessitated the need for efficient and fast-converging complex digital signal processing techniques. In this research, novel complex adaptive digital signal processing techniques are presented, which derive optimal convergence factors or step sizes for adjusting the adaptive system coefficients at each iteration. In addition, the real and imaginary components of the complex signal and complex adaptive filter coefficients are treated as separate entities, and are independently updated. As a result, the developed methods efficiently utilize the degrees of freedom of the adaptive system, thereby exhibiting improved convergence characteristics, even in dynamic environments.

In wireless communications, acceptable co-channel, adjacent channel, and image interference rejection is often one of the most critical requirements for a receiver. In this regard, the fixed-point complex Independent Component Analysis (ICA) algorithm, called Complex FastICA, has been previously applied to realize digital blind interference suppression in stationary or slow fading environments. However, under dynamic flat fading channel conditions frequently encountered in practice, the performance of the Complex FastICA is significantly degraded. In this dissertation, novel complex block adaptive ICA algorithms employing optimal convergence factors are presented, which exhibit superior convergence speed and accuracy in time-varying flat fading channels, as compared to the Complex FastICA algorithm. The proposed algorithms are called Complex IA-ICA, Complex OBA-ICA, and Complex CBC-ICA.

For adaptive filtering applications, the Complex Least Mean Square algorithm (Complex LMS) has been widely used in both block and sequential form, due to its computational simplicity. However, the main drawback of the Complex LMS algorithm is its slow convergence and dependence on the choice of the convergence factor. In this research, novel block and sequential based algorithms for complex adaptive digital filtering are presented, which overcome the inherent limitations of the existing Complex LMS. The block adaptive algorithms are called Complex OBA-LMS and Complex OBAI-LMS, and their sequential versions are named Complex HA-LMS and Complex IA-LMS, respectively. The performance of the developed techniques is tested in various adaptive filtering applications, such as channel estimation, and adaptive beamforming.

The combination of Orthogonal Frequency Division Multiplexing (OFDM) and the Multiple-Input-Multiple-Output (MIMO) technique is being increasingly employed for broadband wireless systems operating in frequency selective channels. However, MIMO-OFDM systems are extremely sensitive to Intercarrier Interference (ICI), caused by Carrier Frequency Offset (CFO) between local oscillators in the transmitter and the receiver. This results in crosstalk between the various OFDM subcarriers resulting in severe deterioration in performance. In order to mitigate this problem, the previously proposed Complex OBA-ICA algorithm is employed to recover user signals in the presence of ICI and channel induced mixing. The effectiveness of the Complex OBA-ICA method in performing ICI mitigation and signal separation is tested for various values of CFO, rate of channel variation, and Signal to Noise Ratio (SNR).

This work is dedicated to my parents.

ACKNOWLEDGMENTS

Firstly, I am deeply grateful to my advisor, Dr Wasfy Mikhael for his constant motivation and guidance during the course of my PhD. His timely encouragement helped me overcome various obstacles in both academic and personal fronts.

I would like to express my thanks to the member of the dissertation committee.

I sincerely appreciate the constructive comments and guidance of Dr Brent Myers. In addition, I would like to thank Conexant Corporation for supporting the work.

I am indebted to my wonderful parents for their continuous and unconditional support during my PhD study.

TABLE OF CONTENTS

LIST OF FIGURES

LIST OF TABLES

CHAPTER ONE: INTRODUCTION

Complex signal processing has attracted enormous research efforts in recent decades. It finds increased applications in numerous areas such as wireless communications, statistical signal processing and biomedical signal processing. In general, a complex signal is the combination of two independent real signals (real and imaginary components) at any instance in time. As a result, it enables independent processing of the real and imaginary components in the digital domain.

The main advantage of employing complex signal representations is that it often allows for image-reject architectures to be described more compactly [1,2]. In addition, many spectrally efficient and high bit rate modulation schemes like Quadrature Phase Shift Keying (QPSK), Quadrature Amplitude Modulation (QAM), Orthogonal Frequency Division Multiplexing (OFDM), etc. are based on complex signal concepts.

Traditionally, complex signal processing in wireless transceivers was performed using complex analog filters [3-7]. However, complex analog filters suffer from inherent mismatches causing unwanted image signal energy to alias into the desired signal band [8]. Furthermore, they do not permit a high degree of integration which is an essential requirement for the development of the highly-integrated multi-standard receiver or Software Defined Radio [9]. In recent decades, the development of complex digital filters [10, 11] and efficient Digital Signal Processors has enabled demodulation and signal processing operations like image rejection, channel equalization and interference suppression to be performed entirely in the digital domain using adaptive techniques [12-15].

1.1 MIMO Technology

In mobile radio communications, there is a never-ending demand for increased capacity and improved quality. MIMO (multiple input, multiple output) is a smart antenna technology for wireless communications which supplies this demand. MIMO utilizes multiple antennas at both the source (transmitter) and the destination (receiver) and is sometimes referred to as spatial multiplexing [16-19]. MIMO is one of several forms of smart antenna technology, the others being MISO (multiple input, single output) and SIMO (single input, multiple output). The use of MIMO in wireless systems has several advantages such as

- Significant increase in data throughput and spectral efficiency
- Reduced fading because of antenna diversity
- Increased user capacity
- Greater immunity to interference

MIMO combined with Orthogonal Frequency Division Multiplexing (OFDM) delivers significant performance improvements for wireless LANs, enabling them to serve existing applications more cost-effectively, as well as making new, more demanding applications possible [20,21]. In fact, MIMO-OFDM is the basis for the recently developed 802.11n standard [22].

1.2 Fading Channels

In wireless communications, various elements in the environment reflect the transmitted signal creating multiple paths between the transmitter and the receiver. In each path, the transmitted signal encounters different levels of attenuation, delay and phase shift. These multiple copies of the transmitted signal combine at the receiver,

causing constructive or destructive interference. This causes a residual amplification or attenuation of the signal power at the receiver. In some situations, strong destructive interference results in a sudden and sharp decrease in signal power causing a **deep fade** and temporary loss of the communication signal. Mathematically, fading can be modeled as a time-varying random change in the amplitude and phase of the transmitted signal.

1.2.1 Slow and Fast Fading

The wireless channel induces magnitude and phase changes in the transmitted signal. The rate at which these changes imposed by the channel vary with time is referred to as slow and fast fading. The fading of the channel depends on the **coherence time**, which describes the time duration over which the response of the channel can be considered correlated [23, 24].

- Slow fading occurs when the coherence time of the channel is large relative to the symbol duration. In this scenario, the amplitude and phase change induced by the channel is approximately constant over the symbol period. Slow fading is caused by events such as **shadowing**, where the main signal path between the transmitter and receiver is obscured by a large obstacle such as a mountain or large building.
- Fast fading occurs when the coherence time of the channel is smaller than the symbol duration. In this case, the properties of the channel vary at a rapid rate causing severe fluctuations in the amplitude and phase of the signal. Fast fading typically varies about a mean value and often fast fading is superimposed on slow fading.

1.2.2 Flat and Frequency-Selective Fading

The response of a wireless channel to a communication signal may be frequency specific. In this regard, the coherence bandwidth is a statistical measurement of the range of frequencies over which the response of the channel can be considered constant. It is also defined as the approximate maximum bandwidth or frequency interval over which two frequencies of a signal are likely to experience comparable or correlated amplitude fading.

- In flat fading, the coherence bandwidth of the channel is larger than the bandwidth of the signal. As a result, all the frequency components of the signal experience the same degree of fading.
- In contrast, frequency-selective fading causes different frequencies of an input signal to be attenuated and phase shifted differently in a channel. This occurs when the coherence bandwidth of the channel is smaller than the bandwidth of the signal. Frequency-selective fading gives rise to notches in the frequency response of the channel.

Frequency-selective fading can be viewed in the frequency domain, although in the time domain, it is called multipath delay spread (T_D), which is the total time interval during which reflections with significant energy arrive. In practice, a channel can be considered flat when T_D/T is less than 0.1 where T is the symbol period.

In a frequency-selective fading channel, since different frequency components of the signal are affected independently, it is highly unlikely that all parts of the signal will be simultaneously affected by a deep fade. Certain modulation schemes such as OFDM and CDMA are well-suited to employing frequency diversity to provide robustness to fading.

OFDM divides the wideband signal into many slowly modulated narrowband subcarriers, each exposed to flat fading rather than frequency selective fading.

Frequency-selective fading channels are also dispersive, in that the signal energy associated with each symbol is spread out in time. This causes transmitted symbols that are adjacent in time to interfere with each other causing Inter Symbol Interference (ISI). Inter-symbol interference is avoided by introducing a guard interval between the symbols [25].

1.3 Research Statement

With the ever-increasing demand for higher capacity in wireless communication systems, novel interference rejection techniques are becoming critically important and attracting huge research efforts. Co-Channel Interference (CCI), adjacent channel interference, and interference due to image frequencies are the three types of interference that pose major challenges for wireless transceiver design.

Co-channel interference is caused by another signal or user sharing the same frequency band as the desired signal. In cellular communications, this problem becomes more severe when the cell size is decreased in order to increase the frequency reuse, and hence capacity of the system. The highly selective analog filters are incapable of suppressing CCI. Adjacent channel interference is caused by unwanted signal energy from an adjacent channel leaking into the desired signal band. Adjacent channel interference is typically caused by inadequate filtering, such as incomplete filtering of unwanted modulation products.

The image frequency is an unwanted signal located at twice the intermediate Frequency (IF) from the desired RF signal. After frequency translation from the down-

conversion mixer, the unwanted image signal and desired RF signal both lie in the IF band and cannot be distinguished. The image signal may be much larger than the desired signal and therefore significantly degrades the system sensitivity. In theory, I/Q signal processing can completely attenuate the image signal band. The major difficulty in analog I/Q processing is that perfect image rejection can be realized only if the two branches (I and Q) of such a system are completely matched (equal amplitudes and a phase difference of 90). This is very difficult, if not impossible to obtain with practical analog circuits [26-28]. Especially, if the analog I/Q processing is applied to a wideband multichannel signal, the image attenuation requirements become extremely stringent.

Substantial advances in Analog-to-Digital Converter (ADC) and Digital Signal Processor (DSP) technology make it increasingly feasible to incorporate most radio functionalities, including interference suppression in the digital domain. This would significantly reduce the complexity of the analog front-end making it easily programmable and upgradeable. In addition, it will be a considerable step toward the development of the software-defined radio.

In the presented research, novel techniques for blind suppression of such interfering signals for complex baseband modulation schemes such as QAM, and QPSK, are described.

Independent Component Analysis (ICA) combined with receiver diversity has been successfully applied to perform blind digital interference suppression [29, 30]. In this regard, the FastICA is a highly accurate and fast-converging algorithm in performing signal separation or interference mitigation for real signals. However, in any practically

encountered time-varying scenario, the performance of the FastICA starts deteriorating [31-34].

In wireless communications, a significant increase in the application of complex baseband modulation schemes such as QPSK, QAM, etc. has propelled the need for efficient complex signal processing and interference suppression techniques. In this regard, the Complex FastICA extends the principle of the FastICA to the separation of complex valued signals. However, similar to the FastICA, the convergence speed and accuracy are significantly affected in non stationary environments. In the first part of this research, various novel complex adaptive ICA techniques are presented which optimally and independently update the real and imaginary components of the complex separating weight vector. The proposed algorithms are applied to interference suppression for diversity wireless receivers in dynamic wireless channel conditions [35-39]. Extensive simulation results show that in comparison to the Complex FastICA, the presented methods exhibit superior convergence properties, particularly convergence speed and accuracy in time-varying flat fading channel conditions.

In complex adaptive filtering applications, the Complex Least Mean Square (LMS) algorithm has been frequently applied in both block and sequential form, because of its relatively simple implementation [40-42]. However, the choice of the learning rate or convergence factor in the Complex LMS is made empirically. In addition, this constant convergence factor controls the rate of adaptation of both the real and imaginary components of the complex adaptive filter coefficients. Hence, it is highly ineffective in utilizing the degrees of freedom of the adaptive system. In this dissertation, novel complex adaptive LMS algorithms are presented which independently adjust the real and

imaginary components of the complex adaptive filter weights employing optimally derived convergence factors [43-46]. As a result, the performance of the proposed techniques is independent of the choice of the convergence factor, in contrast to the complex LMS. The presented methods are applied in various adaptive filtering applications such as channel estimation, and beamforming.

The advantages of spatial and frequency diversity are effectively exploited by combining OFDM modulation and the Multiple-Input-Multiple-Output (MIMO) technique. Hence, MIMO-OFDM systems are able to achieve high data rates required for broadband wireless applications. However, due to Carrier Frequency Offset (CFO) between local oscillators in the transmitter and the receiver, the subcarriers in each OFDM symbol cease to be orthogonal. This causes Intercarrier Interference (ICI) resulting in severe deterioration in receiver performance. To mitigate the ICI issue, a blind signal processing approach is presented in this dissertation by employing the previously proposed Complex Optimum Block Adaptive ICA (Complex OBA-ICA) algorithm.

1.4 Organization of the dissertation

The dissertation is organized as follows:

Chapter Two outlines the concept of ICA for real and complex-valued signals.

Chapter Three presents the formulation of the novel complex adaptive ICA algorithms and its application to interference suppression in dynamic channel conditions.

Chapter Four describes a novel realization of one of the proposed complex adaptive ICA algorithms for separating complex-valued signals with known source distributions.

Chapter Five presents a novel Complex Block Conjugate ICA algorithm which incorporates the conjugate gradient principle in Complex Adaptive ICA.

Chapter Six proposes sequential and block based complex adaptive LMS algorithms employing optimal and time-varying convergence factors.

Chapter Seven applies the novel complex block adaptive LMS algorithms to the estimation of a wireless channel modeled as a complex Finite Impulse Response (FIR) filter. Through extensive simulations, its performance, in terms of convergence speed and accuracy, is shown to be superior to the traditional block complex LMS algorithm.

Chapter Eight presents an adaptive beamforming application employing the proposed sequential and block based Complex LMS algorithms.

Chapter Nine describes the application of the proposed Independent Component Analysis (ICA) technique called Complex Optimum Block Adaptive ICA (Complex OBA-ICA) to recover user signals in the presence of Carrier Frequency Offset and channel induced mixing for MIMO-OFDM receivers.

Chapter Ten summarizes the presented research and suggests future research directions.

CHAPTER TWO: INDEPENDENT COMPONENT ANALYSIS

Independent Component Analysis (ICA) is a statistical signal processing technique for recovering statistically independent source signals from their linear mixtures [47-50]. ICA is very closely related to the method called *blind source separation* (BSS) or blind signal separation [51-53]. The term "Blind" refers to the fact that we have little or no knowledge about the system which induces mixing of the source signals.

The basic ICA model describes how the observed data are generated by a process of mixing the source signals. ICA attempts to estimate both the mixing matrix and the Independent Components (ICs) using only the signal observations. In practice, the ICA model can be applied with the following assumptions and restrictions:

- The source signals are assumed to be statistically independent.

  Fortunately, in most applications, this assumption is valid.
- The source signals should have nongaussian probability distributions or at most one source signal should be gaussian.

  This is because higher order statistics that are essential for ICA is zero for gaussian distributions. Hence, recovery of the source signals from their mixtures becomes impossible.
- The unknown mixing matrix is assumed to be square and invertible.

  This implies that the number of source signals is the same as the number of observations for simplicity of estimation.

Fortunately, in most practical situations, the assumptions for the ICA model are valid. As a result, ICA is a powerful method that finds extensive applications in many areas, such as financial applications [54], brain imaging [55, 56], telecommunications [57, 58], and feature extraction [59, 60].

2.1 ICA Signal Model

In the simplest form of ICA, we observe m scalar random variables $x_1, x_2, ..., x_m$, which are assumed to be linear combinations of n unknown statistically independent components (ICs), denoted by $s_i, i = 1,2..., n$. Arranging the observed variables x_j, $j = 1,2..., m$ into a vector $X = (x_1, x_2, ..., x_m)^T$ and the ICs into a vector S, respectively, then the linear relationship is given by

$$X = AS \tag{2.1}$$

Here, A is an unknown m x n matrix of full column rank, called the mixing matrix. The basic problem of ICA is to estimate both the mixing matrix A and the realizations of the ICs using *only observations of the mixtures* X. ICA attempts to find a suitable linear transformation of the observed variables X or a separating matrix W, such that the statistical dependence of the components of WX is minimized. When this happens, the original source signals are easily recovered, i.e.

$$S = WX \tag{2.2}$$

2.2 Principles of ICA

2.2.1 Maximization of Nongaussianity

ICA by maximization of nongaussianity is motivated by the *Central Limit Theorem*, which states that when statistically independent source signals are added, their combined probability distribution tends to become more gaussian than their individual distributions. Hence, the original source signals can be recovered from their linear combinations up to a multiplicative constant by maximizing their nongaussianity. This can be achieved by fixed-point or gradient search methods.

Kurtosis as a nongaussianity measure:

The classical measure of nongaussianity is the kurtosis or fourth-order cumulant which is zero for gaussian variables. The kurtosis of a zero-mean real variable z, denoted as $kurt(z)$, is defined as

$$kurt(z) = E\{z^4\} - 3(E\{z^2\})^2 \tag{2.3}$$

For a zero-mean complex-valued variable z, the kurtosis is given by

$$kurt(z) = E\{|z|^4\} - 2(E\{|z|^2\})^2 - |E\{z^2\}|^2 \tag{2.4}$$

Kurtosis can be positive or negative. Variables that have a negative kurtosis are called subgaussian, whereas those with positive kurtosis are called supergaussian. In practice, the absolute value or the square of the kurtosis is used as a measure of nongaussianity. Kurtosis is widely used in ICA estimation, because of its theoretical and computational simplicity.

Negentropy as a nongaussianity measure:

The inherent drawback of utilizing the kurtosis is its sensitivity to outliers. Negentropy is another measure of nongaussianity that is robust, yet computationally intensive [50]. It is a normalized version of differential entropy and is defined as

$$J(z) = H(z_{gauss}) - H(\boldsymbol{z}) \tag{2.5}$$

Where, the entropy H of a random vector $\boldsymbol{z}$ with density $p_z(\eta)$ is given by

$$H(\boldsymbol{z}) = -\int p_z(\eta) \log p_z(\eta) d\eta \tag{2.6}$$

z_{gauss} is a gaussian random variable of the same variance as $\boldsymbol{z}$. From information theory, we know that a gaussian random variable has the largest entropy or unpredictability among all variables with equal variance. As a result, Negentropy is zero for gaussian variables and nonnegative in other cases.

2.2.2 Maximum Likelihood Estimation

A widely used approach for ICA is maximum likelihood (ML) estimation [93]. In ML estimation, the likelihood is expressed as a function of the parameters of the ICA model, which are the elements of the mixing matrix. The parameter values which give the highest probability or likelihood for the observations are taken as estimates.

However, in the ICA model, the densities of the independent source signals have to be estimated as well. This complicates the problem of source recovery, as the estimation of densities is *nonparametric* with infinite number of parameters. In practice, the densities of the source signals are approximated by a family of nonlinear functions with limited number of parameters.

2.2.3 Minimization of Mutual Information

Using the concept of differential entropy, the mutual information I between m scalar random variables, $z_i, i = 1,2,....,m$ is defined as

$$I(z_1, z_2,....., z_m) = H(z_i) - H(\boldsymbol{z}) \tag{2.7}$$

As the name suggests, mutual information is a measure of the statistical dependence between observed variables. It is always non-negative, and zero if and only if the variables are statistically independent.

ICA by minimization of mutual information of an observed vector X involves a linear transformation $S = WX$, where W is determined such that the *mutual information of the transformed components* s_i is minimized. In this way, the statistically independent source signals s_i can be recovered from their linear mixtures.

2.3 FastICA algorithm

The FastICA algorithm is a block algorithm based on a fixed-point iteration scheme maximizing non-gaussianity as a measure of statistical independence [61, 62]. It can also be derived as an approximate Newton iteration. As a result, it eliminates the need for choosing a convergence factor or learning rate resulting in extremely fast convergence. The algorithm finds the direction for the weight vector W maximizing the non-gaussianity of the projection $W^T X$ for the observation vector X. It finds numerous applications in biomedical and wireless communications for separating real signals.

The FastICA employs the kurtosis given in (2.3) as a measure of non-gaussianity. Typically, the algorithm operates in batch mode on a N X L observation matrix X, where, N is the number of observations, and L is the processing block or frame length. The algorithm attempts to recover all the p independent source components, one at a time. The description of the algorithm as a series of steps is given below.

Step 1: Set p =1. The observation matrix X is whitened using Eigenvalue decomposition (EVD).

Step 2: The p^{th} row of the separating or demixing matrix W, namely, w_p is initialized to any unit random vector.

Step 3: Update w_p as

$$w_p = \frac{1}{N_f}\sum_{n=1}^{N_f}\{[w_p X(n)]^3 X(n)\} - 3w_p$$

Step 4: If $p > 1$, the previously extracted rows of W, i.e., w_1,....., w_{p-1} are decorrelated using Gram-Schmidt like decorrelation as follows:

$$w_p = w_p - \sum_{k=1}^{p-1}(w_p^T w_k w_k)$$

Step 5: w_p is normalized to unit length

Step 6: If w_p has converged to a certain predetermined accuracy , Goto Step 7, else Goto Step 3.

Step 7: Iterate $p = p + 1$ and if $p \leq N$, Goto Step 2

From Step 3 of the algorithm, it can be inferred that the FastICA algorithm has cubic convergence without having to choose an appropriate learning rate. As a result, it displays fast convergence in stationary environments, as compared to a gradient based approach.

2.4 Complex FastICA algorithm

With the increased application of complex baseband modulation schemes and complex signal processing techniques in wireless communications and receiver filter design, separation of complex-valued signals has received major attention in recent times. In this regard, the Complex FastICA is also a fixed-point algorithm which extends the capability of the FastICA in separating complex-valued signals [63, 64].

The kurtosis given in (2.4) is used as the measure of non-gaussianity. In addition, the projection of the complex demixing weight matrix W onto the observation matrix X is expressed as $W^H X$, as compared to $W^T X$ for the FastICA. H denotes the conjugate transpose or the Hermitian operator, and * represents the complex conjugate. The complex FastICA algorithm is described below in step form as follows:

Step 1: Set p =1. The observation matrix X is whitened using Eigenvalue decomposition (EVD).

Step 2: The p^{th} row of the separating or demixing matrix W , namely, w_p is initialized to any unit random vector.

Step 3: Update w_p as

$$w_p = \frac{2}{N_f}\sum_{n=1}^{N_f}\{X(n)[w_p{}^H X(n)]^* - 2w_p\}\left|w_p^H X(n)\right|^2$$

Step 4: If $p > 1$, the previously extracted rows of W, i.e., w_1,....., w_{p-1} are decorrelated using Gram-Schmidt like decorrelation as follows:

$$w_p = w_p - \sum_{k=1}^{p-1} (w_p^H w_k w_k)$$

Step 5: w_p is normalized to unit length

Step 6: If w_p has converged to a certain predetermined accuracy , Goto Step 7, else Goto Step 3.

Step 7: Iterate $p = p + 1$ and if $p \leq N$, Goto Step 2

Similar to the FastICA, the complex FastICA exhibits extremely fast convergence and excellent accuracy in stationary or slow time-varying environments. However, it assumes that the mixing matrix is stationary or quasi-stationary within one processing block. In practical wireless or cellular communications, such an assumption is not valid, as the fading coefficients of the channel or mixing matrix vary significantly in a data block.

In such a scenario, a gradient based algorithm can be used for tracking the channel variations. However, the drawback of such gradient based algorithms is their slow convergence characteristics and the performance dependence on the choice of convergence factor or learning rate. In the following chapters 3, 4 and 5, novel complex adaptive ICA algorithms are developed which optimally derive the convergence factor at each iteration, thereby displaying fast convergence speed and accuracy in tracking the dynamics of the channel in time-varying flat fading scenarios.

2.5 Conclusions

In this chapter, a statistical technique called Independent Component Analysis was introduced. The ICA signal model and the principles used in ICA were briefly reviewed.

Two existing fixed-point algorithms called FastICA and complex FastICA were described for the separation of real and complex-valued signals, respectively.

CHAPTER THREE: COMPLEX BLOCK ADAPTIVE ICA WITH INDIVIDUAL ADAPTATION (COMPLEX IA-ICA)

The technique of Complex Independent Component Analysis (ICA) has been employed for various applications involving the separation of complex signals. In this regard, the Complex FastICA is a highly efficient and widely used algorithm in stationary or slow time-varying channel conditions. However, it does not perform as well in dynamic environments. In practice, such dynamic changes in the channel are frequently encountered in wireless communications. In this chapter, a novel complex adaptive ICA algorithm with individual adaptation (Complex IA-ICA) is developed. The algorithm independently updates the real and imaginary components of each complex adaptive filter weight of the adaptive system employed for interference suppression. This is achieved by optimally deriving a unique convergence factor for each part of each weight. Furthermore, the convergence factors are updated at every block iteration. As a result, it is most efficient in utilizing the degrees of freedom of the adaptive system. The proposed algorithm is applied to interference suppression in both linearly and abruptly time-varying flat fading channel conditions, for wireless receivers employing Quadrature Phase Shift Keying (QPSK). The effectiveness of the proposed algorithm is compared with the Complex FastICA, under these dynamic environments. Simulation results confirm the improved performance of the proposed technique, in terms of convergence speed and accuracy.

3.1 Proposed Complex IA-ICA Algorithm: Formulation

The basic principle of any adaptive algorithm is to either maximize or minimize a cost function in order to arrive at the optimal solution. In the case of the Complex IA-ICA, the cost function used is the absolute value of the kurtosis which has to be maximized. The primary reason for using the kurtosis as a measure of non-gaussianity is its theoretical and computational simplicity.

The objective of the Complex IA-ICA is to find a complex separation matrix W, such that the source signals can be recovered when the observation matrix X is multiplied by W. This is achieved by making each component in the resulting matrix $W^H X$, H representing the Hermitian, as statistically independent as possible by maximizing the kurtosis.

The formulation of the Complex IA-ICA is given as follows

Firstly, the following parameters are defined.

k : Iteration index

$j = \sqrt{-1}$

M: number of observations

L : Block Size

$w(k) = [w_1(k)\, w_2(k) .... w_M(k)]^T$: The current row of the complex separation matrix for the k th iteration. The real and imaginary components of $w(k)$ at the k th iteration are represented as $w_R(k)$ and $w_I(k)$ respectively

$x_{l,i}(k)$: The i th complex signal in the l th observation data vector for the k th iteration. (l =1, 2… L)

$X_l(k) = [x_{l,1}(k)\ \ x_{l,2}(k).....x_{l,M}(k)]^T$: l th signal observation for the k th iteration.

$[G]_k = [X_1(k)\ X_2(k).....X_L(k)]^T$: Observation matrix for the k th iteration

The l th kurtosis value for the k th iteration is expressed as

$$kurt_l(k) = E[\left|w^H(k)X_l(k)\right|^4] - 2 \tag{3.1}$$

$$\underline{kurt(k)} = [kurt_1(k)\, kurt_2(k)....kurt_L(k)]^T \tag{3.2}$$

is the kurtosis vector for the k th iteration.

In practice, the expectations in (3.1) are replaced by estimates.

As mentioned previously, the proposed Complex IA-ICA algorithm employs independent convergence factors for the real and imaginary components of the weight vector.

Therefore, the independent weight update equations for the real and imaginary components of the weight vector are expressed as

$$w_R(k+1) = w_R(k) + [MU]_{kR}\nabla_{BR}(k) \tag{3.3}$$

$$w_I(k+1) = w_I(k) + [MU]_{kI}\nabla_{BI}(k) \tag{3.4}$$

Where,

$$\nabla_{BR}(k) = \frac{\partial\{\underline{kurt}^T(k)\underline{kurt}(k)\}}{\partial w_R(k)} \tag{3.5}$$

$$\nabla_{BI}(k) = \frac{\partial\{\underline{kurt}^{T}(k)\underline{kurt}(k)\}}{\partial w_{I}(k)} \tag{3.6}$$

are the gradients of the square of the kurtosis with respect to the real and imaginary components of the weight vector, respectively.

$[MU]_{kR}$ and $[MU]_{kI}$ are the matrices containing the convergence factors for each coefficient of $w_R(k)$ and $w_I(k)$, respectively, at each block iteration.

$$[MU]_{kR} = \begin{bmatrix} \mu_{1R}(k) & \dots & 0 \\ \dots & \dots & \dots \\ 0 & \dots & \mu_{MR}(k) \end{bmatrix} \tag{3.7}$$

$$[MU]_{kI} = \begin{bmatrix} \mu_{1I}(k) & \dots & 0 \\ \dots & \dots & \dots \\ 0 & \dots & \mu_{MI}(k) \end{bmatrix} \tag{3.8}$$

Substituting from (3.2) in (3.5) and (3.6), and evaluating the resulting expression, we obtain

$$\nabla_{BR}(k) = \frac{8}{L}[\mathrm{Re}\{[G]_k^T[C]_k\}\underline{kurt(k)}] \tag{3.9}$$

$$\nabla_{BI}(k) = \frac{8}{L}[\mathrm{Im}\{[G]_k^T[C]_k\}\underline{kurt(k)}] \tag{3.10}$$

Where,

$$[C]_k = \begin{bmatrix} \{w^H(k)X_1(k)\}^*\left|w^H(k)X_1(k)\right|^2 & \dots & 0 \\ 0 & \dots & 0 \\ 0 & 0 & \{w^H(k)X_L(k)\}^*\left|w^H(k)X_L(k)\right|^2 \end{bmatrix} \tag{3.11}$$

is a diagonal matrix. Re {.} and Im {.} represents the real and imaginary components of {.}, respectively.

Substituting (3.9) in (3.3) gives us

$$w_R(k+1) = w_R(k) + [MU]_{kR} \frac{8}{L} [\mathrm{Re}\{[G]_k^T [C]_k\} \underline{kurt(k)}] \qquad (3.12)$$

Similarly, by substituting (3.10) in (3.4) we obtain

$$w_I(k+1) = w_I(k) + [MU]_{kI} \frac{8}{L} [\mathrm{Im}\{[G]_k^T [C]_k\} \underline{kurt(k)}] \qquad (3.13)$$

In order to obtain the optimal convergence factors $[MU]_{kR}$ and $[MU]_{kI}$, the total squared kurtosis has to be maximized with respect to the real and imaginary components of the weight vector independently.

To achieve this, the l th kurtosis values in the $(k+1)$ th iteration are expressed in a Taylor Series expansion as follows:

$$kurt_{lR}(k+1) = kurt_l(k) + \sum_{i=1}^{M} \frac{\partial kurt_l(k)}{\partial w_{iR}(k)} \Delta w_{iR}(k) +_{\ldots}$$

$$l = 1,2 \ldots . L \qquad (3.14)$$

$$kurt_{lI}(k+1) = kurt_l(k) + \sum_{i=1}^{M} \frac{\partial kurt_l(k)}{\partial w_{iI}(k)} \Delta w_{iI}(k) +_{\ldots}$$

$$l = 1,2 \ldots . L \qquad (3.15)$$

From (3.3) and (3.4) we have,

$$\Delta w_{iR}(k) = [MU]_{kR} \nabla_{BR}(k) \qquad (3.16)$$

$$\Delta w_{iI}(k) = [MU]_{kI} \nabla_{BI}(k) \tag{3.17}$$

The second and higher terms in the Taylor Series can be ignored if $\Delta w_{iR}(k)$ and $\Delta w_{iI}(k)$ are small, which is indeed the case. Therefore, evaluating the expressions in (3.14) and (3.15) for all the L kurtosis values, we obtain

$$\underline{kurt_R(k+1)} = \underline{kurt_R(k)} + 4\,\mathrm{Re}\{[C]_k[G]_k\}\Delta w_R(k) \tag{3.18}$$

$$\underline{kurt_I(k+1)} = \underline{kurt_I(k)} + 4\,\mathrm{Im}\{[C]_k[G]_k\}\Delta w_I(k) \tag{3.19}$$

Substituting (3.16) and (3.17) in (3.18) and (3.19) respectively, the following expressions are obtained

$$\underline{kurt_R(k+1)} = \underline{kurt_R(k)} + \frac{32}{L}\mathrm{Re}\{[C]_k[G]_k\}[MU]_{kR}\, q_R(k) \tag{3.20}$$

$$\underline{kurt_I(k+1)} = \underline{kurt_I(k)} + \frac{32}{L}\mathrm{Im}\{[C]_k[G]_k\}[MU]_{kI}\, q_I(k) \tag{3.21}$$

Where,

$$q_R(k) = [\mathrm{Re}\{[G]_k^T[C]_k\}\underline{kurt(k)}] \tag{3.22}$$

$$q_I(k) = [\mathrm{Im}\{[G]_k^T[C]_k\}\underline{kurt(k)}] \tag{3.23}$$

Defining

$$[R]_R(k) = [\mathrm{Re}\{[C]_k[G]_k\}]^T\ \mathrm{Re}\{[C]_k[G]_k\} \tag{3.24}$$

and

$$[R]_I(k) = [\mathrm{Im}\{[C]_k[G]_k\}]^T\ \mathrm{Im}\{[C]_k[G]_k\} \tag{3.25}$$

The total squared kurtosis for the $(k+1)$ th iteration in (3.20) can be written as

$$\underline{kurt_R^T(k+1)}\,\underline{kurt_R(k+1)} = S_1 + S_2 + S_3 + S_4 \tag{3.26}$$

Where,

$$S_1 = \underline{kurt_R^T(k)}\,\underline{kurt_R(k)} \tag{3.27}$$

$$S_2 = \frac{1024}{L^2} q_R^T(k)[MU]_{kR}[R]_R(k)[MU]_{kR}\, q_R(k) \tag{3.28}$$

$$S_3 = \frac{32}{L} q_R^T(k)[MU]_{kR}[\mathrm{Re}\{[C]_k[G]_k\}]^T\, \underline{kurt(k)} \tag{3.29}$$

$$S_4 = \frac{32}{L} \underline{kurt^T(k)}[\mathrm{Re}\{[C]_k[G]_k\}][MU]_{kR}\, q_R(k) \tag{3.30}$$

In order to obtain the optimal convergence factors $[MU]_{kR}$ for the real part of the weight vector, the following condition has to be satisfied, i.e.

$$\nabla \frac{\partial\{\underline{kurt_R^T(k+1)}\,\underline{kurt_R(k+1)}\}}{\partial \mu_{Ri}(k)} = 0$$

i =1, 2 …M (3.31)

Substituting (3.26) in (3.31) and evaluating the resulting expression, the following weight update equation is obtained for the real part of the weight vector

$$w_R(k+1) = w_R(k) - 0.25[R_R]_k^{-1} q_R(k) \tag{3.32}$$

Following a similar procedure for the imaginary component of the weight vector, the following update equation is obtained

$$w_I(k+1) = w_I(k) - 0.25[R_I]_k^{-1} q_I(k) \tag{3.33}$$

The complex weight vector is then obtained by combining the real and imaginary components as follows.

$$w(k+1) = w_R(k+1) + jw_I(k+1) \tag{3.34}$$

From the derivation, it can be inferred that the real and imaginary parts of the weights are treated as separate entities and adjusted independently. Hence, the Complex IA-ICA algorithm is most effective in utilizing the degrees of freedom of the adaptive system, giving it much better adaptability in a time-varying environment.

3.2 Computational Complexity

The weight update equations for the Complex IA-ICA algorithm in (3.32) and (3.33) involve matrix inversion, which is computationally intensive and impractical. However, the matrix inversion operation is significantly simplified by replacing the matrix to be inverted with a matrix containing only its diagonal elements. As a result, the computational complexity of the Complex IA-ICA algorithm is considerably reduced to *O (L)* per iteration, similar to the complex FastICA. Even with this approximation, simulation results show that the Complex IA-ICA achieves fast convergence and excellent accuracy [35-37, 65].

3.3 Interference Suppression for Diversity Wireless Receivers in Dynamic Flat Fading Channels

In wireless communications, interference suppression and desired signal recovery pose a considerable challenge. As a signal propagates between the transmitter and receiver, the wireless channel induces mixing between the desired signal and unknown interfering signals. As a result, it becomes essential to retrieve the desired signal from the mixture, before decoding of the received symbols can be done.

In modern receiver design, most radio functionalities are incorporated in software. As a result, interference suppression and signal separation is performed entirely in the digital domain. Hence, digital signal processing algorithms should be efficient and fast-converging in diverse channel conditions.

In this research, the proposed Complex IA-ICA algorithm is applied to blind interference suppression for diversity QPSK receivers under static and dynamic flat fading channel scenarios. The resulting performance is compared to the complex FastICA algorithm. The Symbol Error Rate, Intersymbol Interference (ISI) and the convergence speed are used to compare the performance of the algorithms.

3.4 Diversity Receiver Structure and Signal Model

Fig.1 shows the proposed diversity receiver structure for interference suppression.

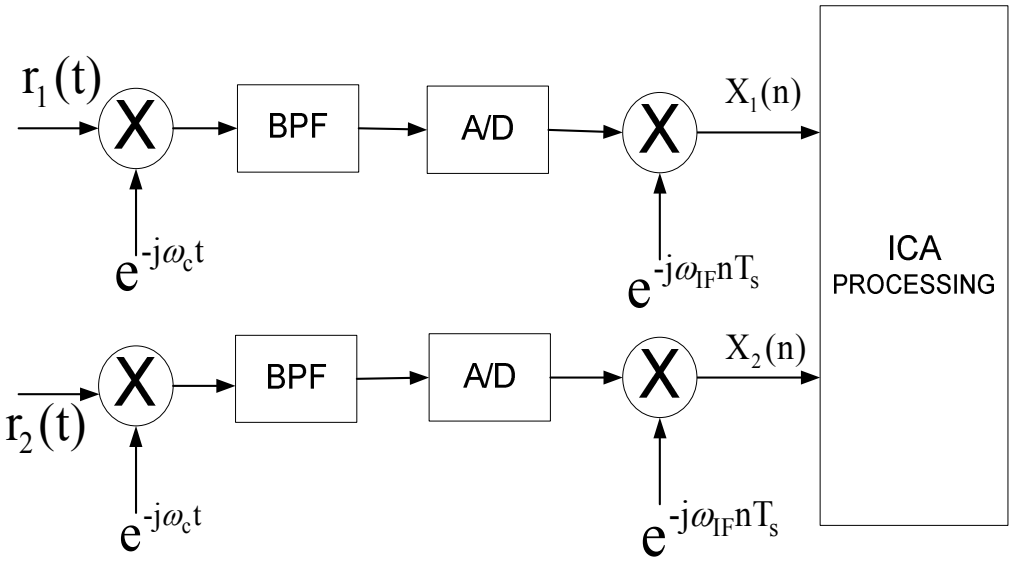

Figure 1: Diversity QPSK Receiver Structure

In this receiver structure, it is assumed that there is no amplitude or phase mismatch between the oscillators in the two receiver paths. In such a scenario, the sole reason for the interfering signal to combine with the desired signal is the time-varying wireless channel.

In Fig.1, $r_1(t)$ and $r_2(t)$ are the Radio Frequency (RF) signals received by the two antennas of the receiver. In the first step of complex downconversion, the signals are translated to an Intermediate Frequency (IF) at which they can be digitized by the A/D converters. In the digital domain, the signals undergo another step of complex downconversion to baseband. At this stage, the signals are processed by the Complex IA-ICA and the Complex FastICA algorithms to perform retrieval of the desired signal.

The mixing matrix is composed of the flat fading coefficients of the wireless channel, and is represented as:

$$A = \begin{bmatrix} f_{s1}(1 + l\Delta) & f_{i1}(1 + l\Delta) \\ f_{s2}(1 + l\Delta) & f_{i2}(1 + l\Delta) \end{bmatrix}$$

$$l = 1, 2 \ldots . L \qquad (3.35)$$

Where, Δ is the complex parameter reflecting the speed of channel variation in amplitude and phase and L is the block size in symbols. For a static channel, Δ becomes 0. As long as the mixing matrix A is non singular, the ICA signal model can be applied, irrespective of the magnitude and phase of the fading coefficients and the relative timing phase of the desired and interfering signals. In addition, the relative strength of the desired and interfering signals does not affect the performance of ICA based algorithms.

The ICA signal model is developed as follows. Let $s(l)$ and $i(l)$ denote the elements of the baseband source signal vector S of the desired signal and the interfering signal, respectively. The elements $X_1(l)$ and $X_2(l)$ of the baseband observation matrix X are given by:

$$\begin{bmatrix} X_1(l) \\ X_2(l) \end{bmatrix} = \begin{bmatrix} f_{s1}(1+l\Delta) & f_{i1}(1+l\Delta) \\ f_{s2}(1+l\Delta) & f_{i2}(1+l\Delta) \end{bmatrix} \begin{bmatrix} s(l) \\ i(l) \end{bmatrix}$$

$$l = 1,2\ldots. L \qquad (3.36)$$

or

$$X = AS \qquad (3.37)$$

3.5 Simulation Results

As a signal propagates through a wireless channel, it experiences random fluctuations in time if the transmitter, receiver, or surrounding objects are moving because of changing reflections and attenuation. Hence the characteristics of the channel appear to change randomly with time. In addition, the properties of the wireless channel itself, varies with time.

In the simulations, the Complex IA-ICA and the Complex FastICA are applied to interference suppression in static, linearly varying and abruptly varying flat fading channel conditions. In achieving this objective, their performances in terms of Symbol Error Rate (SER), speed of convergence in terms of number of iterations and Inter Symbol Interference (ISI) are compared.

From [37], the ISI is given by the following expression:

$$\mathrm{ISI} = \frac{1}{2\mathrm{N}}\sum_{m}\left(\sum_{n}\frac{\left|p_{mn}\right|^2}{(\max\left|\mathrm{P_m}\right|)^2} - 1\right) + \frac{1}{2\mathrm{N}}\sum_{n}\left(\sum_{m}\frac{\left|p_{mn}\right|^2}{(\max\left|\mathrm{P_n}\right|)^2} - 1\right) \quad (3.38)$$

Where, N is the length of the complex weight vector w, $\mathrm{P} = W^H A$ is the permutation matrix with coefficients p_{mn}, max $\left|\mathrm{P_m}\right|$ and max $\left|\mathrm{P_n}\right|$ are the absolute maximum values of the m th row and n th column of P, respectively. Since the number of signals to be separated is 2, P is a 2 X 2 matrix. Furthermore, in all the simulations, Additive White Gaussian Noise (AWGN) is added to the signal observations to realize a signal to noise ratio (SNR) of 20 dB.

3.5.1 Static Channels

For the first simulation, a static channel is considered, i.e. $\Delta = 0$. The Inter Symbol Interference (ISI) in dB and the number of iterations required for convergence are illustrated in Figs. 2 and 3 respectively. The corresponding SER achieved is shown in Fig 4. As can be seen, the complex FastICA exhibits extremely fast convergence and accuracy in stationary channel conditions due to its Newton's type iteration. In comparison, the Complex IA-ICA achieves similar interference suppression with slightly more iterations for convergence.

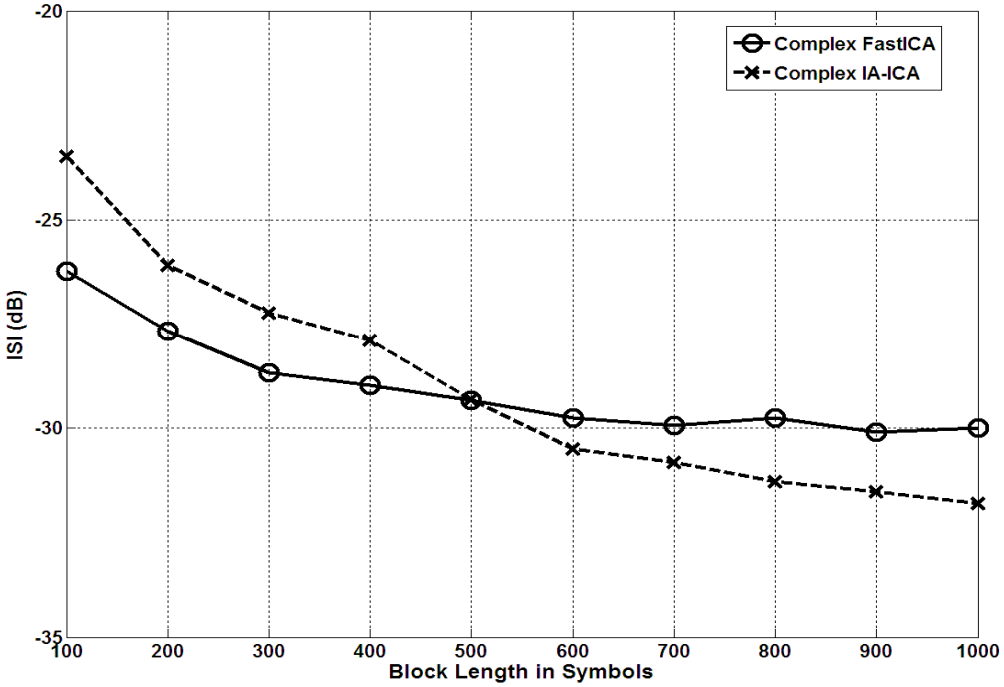

Figure 2: ISI (dB) achieved in Static Channels

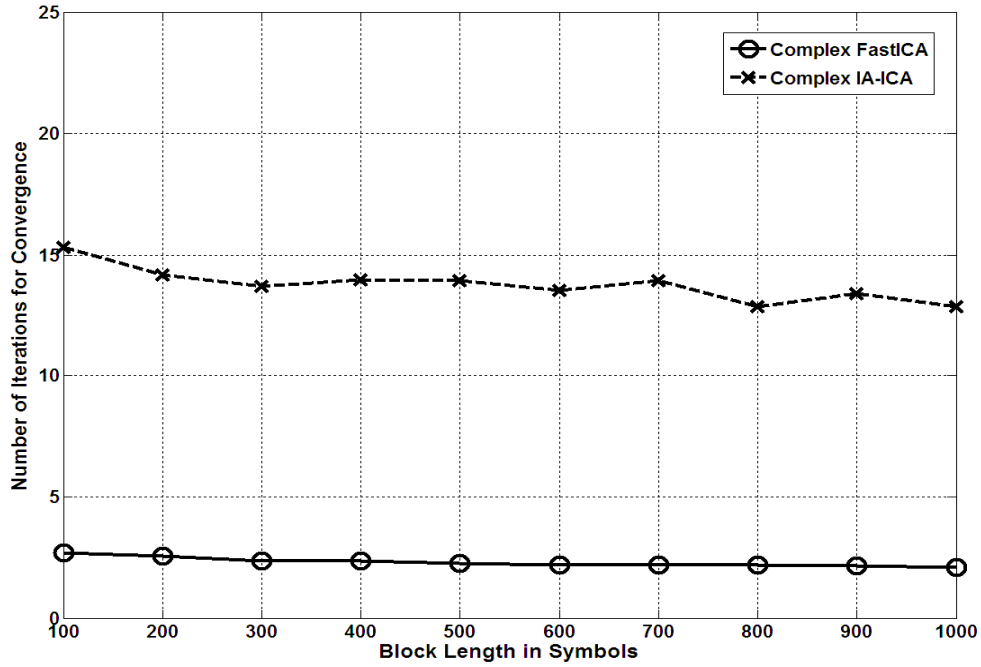

Figure 3: Number of Iterations for Convergence in Static Channels

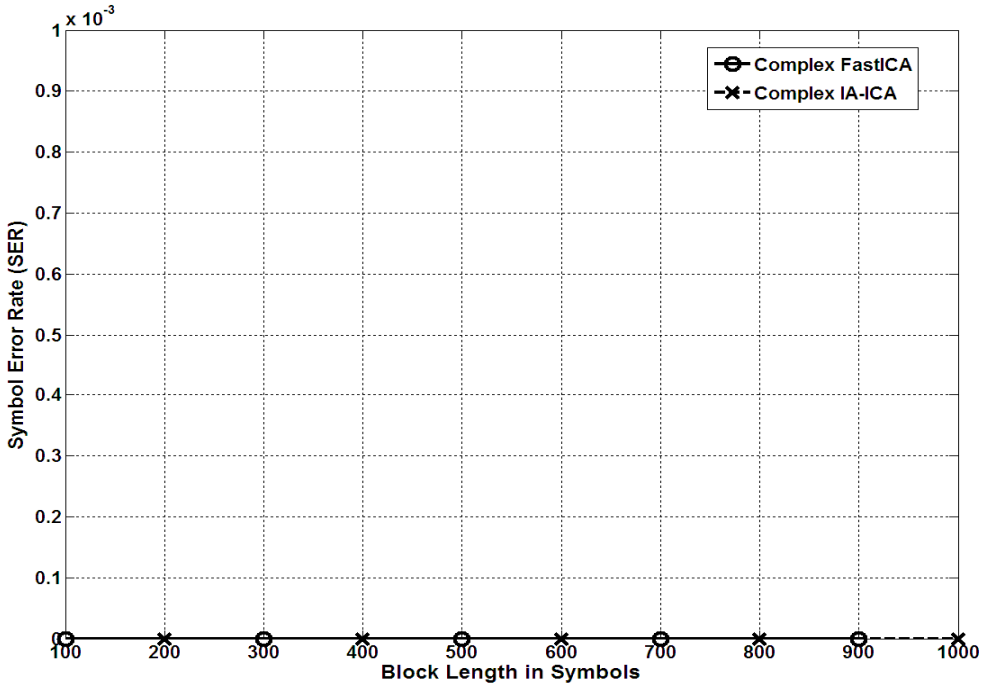

Figure 4: SER achieved in Static Channels

3.5.2 Linearly and Abruptly Flat Fading Channels

In cellular communications, the properties of the wireless channel change much more frequently due to relative motion between the user and base station. This could manifest itself as a continuous linear change in the magnitude and phase of the mixing matrix coefficients. In such situations, the complex ICA algorithm tries to derive an average demixing matrix to separate the desired and interfering signals.

A significant change in the wireless environment is caused either by handoff between two towers or the mobile user entering a building or tunnel. This results in an instantaneous abrupt change in the mixing matrix coefficients or channel parameters within the processing block. In this scenario, the complex ICA algorithm has to converge to a new demixing matrix after the change occurs. As a result, these algorithms need to

exhibit excellent adaptability and accuracy to efficiently track the dynamics of the wireless channel.

In this research, the performance of the proposed Complex IA-ICA algorithm is studied in such linear and abruptly flat fading channels. The signal model given in (3.36) with $\Delta = 0.0022$ is used to simulate the linearly flat fading scenario. The ISI (dB) achieved by both algorithms and the number of iterations required for convergence are illustrated in Figs. 5 and 6 respectively. The corresponding SER realized is shown in Fig 7. Simulation results show that as the block length increases, the Complex FastICA requires many more iterations to achieve comparable interference suppression and SER as the Complex IA-ICA.

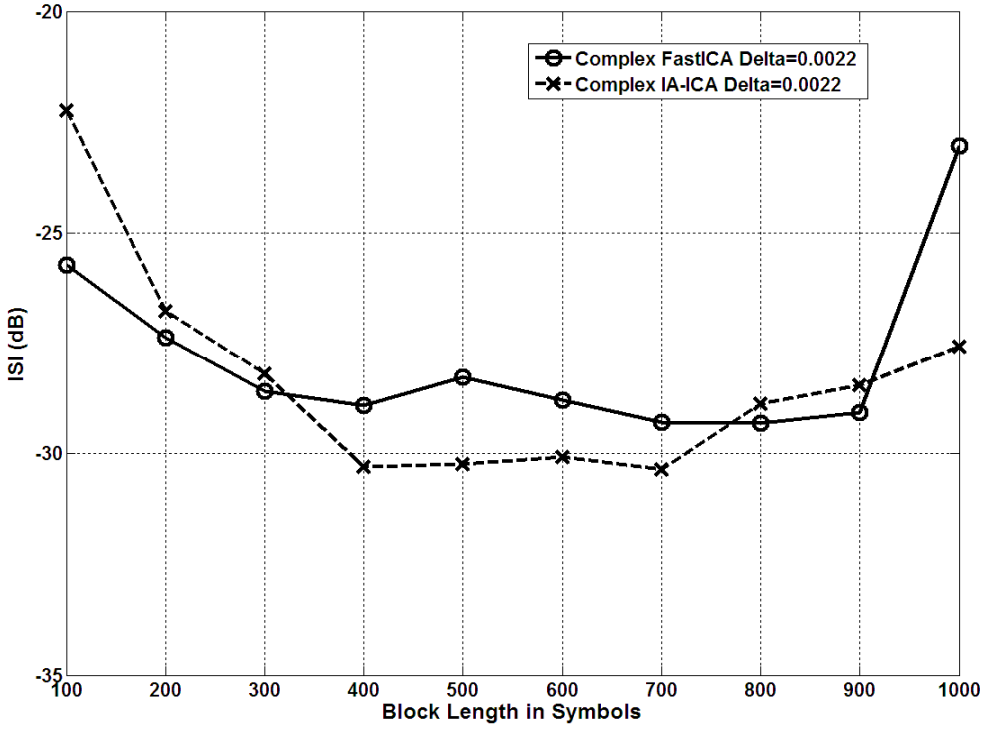

Figure 5: ISI (dB) achieved in Linearly Flat Fading Channels

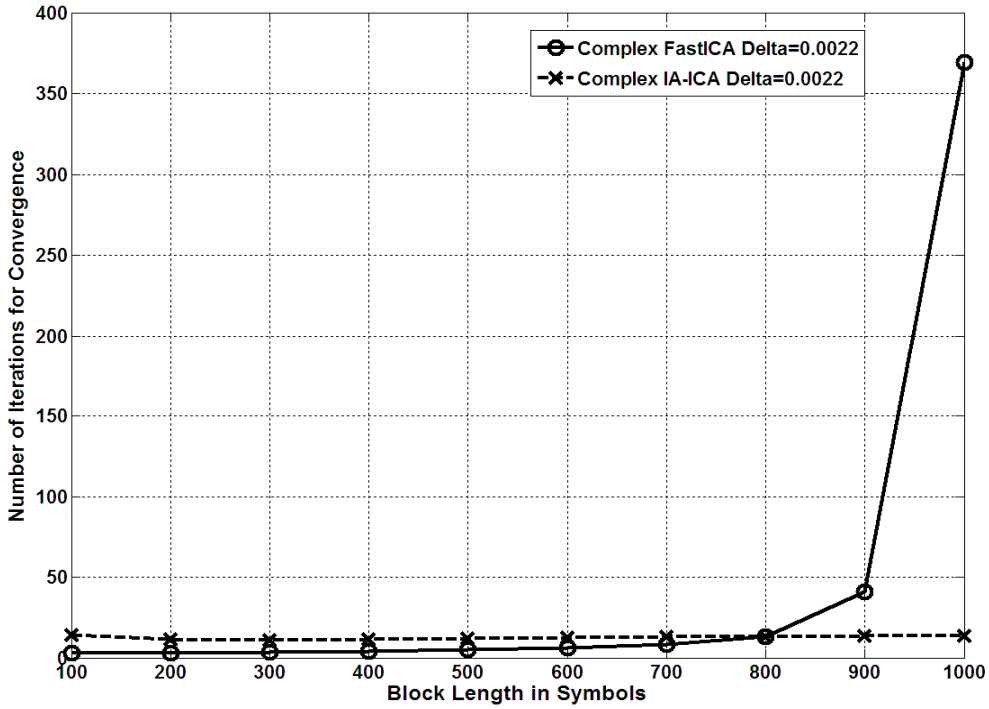

Figure 6: Number of Iterations for Convergence in Linearly Flat Fading Channels

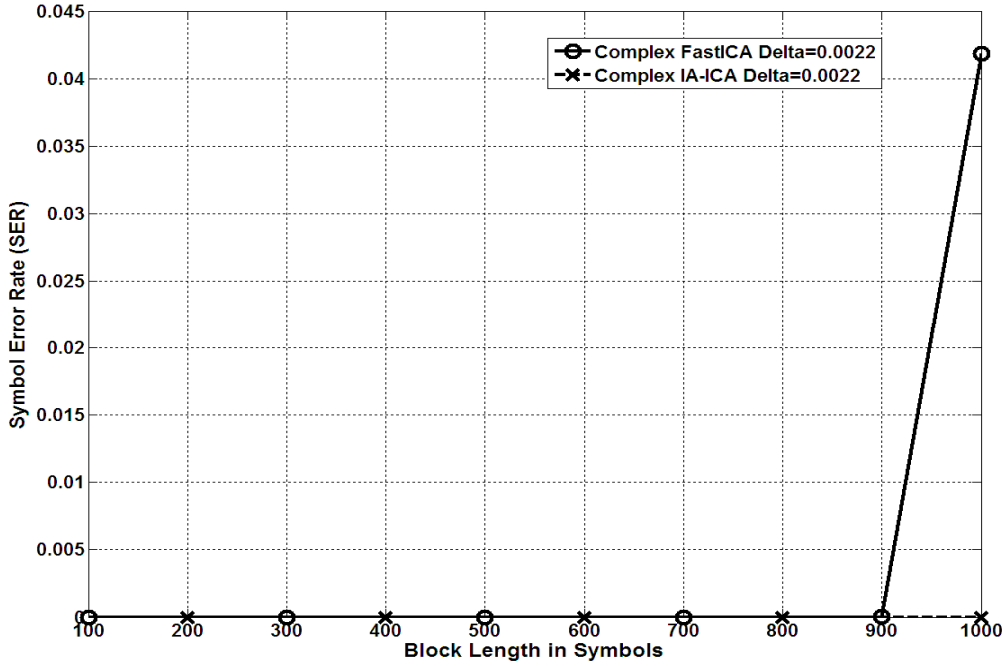

Figure 7: SER achieved in Linearly Flat Fading Channels

An abruptly flat fading channel is modeled by simulating an instantaneous change in the mixing matrix coefficients in the middle of the processing block. When this happens, the complex ICA algorithm has to quickly recover from this variation and re-converge to a new demixing matrix before the end of the data block. In this scenario, the convergence speed and accuracy of the Complex FastICA and Complex IA-ICA are compared for different block lengths L. For each L, the performance is averaged over 100 Monte Carlo runs for a SNR of 20 dB. The ISI (dB) realized, and the number of iterations for convergence for different values of L is illustrated in Figs. 8 and 9, respectively. The corresponding SER achieved is shown in Fig. 10.

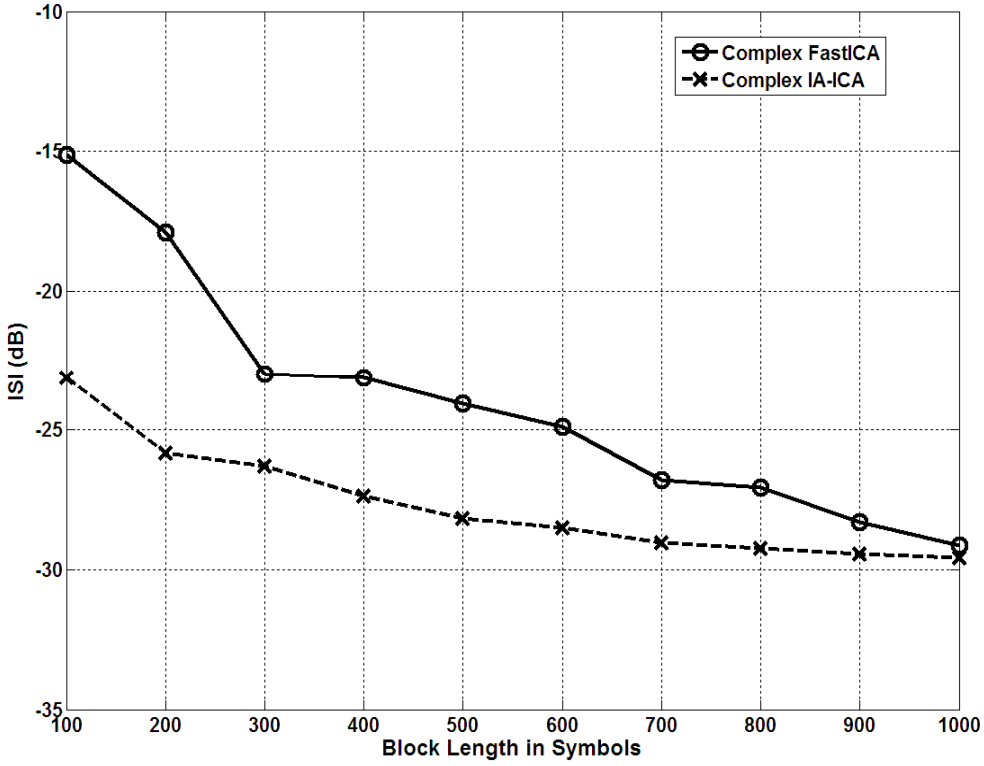

Figure 8: ISI (dB) achieved in Abruptly Flat Fading Channels

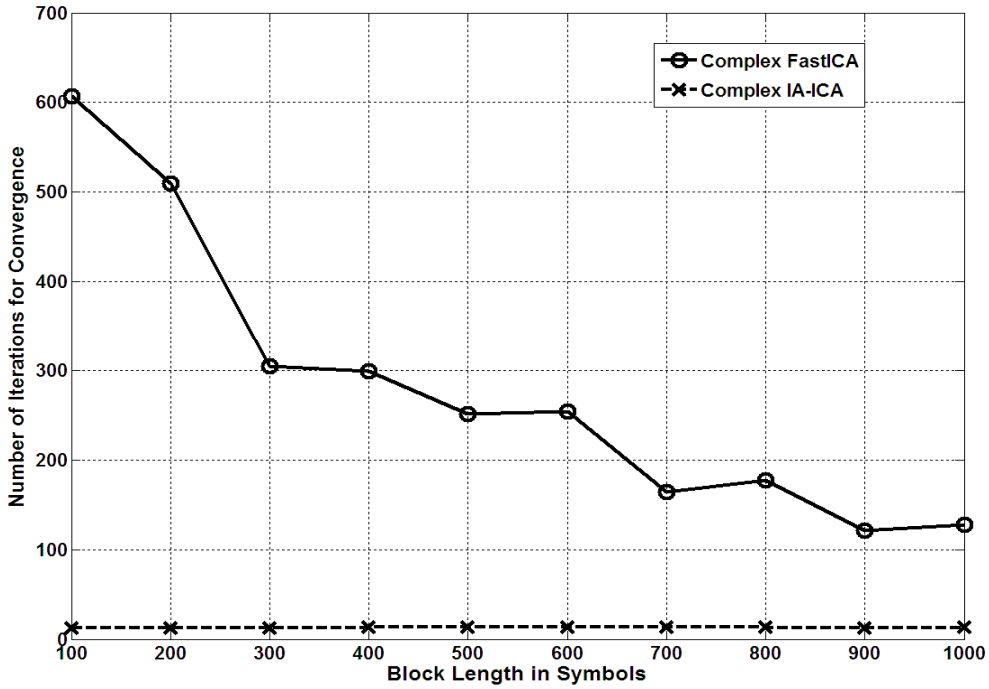

Figure 9: Number of Iterations for Convergence in Abruptly Flat Fading Channels

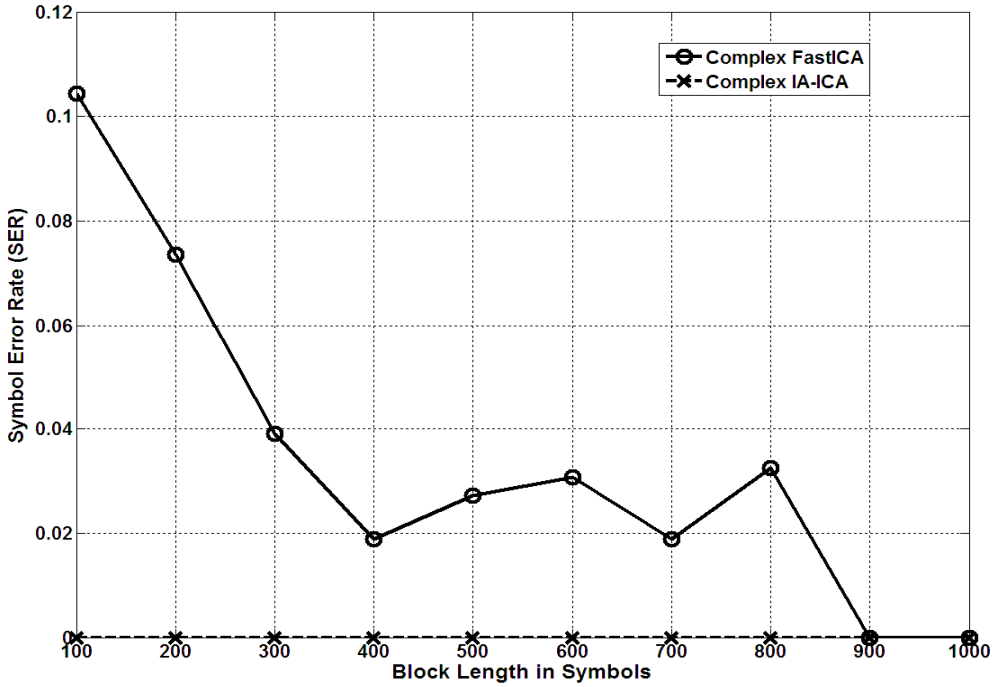

Figure 10: SER achieved in Abruptly Flat Fading Channels

In order to study the effect of Δ on the convergence properties for a constant block length, Δ is varied between 0 and .0025 with a step size of .0005. The block length is set at 1000 symbols. The ISI (dB), and number of iterations for convergence are shown in Figs. 11, and 12, respectively. The corresponding SER achieved for each Δ is shown in Fig. 13. It is worth mentioning that the Complex FastICA failed to converge for values of Δ greater than .0025. In contrast, the Complex IA-ICA continued to converge in less than 20 iterations, while achieving satisfactory SER and ISI.

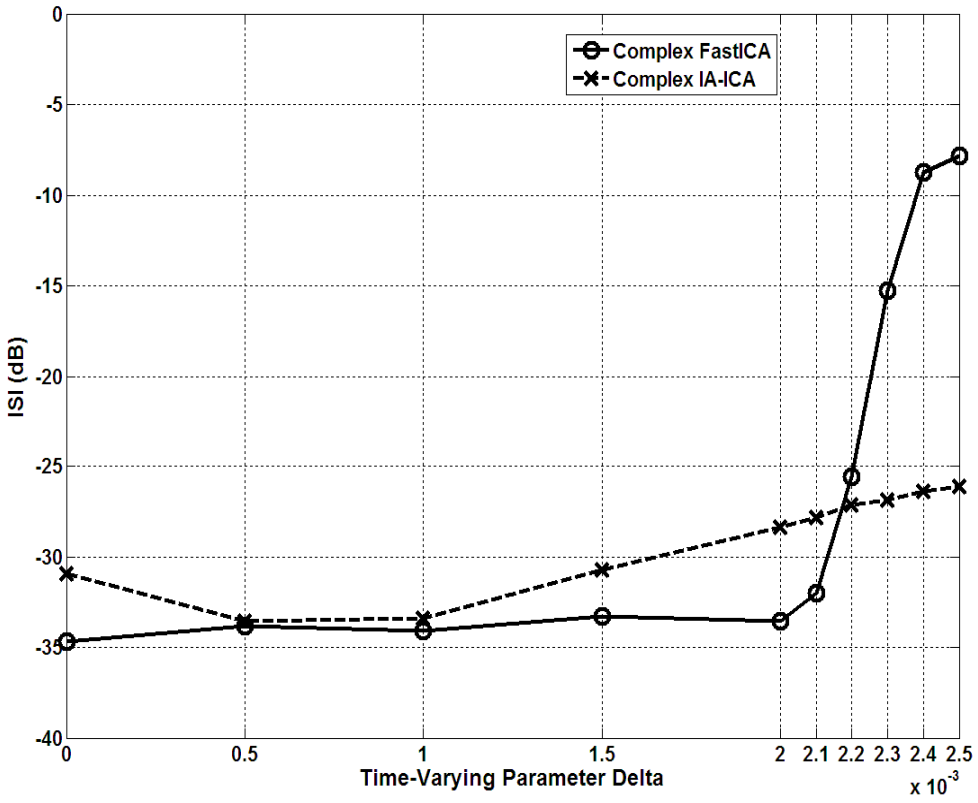

Figure 11: ISI (dB) achieved for Different Values of Δ and L =1000 symbols

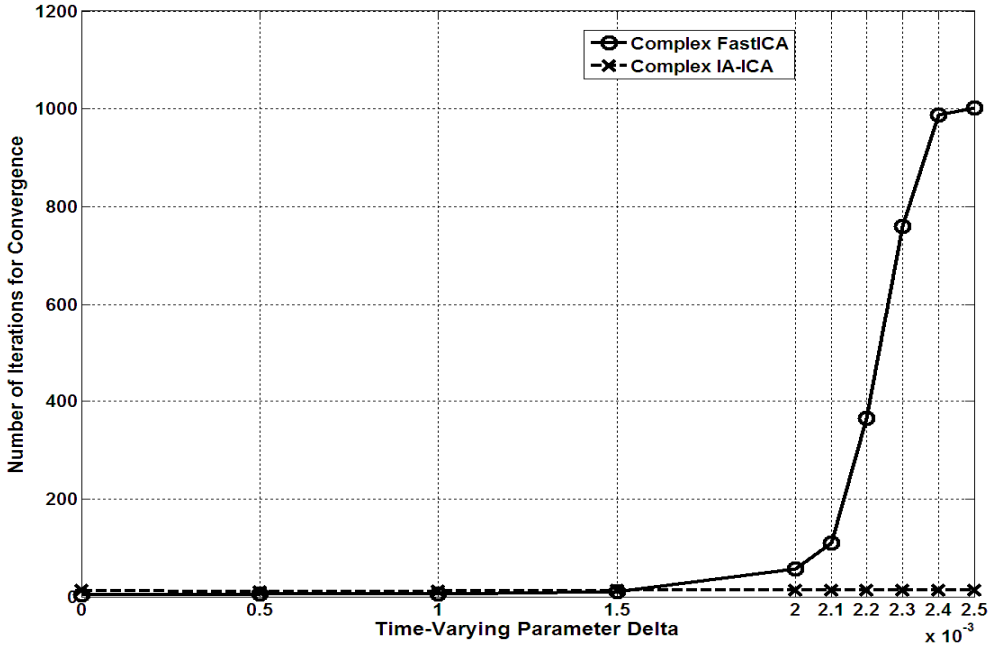

Figure 12: Number of Iterations for Convergence for Different Values of Δ and L =1000 symbols

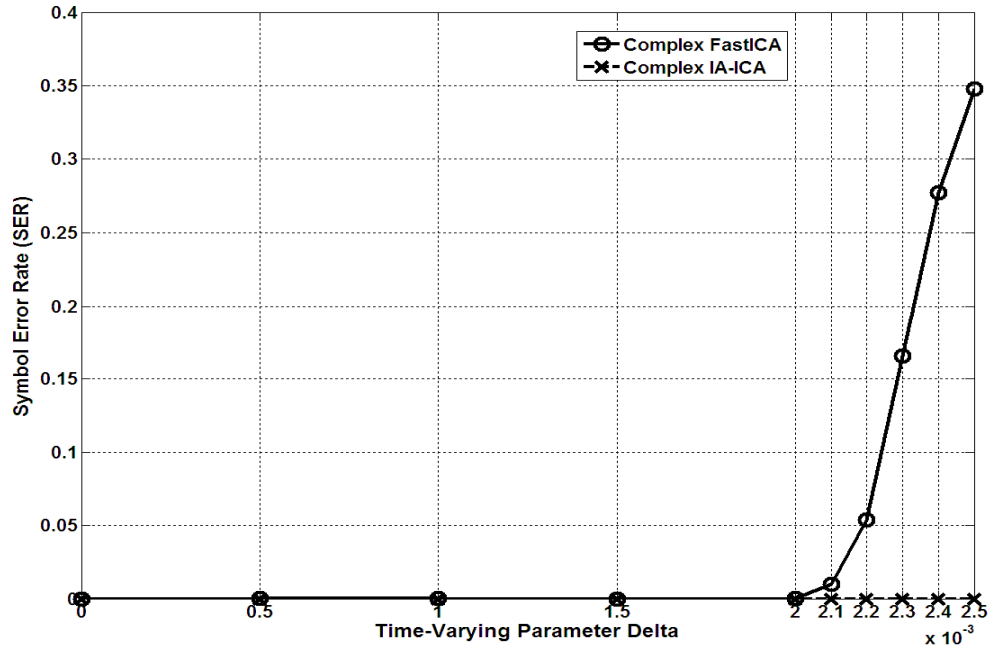

Figure 13: SER achieved for Different Values of Δ and L =1000 symbols

From the extensive simulation results presented, it is evident that the proposed Complex IA-ICA algorithm converges in less than 20 iterations with excellent accuracy, in both static and dynamic flat fading conditions. This can be attributed to the individual convergence factors optimally derived for each component of each weight, which maximally utilize the degrees of freedom of the adaptive system. As a result, it is highly effective in tracking the linear and abrupt variations in the complex channel parameters. In contrast, for linearly fading channels, it can be inferred from Figs. 6 and 7, that the convergence properties and SER of the Complex FastICA deteriorates with increasing block length and Δ, as it is unable to find a demixing matrix which approximates the linear variation. Furthermore, Figs. 8-10 show that in abruptly fading channels the Complex FastICA fails to achieve acceptable SER and interference suppression, especially for small block lengths. This is due to the fact that as the block length is reduced, the Complex FastICA finds the number of samples in the block insufficient to converge to a new demixing matrix. This limits the application of the Complex FastICA in wireless receivers with small processing block lengths. In comparison, the Complex IA-ICA quickly recovers from the sudden change, irrespective of the block length to yield excellent convergence properties.

3.6 Conclusions

In this chapter, the Complex ICA with Individual Adaptation (Complex IA-ICA) was presented. The square of the kurtosis was used as the cost function to be maximized and as a measure of statistical independence. The proposed algorithm optimally adapts each real and imaginary component of the complex weight vector using independent convergence factors. This is achieved by employing the Taylor's Series expansion in

combination with block gradient based optimization. In addition, the convergence factors are updated at the iteration of each block. As result, this novel formulation is most effective in utilizing all the degrees of freedom of the adaptive system in tracking the dynamics of the flat fading channel. Furthermore, the computational complexity involved in the matrix inversion operation was reduced to the order of L by inverting only the diagonal elements of the matrix. Simulation results confirm the remarkable improvement achieved in interference suppression and convergence speed over the Complex FastICA in dynamic environments.

CHAPTER FOUR: COMPLEX OPTIMUM BLOCK ADAPTIVE ICA (COMPLEX OBA-ICA) FOR SEPARATING COMPLEX SIGNALS WITH KNOWN SOURCE DISTRIBUTIONS

In the previous chapter, the formulation for the Complex IA-ICA was presented. The computational complexity of the Complex IA-ICA can be further reduced by employing only two convergence factors, one for all the real components of the complex weights, and another for all the imaginary components, instead of one for each component of each weight. This leads to a different formulation called Complex Optimum Block Adaptive ICA (Complex OBA-ICA).

Typically, in wireless communications, the receiver has prior knowledge regarding the modulation scheme of the desired communication signal. As a result, the statistical properties, including the probability distribution and higher order statistics of the desired signal are available information. In this chapter, this prior information is exploited to derive a modification of the Complex OBA-ICA algorithm for separation of complex signals with known distributions. The new realization is applied to interference suppression in dynamic environments for diversity QPSK receivers. Simulation results indicate that the proposed algorithm exhibit much better convergence speed and accuracy, in comparison with the Complex FastICA.

4.1 Proposed Complex OBA-ICA: Formulation

Similar to the Complex IA-ICA, the objective of the Complex OBA-ICA is to find a complex separating matrix W, such that its projection on the observation vector X, i.e. $W^H X$, yields the original source signals. In this process, it utilizes the square

of the kurtosis of $W^H X$ as an estimate of statistical independence, and tries to maximize it though a block gradient ascent approach.

The real and imaginary components of W at iteration index k, are defined as $w_R(k)$ and $w_I(k)$, respectively. The previously defined diagonal matrices $[MU]_{kR}$ and $[MU]_{kI}$ in (3.5) and (3.6), that represented the individual convergence factors for $w_R(k)$ and $w_I(k)$, respectively, are replaced by single convergence factors, i.e., $\mu_R(k)$ and $\mu_I(k)$. In other words,

$$\mu_{R1}(k) = \mu_{R2}(k) = \ldots\ldots\ldots = \mu_{RM}(k) = \mu_R(k) \tag{4.1}$$

and

$$\mu_{I1}(k) = \mu_{I2}(k) = \ldots\ldots\ldots = \mu_{IM}(k) = \mu_I(k) \tag{4.2}$$

Hence, the update equations for $w_R(k)$ and $w_I(k)$ become as follows:

$$w_R(k+1) = w_R(k) + \mu_R(k)\nabla_{BR}(k) \tag{4.3}$$

$$w_I(k+1) = w_I(k) + \mu_I(k)\nabla_{BI}(k) \tag{4.4}$$

Where,

$$\nabla_{BR}(k) = \frac{\partial\{\underline{kurt}^T(k)\underline{kurt}(k)\}}{\partial w_R(k)} \tag{4.5}$$

$$\nabla_{BI}(k) = \frac{\partial\{\underline{kurt}^T(k)\underline{kurt}(k)\}}{\partial w_I(k)} \tag{4.6}$$

are the block gradient vectors for the square of the kurtosis with respect to $w_R(k)$ and $w_I(k)$, respectively.

Evaluating (4.5) and (4.6), we obtain

$$\nabla_{BR}(k) = \frac{8}{L}[\mathrm{Re}\{[G]_k^T[C]_k\}\underline{kurt(k)}] \tag{4.7}$$

$$\nabla_{BI}(k) = \frac{8}{L}[\mathrm{Im}\{[G]_k^T[C]_k\}\underline{kurt(k)}] \tag{4.8}$$

Where,

$$[C]_k = \begin{bmatrix} \{w^H(k)X_1(k)\}^*\left|w^H(k)X_1(k)\right|^2 & \ldots & 0 \\ 0 & \ldots & 0 \\ 0 & 0 & \{w^H(k)X_L(k)\}^*\left|w^H(k)X_L(k)\right|^2 \end{bmatrix} \tag{4.9}$$

is a diagonal matrix. Re {.} and Im {.} represents the real and imaginary components of {.}, respectively.

Substituting (4.7) in (4.3), we get

$$w_R(k+1) = w_R(k) + \mu_R(k)\frac{8}{L}[\mathrm{Re}\{[G]_k^T[C]_k\}\underline{kurt(k)}] \tag{4.10}$$

Similarly, by substituting (4.8) in (4.4) we obtain

$$w_I(k+1) = w_I(k) + \mu_I(k)\frac{8}{L}[\mathrm{Im}\{[G]_k^T[C]_k\}\underline{kurt(k)}] \tag{4.11}$$

The l th kurtosis values for the real and imaginary parts of the weight update equation in the $(k+1)$ th iteration are expressed in a Taylor Series expansion as follows:

$$kurt_{lR}(k+1) = kurt_l(k) + \sum_{i=1}^{M}\frac{\partial kurt_l(k)}{\partial w_{iR}(k)}\Delta w_{iR}(k) +\ldots$$

$$l = 1,2\ldots. L \tag{4.12}$$

$$kurt_{lI}(k+1) = kurt_{l}(k) + \sum_{i=1}^{M} \frac{\partial kurt_{l}(k)}{\partial w_{iI}(k)} \Delta w_{iI}(k) +_{\ldots}$$

$$l = 1,2 \ldots . L \qquad (4.13)$$

Evaluating (4.12) and (4.13) for all L, we get

$$\underline{kurt_{R}(k+1)} = \underline{kurt_{R}(k)} + 4\,\mathrm{Re}\{[C]_{k}[G]_{k}\}\underline{\Delta w_{R}(k)} \qquad (4.14)$$

$$\underline{kurt_{I}(k+1)} = \underline{kurt_{I}(k)} + 4\,\mathrm{Im}\{[C]_{k}[G]_{k}\}\underline{\Delta w_{I}(k)} \qquad (4.15)$$

From (4.3) and (4.4), we have,

$$\Delta w_{R}(k) = \mu_{R}(k)\nabla_{BR}(k) \qquad (4.16)$$

$$\Delta w_{I}(k) = \mu_{I}(k)\nabla_{BI}(k) \qquad (4.17)$$

Substituting (4.16) and (4.17) in (4.14) and (4.15), respectively, and evaluating the resulting expressions, we obtain the following:

$$\underline{kurt_{R}(k+1)} = \underline{kurt_{R}(k)} + \frac{32}{L}\mu_{R}(k)\,\mathrm{Re}\{[C]_{k}[G]_{k}\}q_{R}(k) \qquad (4.18)$$

$$\underline{kurt_{I}(k+1)} = \underline{kurt_{I}(k)} + \frac{32}{L}\mu_{I}(k)\,\mathrm{Im}\{[C]_{k}[G]_{k}\}q_{I}(k) \qquad (4.19)$$

Where,

$$q_{R}(k) = [\mathrm{Re}\{[G]_{k}^{T}[C]_{k}\}\underline{kurt(k)}] \qquad (4.20)$$

$$q_{I}(k) = [\mathrm{Im}\{[G]_{k}^{T}[C]_{k}\}\underline{kurt(k)}] \qquad (4.21)$$

To ensure simplicity, we define the following:

$$[R]_{R}(k) = [\mathrm{Re}\{[C]_{k}[G]_{k}\}]^{T}\ \mathrm{Re}\{[C]_{k}[G]_{k}\} \qquad (4.22)$$

$$[R]_{I}(k) = [\mathrm{Im}\{[C]_{k}[G]_{k}\}]^{T}\ \mathrm{Im}\{[C]_{k}[G]_{k}\} \qquad (4.23)$$

From (4.18), the total squared kurtosis for the $(k+1)$ th iteration is given as:

$$\underline{kurt_R^T(k+1)}\,\underline{kurt_R(k+1)} = S_1 + S_2 + S_3 + S_4 \tag{4.24}$$

Where,

$$S_1 = \underline{kurt_R^T(k)}\,\underline{kurt_R(k)} \tag{4.25}$$

$$S_2 = \frac{1024}{L^2}\,\mu_R{}^2(k)\,q_R^T(k)[R]_R(k)q_R(k) \tag{4.26}$$

$$S_3 = \frac{32}{L}\,\mu_R(k)\,q_R^T(k)[\mathrm{Re}\{[C]_k[G]_k\}]^T\,\underline{kurt(k)} \tag{4.27}$$

$$S_4 = \frac{32}{L}\,\mu_R(k)\,\underline{kurt^T(k)}[\mathrm{Re}\{[C]_k[G]_k\}]q_R(k) \tag{4.28}$$

Since we are optimizing the square of the kurtosis with respect to $\mu_R(k)$, the following equation is applied.

$$\nabla \frac{\partial\{\underline{kurt_R^T(k+1)}\,\underline{kurt_R(k+1)}\}}{\partial\mu_R(k)} = 0 \tag{4.29}$$

Evaluating (4.29), we get

$$\mu_R(k) = -\frac{L}{32}\frac{q_R^T(k)q_R(k)}{q_R^T(k)[R]_R(k)q_R(k)} \tag{4.30}$$

Similarly, by evaluating the derivative of the square of (4.15) with respect to $\mu_I(k)$, we obtain

$$\mu_I(k) = -\frac{L}{32}\frac{q_I^T(k)q_I(k)}{q_I^T(k)[R]_I(k)q_I(k)} \tag{4.31}$$

From (4.10) and (4.11), we have:

$$w_R(k+1) = w_R(k) + \frac{8}{L}\mu_R(k)q_R(k) \tag{4.32}$$

$$w_I(k+1) = w_I(k) + \frac{8}{L}\mu_I(k)q_I(k) \tag{4.33}$$

Substituting (4.30) and (4.31) in (4.32) and (4.33), respectively, we obtain the independent weight update equations for the Complex OBA-ICA algorithm as follows:

$$w_R(k+1) = w_R(k) - 0.25\frac{q_R^T(k)q_R(k)}{q_R^T(k)[R]_R(k)q_R(k)}q_R(k) \tag{4.34}$$

$$w_I(k+1) = w_I(k) - 0.25\frac{q_I^T(k)q_I(k)}{q_I^T(k)[R]_I(k)q_I(k)}q_I(k) \tag{4.35}$$

In contrast with the Complex IA-ICA algorithm presented in (3.32) and (3.33), the Complex OBA-ICA algorithm does not involve a matrix inversion operation. As a result, from the computational viewpoint, it is less intensive.

4.2 Modification of the Complex OBA-ICA for complex signals with known source distributions

In the previous section, the formulation for the Complex OBA-ICA algorithm was presented. However, in most wireless communication applications, the receiver has prior knowledge about the modulation format of the desired source signal. Hence, information regarding higher order statistics, such as kurtosis for the source signal is readily available to the receiver. In this section, this information is utilized to derive a novel realization of the Complex OBA-ICA for separating complex signals with known source distributions [38, 39, and 66].

As the possible values for symbols in the QPSK constellation are $\pm 0.707 \pm 0.707j$, the corresponding kurtosis value is -1. The proposed modification

to the Complex OBA-ICA follows a Newton's type iteration approach to update the weight vectors $w_R(k)$ and $w_I(k)$, such that each of the L elements of $\underline{kurt_R(k+1)}$ and $\underline{kurt_I(k+1)}$ in (4.14) and (4.15), respectively, becomes -1, i.e.,

$$\underline{kurt_R(k+1)} = \underline{kurt_I(k+1)} = -\underline{K} = [-1 \ -1 \ldots\ldots -1]^T \tag{4.36}$$

Defining

$$[R]_R(k) = [\mathrm{Re}\{[C]_k[G]_k\}] \tag{4.37}$$

$$[R]_I(k) = [\mathrm{Im}\{[C]_k[G]_k\}] \tag{4.38}$$

(4.14) and (4.15) become as follows:

$$\Delta w_R(k) = -[R]_R^{\#}(k)(\underline{kurt_R(k)} + \underline{K}) \tag{4.39}$$

$$\Delta w_I(k) = -[R]_I^{\#}(k)(\underline{kurt_I(k)} + \underline{K}) \tag{4.40}$$

Where,

$$[R]_R^{\#}(k) = \begin{cases} [R]_R^T(k)([R]_R(k)[R]_R^T(k))^{-1} & \mathrm{L} < \mathrm{N} \\ ([R]_R^T(k)[R]_R(k))^{-1}[R]_R^T(k) & \mathrm{L} \geq \mathrm{N} \end{cases} \tag{4.41}$$

$$[R]_I^{\#}(k) = \begin{cases} [R]_I^T(k)([R]_I(k)[R]_I^T(k))^{-1} & \mathrm{L} < \mathrm{N} \\ ([R]_I^T(k)[R]_I(k))^{-1}[R]_I^T(k) & \mathrm{L} \geq \mathrm{N} \end{cases} \tag{4.42}$$

$[R]_R^{\#}(k)$ and $[R]_I^{\#}(k)$ are the pseudo-inverses of the matrices $[R]_R(k)$ and $[R]_I(k)$ respectively.

Since the proposed technique tries to achieve separation of signals in one step, a scaling factor μ is introduced to ensure stability of convergence and enhancement of performance. However, the performance is not sensitive to the chosen μ.

Hence, the weight updates for the modified Complex OBA-ICA algorithm employing μ becomes:

$$\Delta w_R(k) = -\mu [R]_R^{\#}(k)(\underline{kurt_R(k)} + \underline{K}) \tag{4.43}$$

$$\Delta w_I(k) = -\mu [R]_I^{\#}(k)(\underline{kurt_I(k)} + \underline{K}) \tag{4.44}$$

4.3 Computational Complexity

The weight update equations for the Complex OBA-ICA algorithm in (4.41) and (4.42) involve matrix inversion, which can be computationally intensive for high order systems. However, the matrix inversion operation can be simplified by replacing the matrix to be inverted in (4.41) and (4.42) with a matrix containing only its diagonal elements. As a result, the computational complexity of the Complex OBA-ICA algorithm is reduced to be linear, which is equivalent to the complex FastICA algorithm. Even with this approximation, simulation results presented in Section 4.4 show that the modified Complex OBA-ICA converges in less than 15 iterations, while achieving efficient interference cancellation.

4.4 Simulation Results

In the simulations, the modified Complex OBA-ICA is applied to interference suppression for diversity QPSK receivers under diverse channel scenarios. In this regard, the performance of the Complex OBA-ICA in terms of ISI, SER and number of iterations for convergence is compared to the Complex FastICA. The expression for ISI is as given in (3.38).

In matrix form, the signal observation model is given as follows:

$$\begin{bmatrix} X_1(l) \\ X_2(l) \end{bmatrix} = \begin{bmatrix} f_{s1}(1+l\Delta) & f_{i1}(1+l\Delta) \\ f_{s2}(1+l\Delta) & f_{i2}(1+l\Delta) \end{bmatrix} \begin{bmatrix} s(l) \\ i(l) \end{bmatrix}$$

$$l = 1,2\ldots. L \qquad (4.45)$$

Δ establishes the speed of flat fading of the wireless channel, which in turn determines the rate of amplitude and phase variation in the observed signals. $X_1(l)$ and $X_2(l)$ represent the baseband samples of the signals received at the two antennas of the receiver. $s(l)$ and $i(l)$ denote the source samples of the desired and interfering signals respectively. f_{s1} and f_{s2} are the channel fading parameters for the two independent paths between desired source transmitter and the two receiving antennas. Similarly, f_{i1} and f_{i2} represent the channel fading parameters between the interfering source transmitter and the two receiving antennas. The diversity receiver structure adopted for the simulation is as shown in Fig. 1. In addition, in all the simulations, the SNR realized is 20 dB. The channel fading parameters are randomly set as follows:

$$f_{s1} = 1+3j,\ f_{s2} = 5+7j,\ f_{i1} = 6+8j, \text{ and } f_{i2} = 2+4j$$

In the first case, stationary channel conditions are simulated, i.e. Δ=0. The ISI, SER and the number of iterations for convergence are illustrated in Figs. 14-16, respectively.

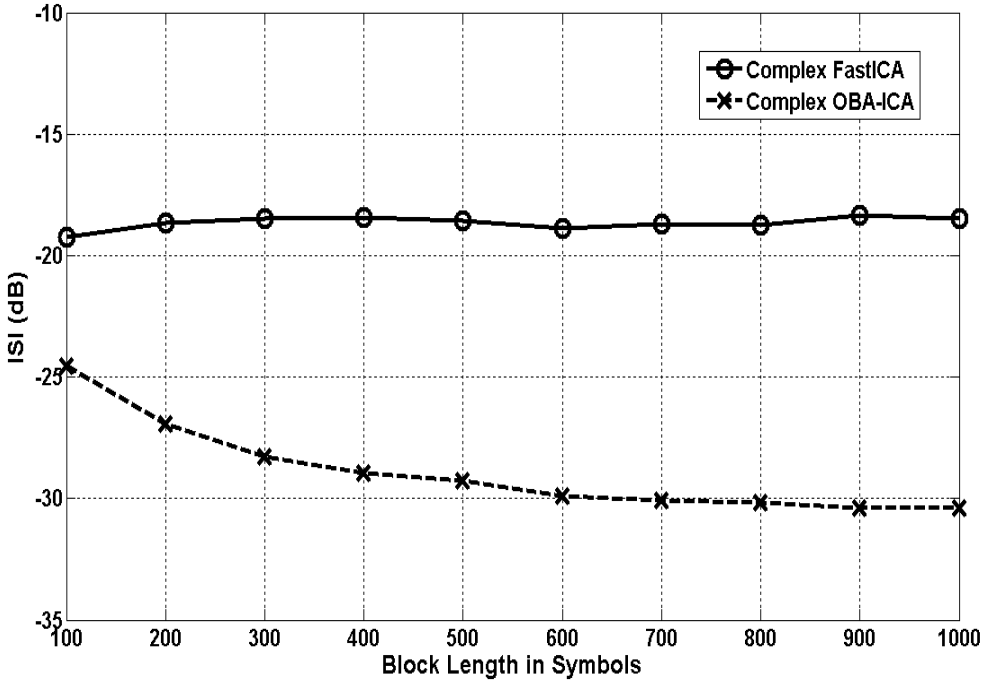

Figure 14: ISI (dB) achieved in Stationary Channels

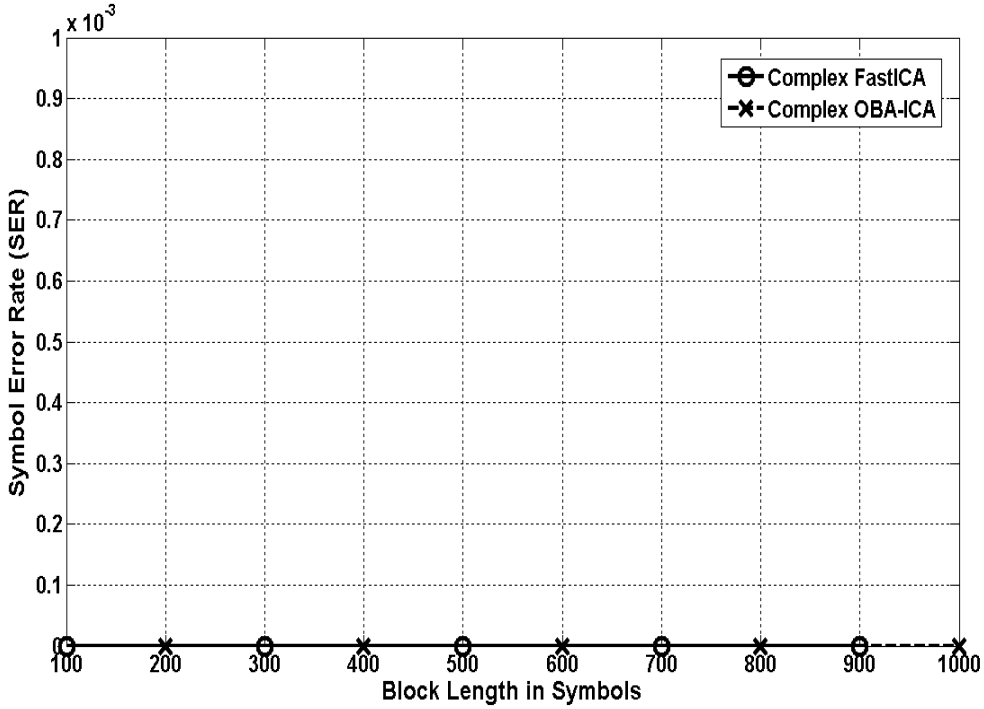

Figure 15: SER achieved in Stationary Channels

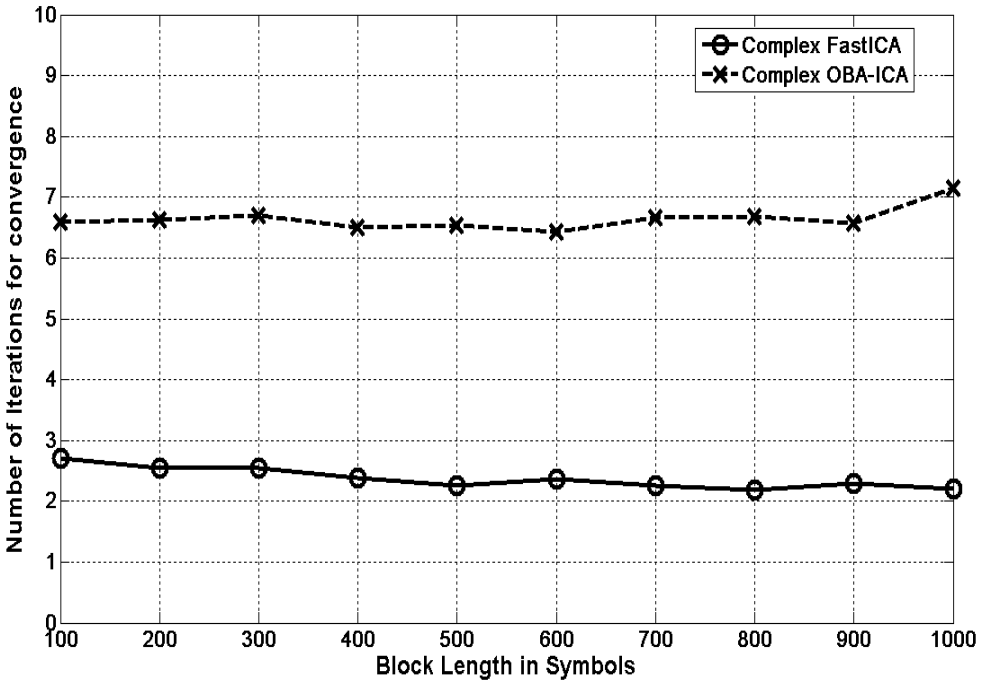

Figure 16: Number of iterations for convergence in Stationary Channels

To model a linearly flat fading scenario, the channel parameters or mixing matrix coefficients are gradually changed over the length of the processing block L. This is achieved by incorporating parameter Δ in (4.45). The performance of the Complex OBA-ICA and Complex FastICA were compared for different values of L. The ISI (dB) achieved by both algorithms for $\Delta = 0.002$ and $\Delta = 0.0022$ is shown in Fig.17. The Complex FastICA failed to converge for higher values of Δ. The SER and number of iterations for convergence for $\Delta = 0.0022$ are plotted in Fig.18 and Fig. 19 respectively.

A highly dynamic environment is simulated by creating a sudden change in the mixing matrix coefficients in the middle of the data block. In this situation, the achieved ISI (dB), SER and number of iterations to converge are illustrated in Figs. 20-22, respectively.

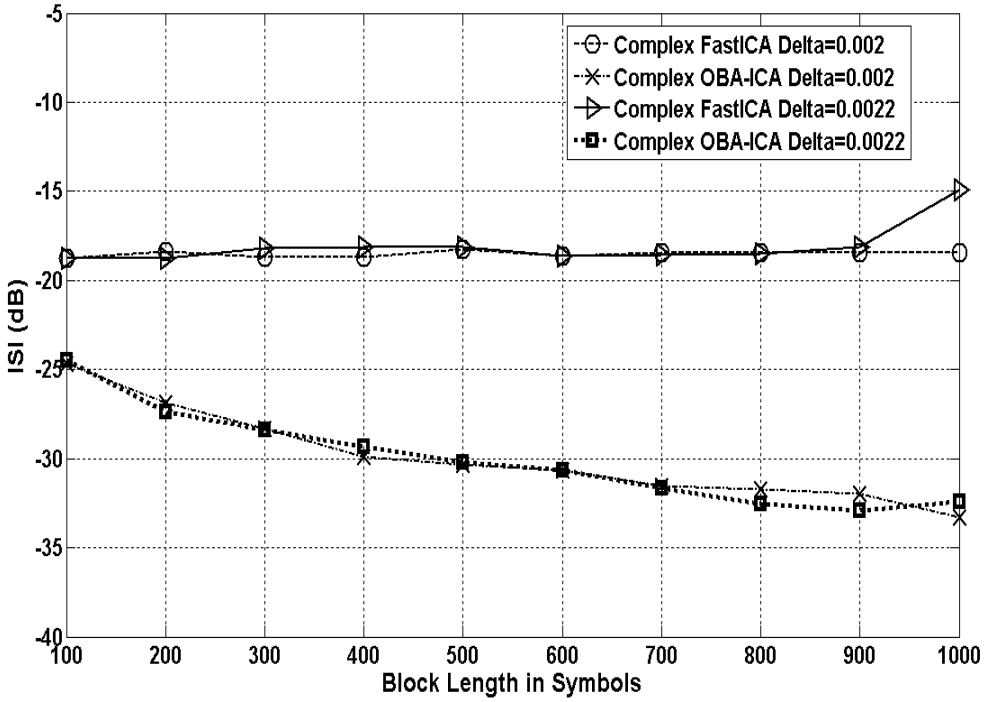

Figure 17: ISI (dB) achieved in Linearly Flat Fading Channels

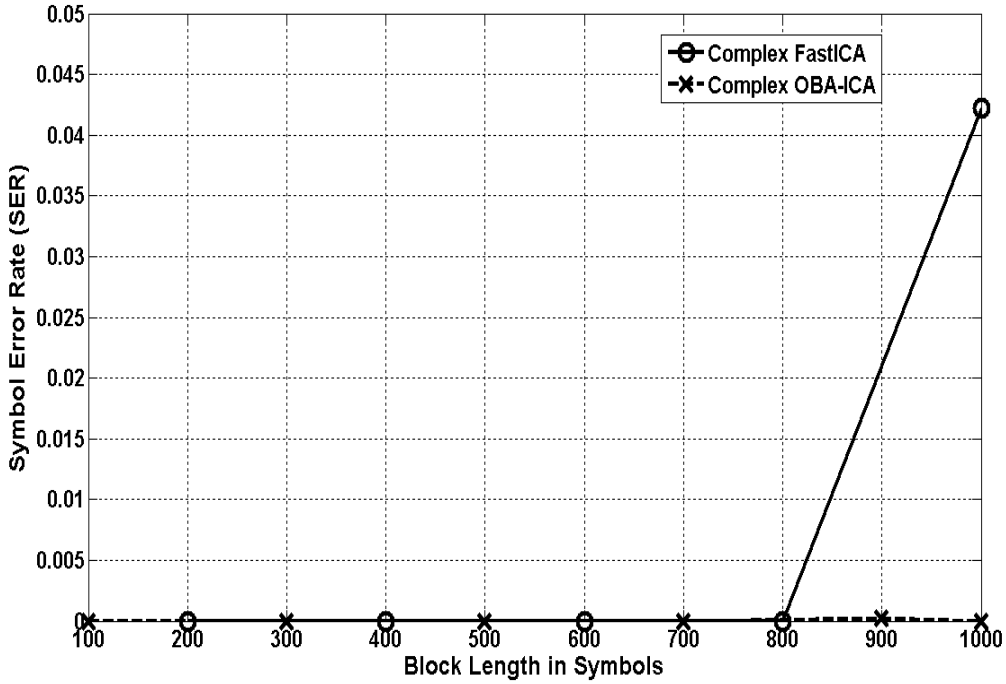

Figure 18: SER achieved for Δ =0.0022

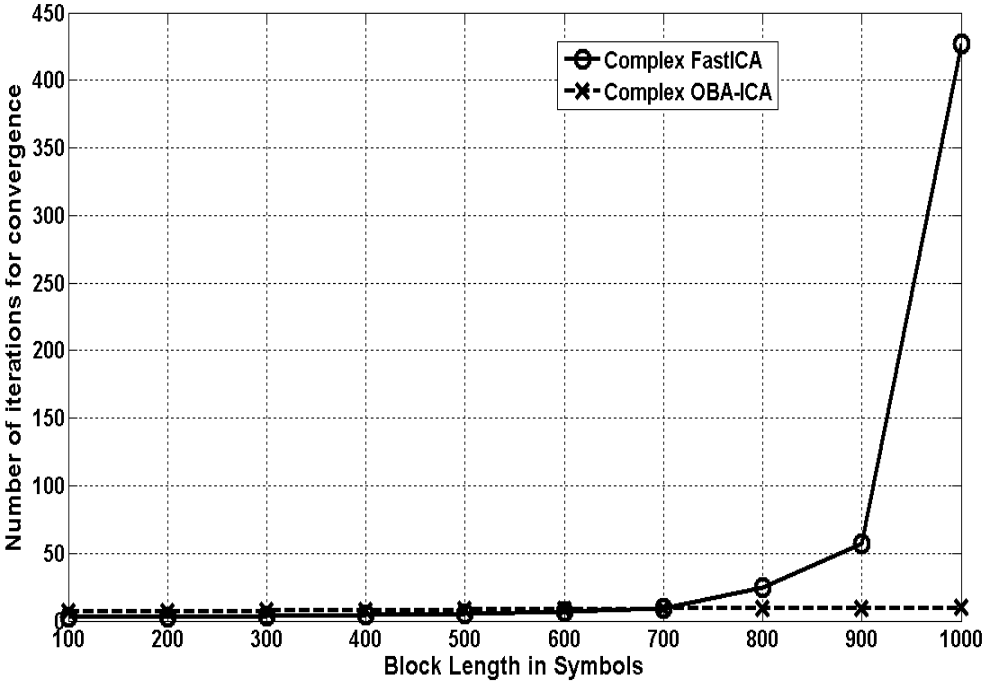

Figure 19: Number of iterations for convergence for Δ =0.0022

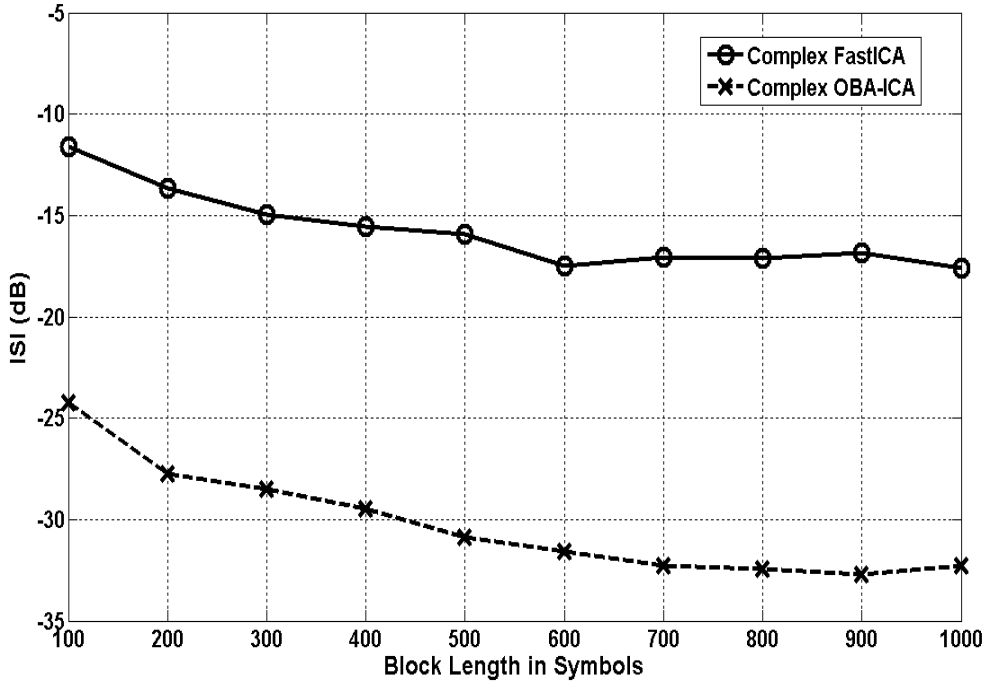

Figure 20: ISI (dB) achieved in abruptly flat fading channels

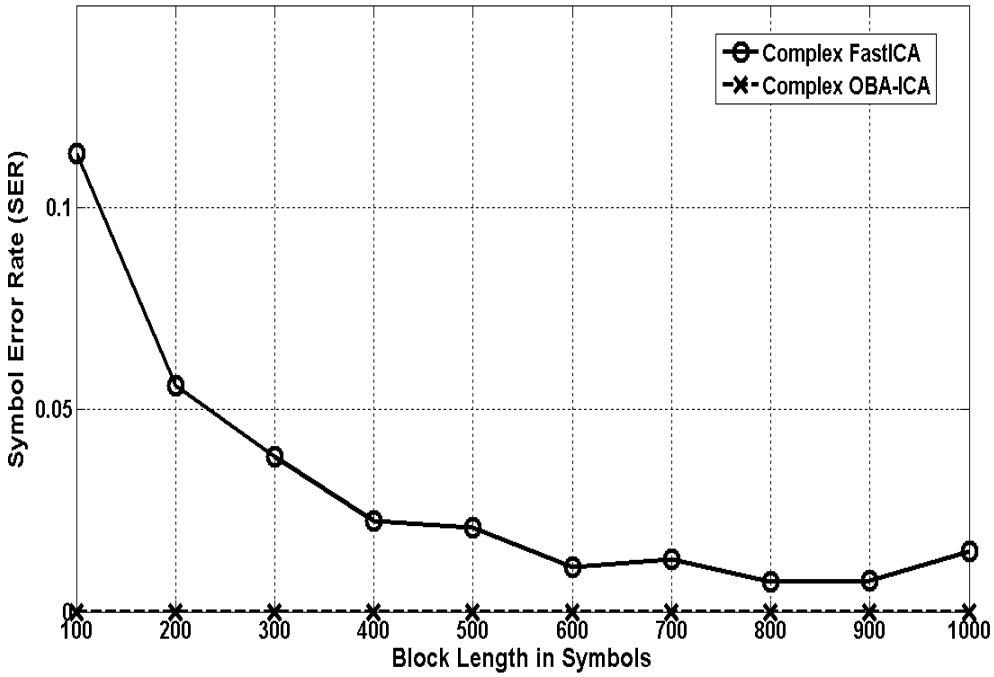

Figure 21: SER achieved in abruptly flat fading channels

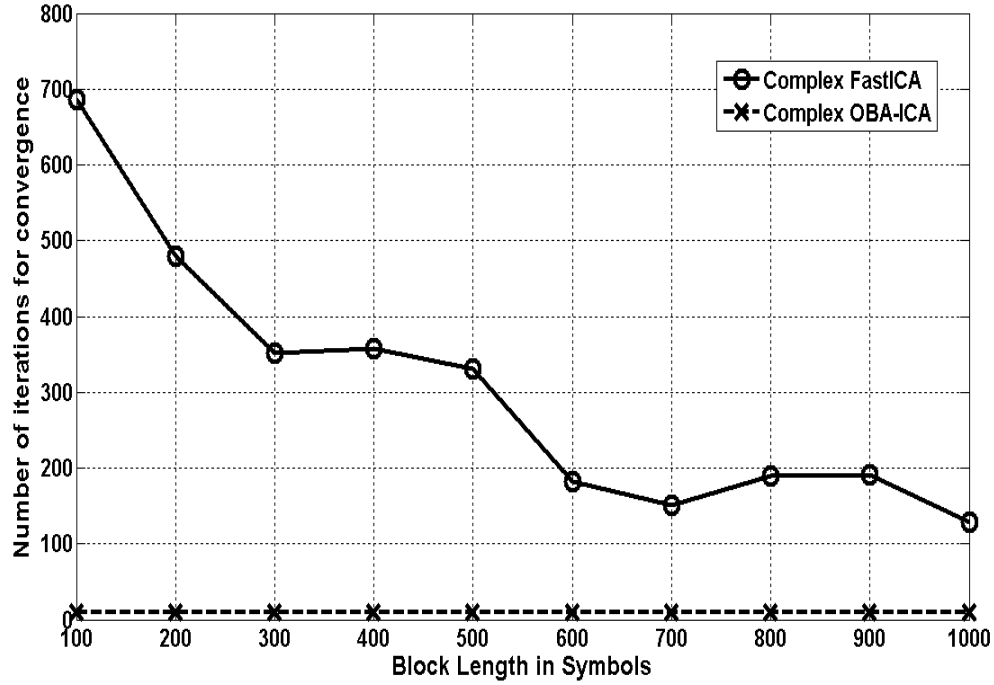

Figure 22: Number of iterations for convergence in abruptly flat fading channels

The illustration in Fig.19 shows that in linearly varying channels, the Complex OBA-ICA consistently converges within 20 iterations for the wide range of block lengths simulated. In addition, from Figs. 17 and 18, it can be inferred that the convergence speed is attained without compromising the SER and ISI performance. In contrast, the Complex FastICA is unable to maintain its accuracy and convergence speed for larger block lengths.

In highly dynamic fading, it can be inferred from Figs. 20-22 that the Complex FastICA is inefficient in adapting to rapid changes in the channel, particularly for small block lengths.

4.5 Conclusions

In this chapter, the formulation of the Complex Optimum Block Adaptive ICA (Complex OBA-ICA) was presented. At each iteration, the proposed technique derives two convergence factors for independent adjustments of the real and imaginary components of the complex demixing vector. This is achieved by optimizing the square of the kurtosis with respect to each convergence factor after a Taylor's series approximation of the kurtosis. As a result, the Complex OBA-ICA has lower computational complexity than the Complex IA-ICA presented in Chapter 3, which employs a convergence factor for each component of each weight. Furthermore, a novel realization of the Complex OBA-ICA was formulated for separating complex signals with known source distributions. The modified technique exploits prior information regarding the statistical properties of the desired signal, namely the kurtosis. Consequently, it updates the weight vector through a Newton's type iteration approach to achieve the kurtosis of the desired signal. In this manner, the desired source signal can be

easily retrieved from the observations. The presented simulation results show that the modified Complex OBA-ICA yields excellent convergence speed and accuracy in both linear and abrupt variations in the flat fading channel, in contrast to the Complex FastICA which demonstrates performance degradation for larger block lengths.

CHAPTER FIVE: CONJUGATE GRADIENT BASED COMPLEX BLOCK ADAPTIVE ICA (CBC-ICA)

The conjugate gradient method is a prominent technique for solving systems of linear equations, and unconstrained optimization problems, including adaptive filtering [67-70]. Since it is an iterative method, it can be particularly applied to solve sparse systems which are too large to be handled by direct methods. The main advantage of the conjugate gradient method is that it employs orthogonal search directions with optimal steps along each direction to arrive at the solution. As a result, it has a much faster convergence speed than the Steepest Descent method which often takes steps in the same direction as earlier steps. Furthermore, it has lower computational complexity than the Newton's iteration approach. This unique tradeoff between convergence speed and computational complexity gives the Conjugate Gradient method desirable properties for application in numerous mathematical optimization problems.

In this chapter, the conjugate gradient principle is applied to Complex Adaptive ICA for maximization of the kurtosis function, to achieve separation of complex-valued signals. The proposed technique is called Complex Block Conjugate Independent Component Analysis (CBC-ICA) algorithm. The CBC-ICA derives independent conjugate-gradient search directions for the real and imaginary components of the complex coefficients of the adaptive system employed for signal separation. In addition, along each conjugate direction an optimal update is generated separately for the real and imaginary components using the Taylor's series approximation [71, 72]. Simulation results confirm that in dynamic flat fading conditions, the CBC-ICA demonstrates

excellent convergence speed, even for large processing block sizes, while maintaining satisfactory SER.

5.1 Conjugate Gradient Principle

As mentioned previously, the Steepest Descent algorithm often derives the same search direction more than once, resulting in slow convergence. Intuitively, we can avoid this by utilizing orthogonal search directions $d_{(0)}, d_{(1)}, \ldots\ldots, d_{(n-1)}$, with optimal steps $\alpha_{(k)}$, along each direction. Hence, the solution can be obtained in just n steps.

To derive unique search directions, the error in the $(k+1)^{th}$ iteration $e_{(k+1)}$, should be orthogonal to the search direction in the k^{th} iteration, $d_{(k)}$, i.e.

$$d_{(k)}^{T} e_{(k+1)} = 0 \tag{5.1}$$

$$d_{(k)}^{T} (e_{(k)} + \alpha_{(k)} d_{(k)}) = 0 \tag{5.2}$$

In this manner, the step size $\alpha_{(k)}$ is computed as:

$$\alpha_{(k)} = -\frac{d_{(k)}^{T} e_{(k)}}{d_{(k)}^{T} d_{(k)}} \tag{5.3}$$

As (5.3) contains the $e_{(k)}$ term which is always unknown, it cannot be used for finding $\alpha_{(k)}$.

A practical approach to this problem would be to replace the orthogonality condition for the search vectors with A-orthogonality. Two search vectors $d_{(i)}$ and $d_{(j)}$ are said to be A-orthogonal if they satisfy the following condition:

$$d_{(i)}^T A d_j = 0 \tag{5.4}$$

Hence, $e_{(k+1)}$ becomes A-orthogonal to $d_{(k)}$, i.e.

$$d_{(k)}^T A e_{(k+1)} = 0 \tag{5.5}$$

Similar to the derivation in (5.3), the expression for $\alpha_{(k)}$ when the search vectors are A-orthogonal is given as:

$$\alpha_{(k)} = -\frac{d_{(k)}^T A e_{(k)}}{d_{(k)}^T A d_{(k)}} \tag{5.6}$$

$$\alpha_{(k)} = \frac{d_{(k)}^T r_{(k)}}{d_{(k)}^T A d_{(k)}} \tag{5.7}$$

$r_{(k)}$ is the residual vector or the negative of the gradient estimate at iteration k given by:

$$\begin{aligned} r_{(k)} &= -A e_{(k)} \\ &= -A(e_{(k-1)} + \alpha_{(k-1)} d_{(k-1)}) \\ &= r_{(k-1)} - \alpha_{(k-1)} A d_{(k-1)} \end{aligned} \tag{5.8}$$

It is worth mentioning that if the residual were the search vector, (5.7) would be identical to the Steepest Descent technique.

In the method of conjugate gradients, the search directions are constructed by conjugation of the residual vectors. In addition, since each residual is orthogonal to the previous search direction, it is also orthogonal to the previous residuals as shown in Fig.23, i.e.

$$r_{(i)}^T r_{(j)} = 0 \qquad i \neq j \tag{5.9}$$

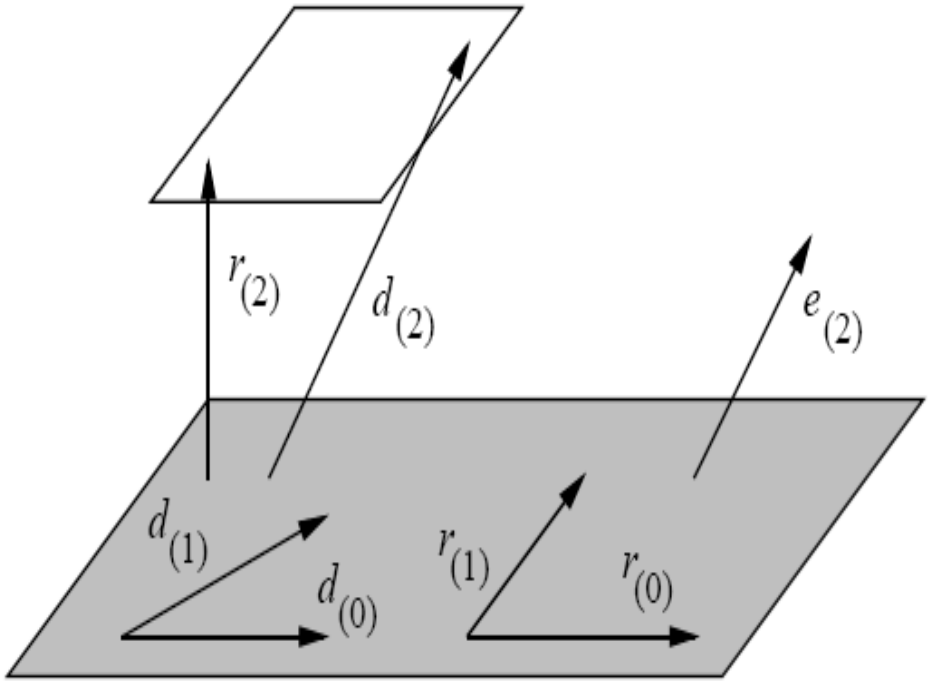

Figure 23: Method of Conjugate Gradients employing orthogonal residuals r_i and A-orthogonal search directions d_i

Applying the inner product of $r_{(i)}$ and (5.8) for $k = j + 1$ results in the following:

$$r_{(i)}^T r_{(j+1)} = r_{(i)}^T r_{(j)} - \alpha_{(j)} r_{(i)}^T A d_{(j)} \tag{5.10}$$

$$\Rightarrow \qquad \alpha_{(j)} r_{(i)}^T A d_{(j)} = r_{(i)}^T r_{(j)} - r_{(i)}^T r_{(j+1)} \tag{5.11}$$

Substituting (5.9) in (5.11), we obtain:

$$r_{(i)}^T A d_{(j)} = \begin{cases} \dfrac{1}{\alpha_{(i)}} r_{(i)}^T r_{(i)} & i = j \\ -\dfrac{1}{\alpha_{(i-1)}} r_{(i)}^T r_{(i)} & i = j+1 \\ 0 & \text{otherwise} \end{cases} \tag{5.12}$$

Employing Gram-Schmidt conjugation [105], the Gram-Schmidt constants are given by:

$$\beta_{ij} = -r_{(i)}^T A d_{(j)} / d_{(j)}^T A d_{(j)} \tag{5.13}$$

Substituting (5.13) in (5.12), gives the following result:

$$\beta_{ij} = \begin{cases} \dfrac{1}{\alpha_{(i-1)}} \dfrac{r_{(i)}^T r_{(i)}}{d_{(i-1)}^T A d_{(i-1)}} & i = j+1 \\ 0 & i > j+1 \end{cases} \tag{5.14}$$

From (5.14), it is evident that the old search vectors need not be stored to ensure the A-orthogonality of new search vectors. As a result, substituting (5.7), (5.14) becomes

$$\begin{aligned} \beta_{ij} &= \frac{r_{(i)}^T r_{(i)}}{d_{(i-1)}^T r_{(i-1)}} \\ &= \frac{r_{(i)}^T r_{(i)}}{r_{(i-1)}^T r_{(i-1)}} \end{aligned} \tag{5.15}$$

In summary, the method of conjugate gradients is given by the following equations:

$$d_{(0)} = r_{(0)} \tag{5.16}$$

$$\beta_{(i+1)} = \frac{r_{(i+1)}^T r_{(i+1)}}{r_{(i)}^T r_{(i)}} \tag{5.17}$$

$$d_{(i+1)} = r_{(i+1)} + \beta_{(i+1)} d_{(i)} \tag{5.18}$$

5.2 Formulation of the Proposed CBC-ICA algorithm

The CBC-ICA applies the conjugate gradient principle independently to the real and imaginary components of the adaptive system coefficients or complex demixing matrix, to achieve maximization of kurtosis or non-gaussianity. In addition, along each

conjugate search direction, optimal step sizes are derived separately for the real and imaginary parts using the Taylor's series approximation.

The formulation of the algorithm as a series of steps is outlined below:

STEP 1: ICA preprocessing operations including mean centering, whitening, and orthogonalization is performed on the observation matrix X and the iteration index k is initialized to 0. In accordance with the ICA model, X can be represented as $X = AS + N$, where A is the unknown mixing matrix or wireless channel, S is the source signal vector, and N is Additive White Gaussian Noise (AWGN). Consequently, the signal separation model is given by $Y = W^H X$, where Y is the vector containing the recovered sources, W is the complex separating or demixing matrix, and H denotes the Conjugate Transpose or Hermitian operator.

STEP 2: Let w_1 be the first column of W, and M be the number of rows of w_1. M is also the number of signal observations or number of signals to be separated. In the presented research, the separation of 2 QPSK signals is considered, hence M = 2. However, the algorithm can be easily extended for separating any number of complex-valued signals.

STEP 3: The gradient vectors $g_R(k)$ and $g_I(k)$, are calculated as the derivative of the kurtosis squared with respect to $w_R(k)$ and $w_I(k)$ respectively:

$$g_R(k) = \frac{\partial\{\underline{kurt}^T(k)\underline{kurt}(k)\}}{\partial w_R(k)} = \frac{8}{L}[\mathrm{Re}\{[X][C]_k\}\underline{kurt}^T(k)] \qquad (5.19)$$

$$g_I(k) = \frac{\partial\{\underline{kurt}^T(k)\underline{kurt}(k)\}}{\partial w_I(k)} = \frac{8}{L}[\mathrm{Im}\{[X][C]_k\}\underline{kurt}^T(k)] \qquad (5.20)$$

where, T denotes the transpose , L is the block length in symbols, X is a matrix of order M x L, $\underline{kurt(k)}$ is a row vector of length L containing the kurtosis values of $w_1(k)^H X$ given by:

$$\underline{kurt(k)} = \left| w_1(k)^H [X] \right|^4 \tag{5.21}$$

and $$[C]_k = diag[\{w_1(k)^H [X]\}^* \left| w_1(k)^H [X] \right|^2] \tag{5.22}$$

is a diagonal matrix, * represents the complex conjugate. Re {.} and Im {.} represents the real and imaginary components of {.}, respectively.

a. The convergence of $w_1 = w_R(k) + jw_I(k)$ is then checked. If the required accuracy has been achieved, proceed to STEP 5.

b. If convergence has not been reached, and $k = 0$, the optimal update directions $d_R(k)$ and $d_I(k)$, for $w_R(k)$ and $w_I(k)$ respectively, are set equal to the gradient vectors, i.e.

$$d_R(k) = g_R(k) \tag{5.23}$$

$$d_I(k) = g_I(k) \tag{5.24}$$

Goto STEP 4.

c. If convergence has not been reached, and $k > 0$, $d_R(k)$ and $d_I(k)$ are calculated as conjugate gradient vectors:

$$d_R(k) = g_R(k) + \frac{g_R{}^T(k) g_R(k)}{g_R{}^T(k-1) g_R(k-1)} d_R(k-1) \tag{5.25}$$

$$d_I(k) = g_I(k) + \frac{g_I^{\,T}(k)g_I(k)}{g_I^{\,T}(k-1)g_I(k-1)} d_I(k-1) \tag{5.26}$$

STEP 4: The independent updates for w_R and w_I are given as:

$$w_R(k+1) = w_R(k) + \alpha_R(k) d_R(k) \tag{5.27}$$

$$w_I(k+1) = w_I(k) + \alpha_I(k) d_I(k) \tag{5.28}$$

where, α_R and α_I at each iteration, are optimally derived as follows:

We express the l th kurtosis value in the $(k+1)$ th iteration in a Taylor Series expansion with respect to w_R and w_I as follows:

$$kurt_{lR}(k+1) = kurt_{lR}(k) + \sum_{i=1}^{M} \frac{\partial kurt_{lR}(k)}{\partial w_{iR}(k)} \Delta w_{iR}(k) + \ldots$$

l=1,2….L (5.29)

$$kurt_{lI}(k+1) = kurt_{lI}(k) + \sum_{i=1}^{M} \frac{\partial kurt_{lI}(k)}{\partial w_{iI}(k)} \Delta w_{iI}(k) + \ldots$$

l=1,2….L (5.30)

Evaluating expressions (5.29) and (5.30) for all L kurtosis values, we obtain,

$$\underline{kurt_R(k+1)} = \underline{kurt_R(k)} + 4\,\mathrm{Re}\{[C]_k[X]^T\}\alpha_R(k) d_R(k) \tag{5.31}$$

$$\underline{kurt_I(k+1)} = \underline{kurt_I(k)} + 4\,\mathrm{Im}\{[C]_k[X]^T\}\alpha_I(k) d_I(k) \tag{5.32}$$

In each iteration, α_R and α_I are optimally computed such that the square of $\underline{kurt_R(k+1)}$ and $\underline{kurt_I(k+1)}$ are maximized in the $(k+1)$ th iteration, i.e.

$$\frac{\partial\{\underline{kurt_R^T(k+1)}\,\underline{kurt_R(k+1)}\}}{\partial \alpha_R(k)} = 0 \tag{5.33}$$

$$\frac{\partial\{\underline{kurt_I^T(k+1)}\underline{kurt_I(k+1)}\}}{\partial\alpha_I(k)}=0 \tag{5.34}$$

Evaluating (5.33) and (5.34) we obtain the following:

$$\alpha_R(k)=-0.25\frac{d_R{}^T(k)q_R(k)}{d_R{}^T(k)[R_R]_k d_R(k)} \tag{5.35}$$

$$\alpha_I(k)=-0.25\frac{d_I{}^T(k)q_I(k)}{d_I{}^T(k)[R_I]_k d_I(k)} \tag{5.36}$$

where,

$$q_R(k)=\mathrm{Re}([X][C]_k)\underline{kurt(k)} \tag{5.37}$$

$$q_I(k)=\mathrm{Im}([X][C]_k)\underline{kurt(k)} \tag{5.38}$$

$$[R_R]_k=[\mathrm{Re}([C]_k[X]^T)]^T\ \mathrm{Re}([C]_k[X]^T) \tag{5.39}$$

$$[R_I]_k=[\mathrm{Im}([C]_k[X]^T)]^T\ \mathrm{Im}([C]_k[X]^T) \tag{5.40}$$

STEP 5: The second column of W, namely w_2, is set orthogonal to w_1, i.e.:

$$w_2=[w_{21}\quad -w_{11}] \tag{5.41}$$

5.3 Application of the CBC-ICA to Interference Suppression in Time-Varying Environments

In this research, the proposed CBC-ICA is applied to the separation of QPSK signals in time-varying flat fading channel situations. The ISI (dB), SER, and the number of iterations for convergence, are used in the performance comparison between the CBC-ICA and complex FastICA algorithms. For each block length L, the performance of both algorithms is averaged over 100 Monte Carlo runs for a SNR of 20 dB. The mixing matrix modeling the time-varying channel is represented in matrix form as

$$A = \begin{bmatrix} f_{11} + l * \Delta * f_{11} & f_{12} + l * \Delta * f_{12} \\ f_{21} + l * \Delta * f_{21} & f_{22} + l * \Delta * f_{22} \end{bmatrix}$$

$$l = 1, 2 ..... L \qquad (5.42)$$

$f_{11}, f_{12}, f_{21}, f_{22}$ denote the channel flat fading parameters which vary within the processing block. Δ is the parameter which reflects the rate of variation of the channel matrix coefficients. L is varied between 1000 and 2000 symbols with a step size of 100. The ISI (dB), SER, and the speed of convergence, in terms of number of iterations, for Δ =0.0011 are shown in Figs. 24-26, respectively. Corresponding results for Δ =0.0012 are illustrated in Figs. 27-29, respectively. For higher values of Δ, the Complex FastICA is unable to achieve the required convergence accuracy.

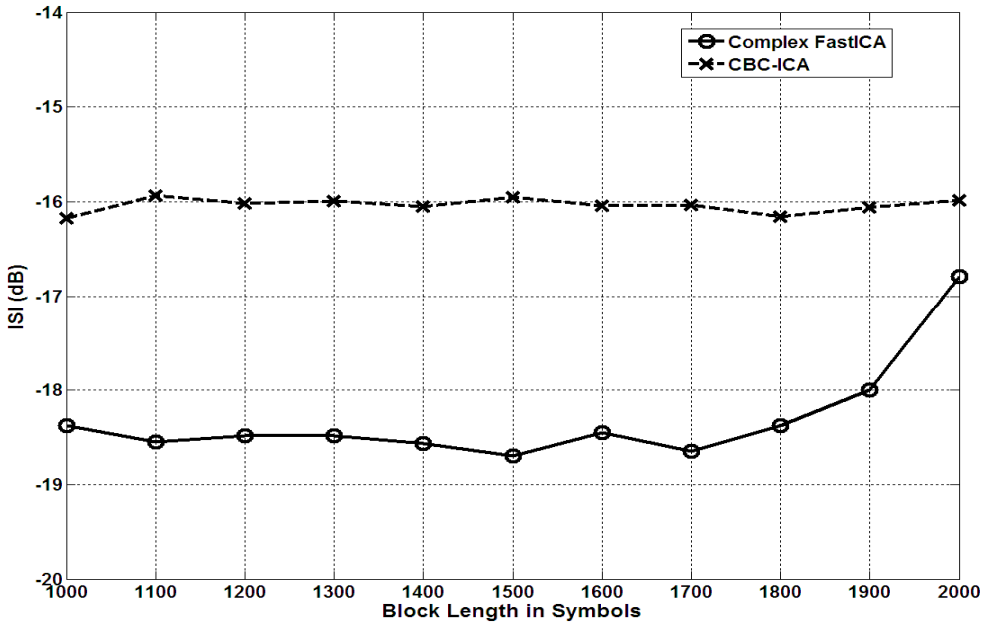

Figure 24: ISI (dB) achieved for Δ =0.0011

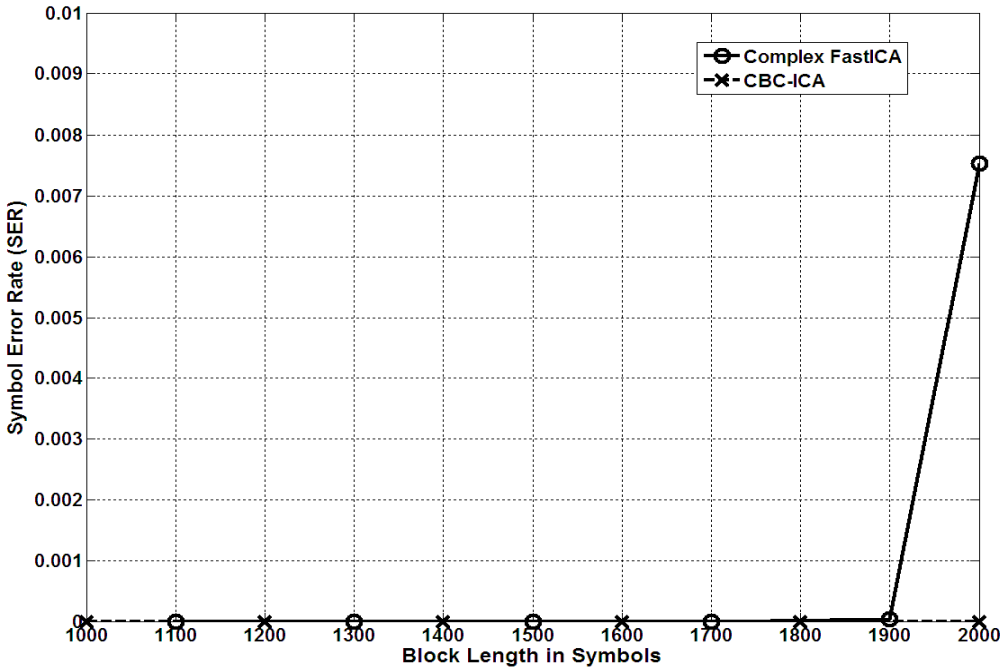

Figure 25: SER achieved for Δ =0.0011

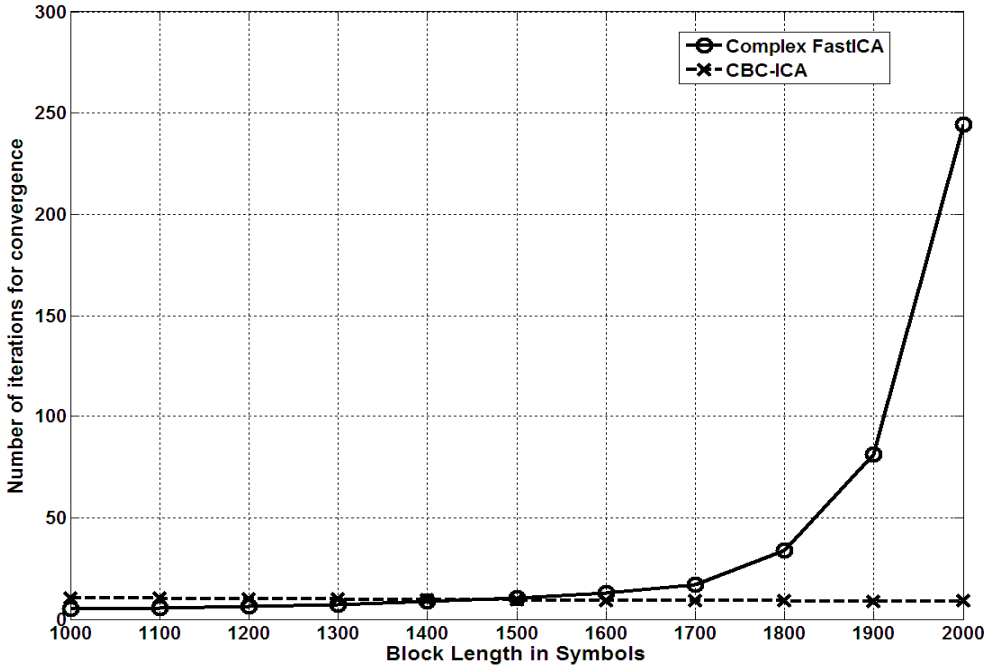

Figure 26: Number of iterations for convergence for Δ =0.0011

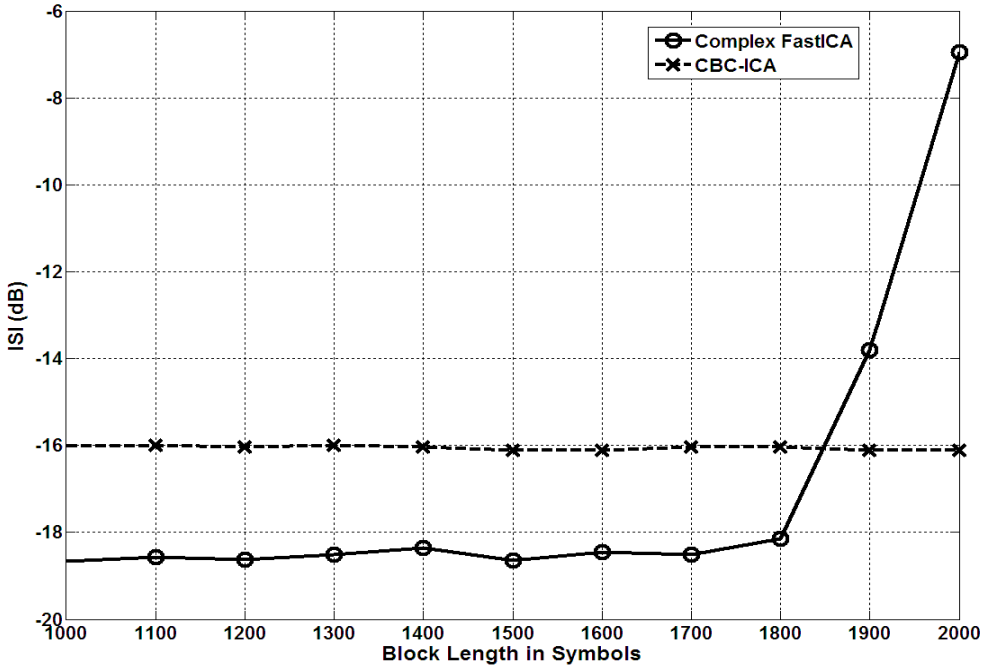

Figure 27: ISI (dB) achieved for Δ =0.0012

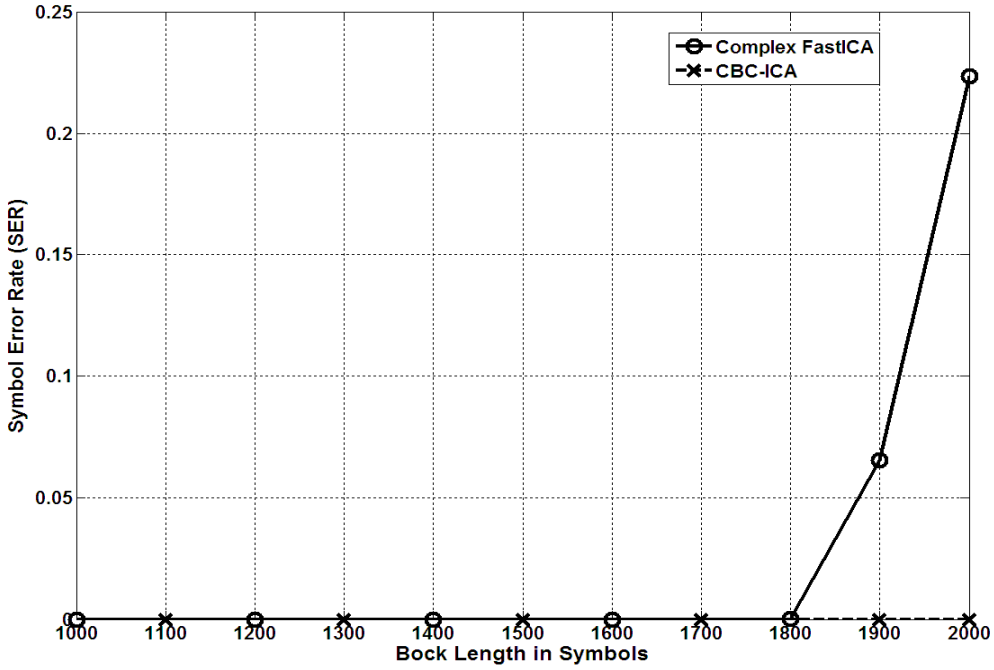

Figure 28: SER achieved for Δ =0.0012

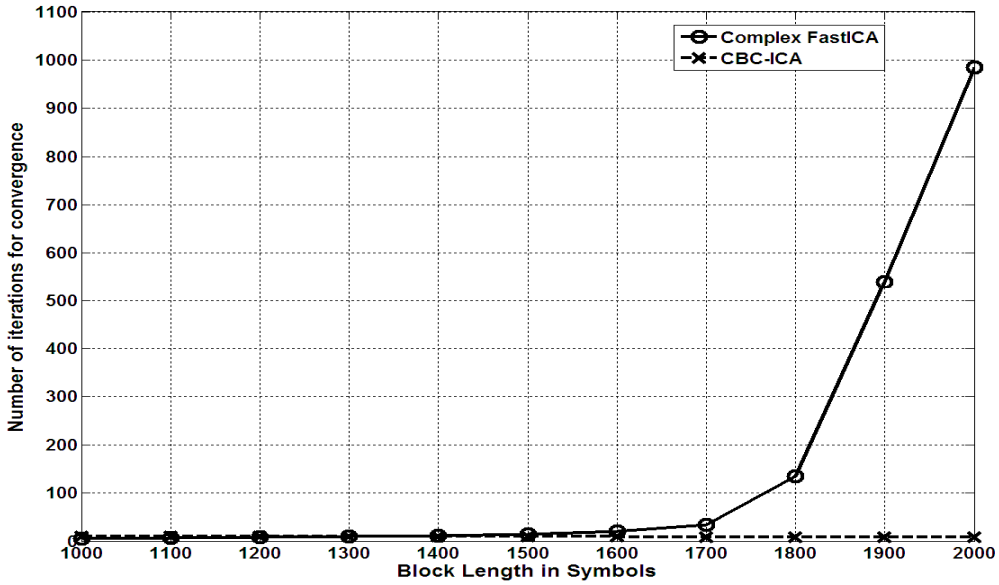

Figure 29: Number of iterations for convergence for Δ =0.0012

To simulate an abrupt channel variation, a sudden change in the mixing matrix coefficients is introduced in the middle of the processing block. In this scenario, the performance comparison between the two algorithms is plotted in Figs 30-32. The simulation results confirm the consistent and improved convergence properties demonstrated by the CBC-ICA algorithm, in terms of convergence speed and accuracy. In contrast, the ISI (dB) and SER of the complex FastICA is significantly affected with increasing values of Δ as can be seen from Figs.27 and 28, respectively. In addition, it can be inferred from Fig. 29 that the convergence speed of the complex FastICA progressively degrades with increasing block length, requiring many more iterations for convergence. Furthermore, Fig. 32 shows that in the abruptly fading case, the complex FastICA needs a larger block size to adapt to the instantaneous variations in the mixing matrix, thereby requiring many more iterations to converge for small block sizes. In

contrast, the CBC-ICA achieves comparable SER and ISI with fewer than 20 iterations for convergence.

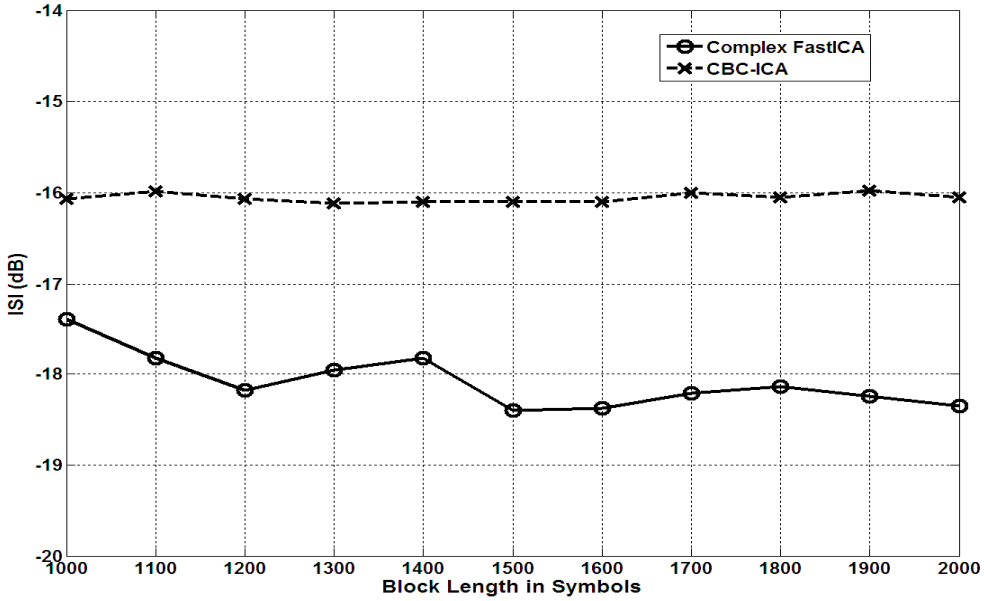

Figure 30: ISI achieved in abruptly flat fading channels

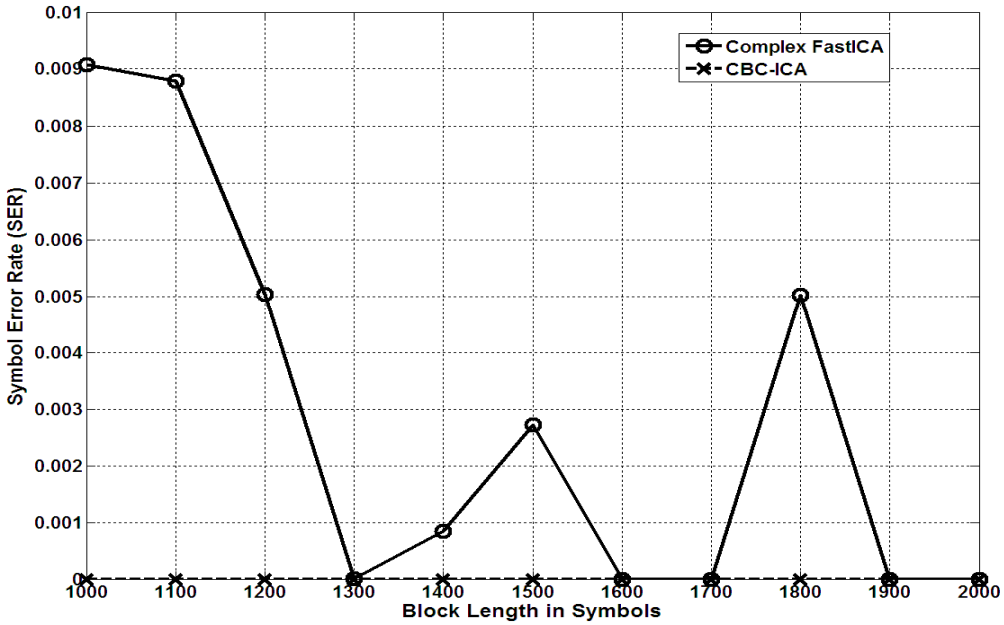

Figure 31: SER achieved in abruptly flat fading channels

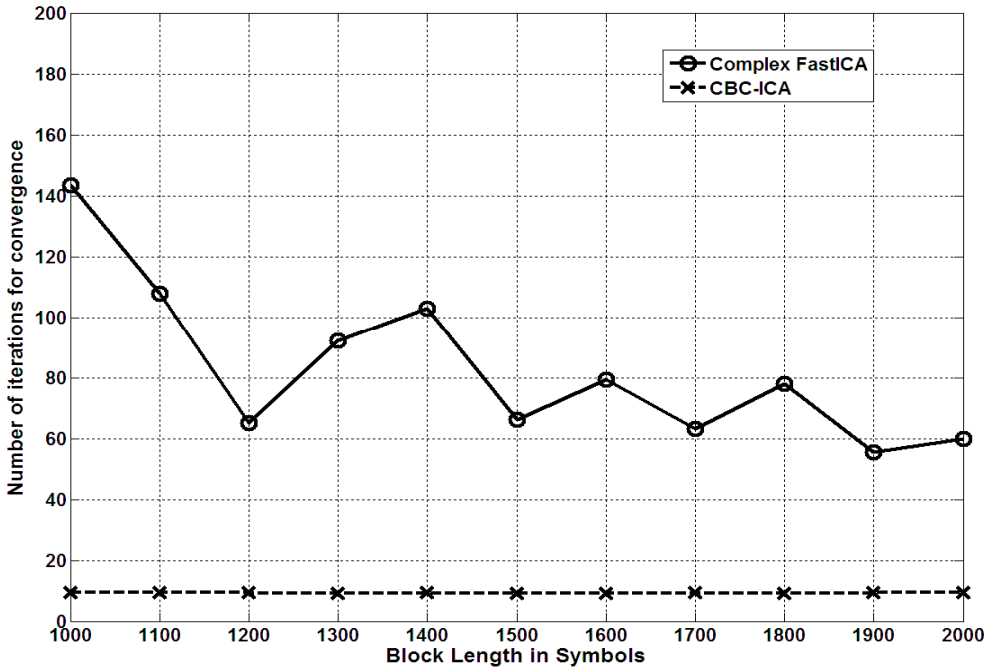

Figure 32: Number of iterations for convergence in abruptly flat fading channels

5.4 Conclusions

In this chapter, a novel Complex Adaptive Independent Component Analysis algorithm employing the conjugate gradient optimization technique (CBC-ICA) is presented. The algorithm updates the real and imaginary components of the adaptive system coefficients or complex separating matrix along independently derived conjugated directions. As a result, the CBC-ICA avoids gradient ascent in the same direction more than once, resulting in fast convergence. In addition, the two step sizes for the real and imaginary components of the complex separating matrix are optimally and separately derived to maximize the kurtosis. This provides the CBC-ICA superior convergence properties in dynamic environments, as compared to the Complex FastICA algorithm. Simulation results confirm the performance improvement yielded by the CBC-ICA, in

terms of ISI, SER and convergence speed. Furthermore, as the formulation for the CBC-IC does not require any matrix inversion, it has similar computational complexity as the Complex FastICA.

CHAPTER SIX: COMPLEX LEAST MEAN SQUARE ALGORITHMS EMPLOYING OPTIMAL TIME-VARYING CONVERGENCE FACTORS

The Complex Least Mean Square (Complex LMS) algorithm has been widely used in various adaptive filtering applications, because of its computational and theoretical simplicity [40]. However, the inherent limitation of the Complex LMS is its dependence on the convergence factor or step size, which is fixed and has to be manually selected depending on the type of application or nature of the input signal. Moreover, a small step size results in slow convergence, and a large step size could cause unstable gradient descent, leading to divergence. Hence, the optimal convergence factor has to be chosen by trial and error. In this chapter, the formulations for novel complex adaptive algorithms are presented that automatically derive optimal convergence factors for the real and imaginary components of the complex adaptive filter coefficients. In addition, the proposed methods independently update the real and imaginary parts of the adaptive filter coefficients at each iteration. The algorithms are called Complex Optimum Block Adaptive LMS (Complex OBA-LMS) and Complex Optimum Block Adaptive LMS with Individual Adaptation (Complex OBAI-LMS), and their sequential versions are called Complex LMS with Homogeneous Adaptation (Complex HA-LMS), and Complex LMS with Individual Adaptation (Complex IA-LMS), respectively. In the Complex OBA-LMS and Complex HA-LMS, two optimal convergence factors are separately derived at each iteration, one for the real components, and one for the imaginary components of the complex adaptive filter coefficients. On the other hand, the Complex OBAI-LMS and Complex IA-LMS derive a unique convergence factor for each component of each

complex adaptive filter weight. As a result, the Complex OBAI-LMS and Complex IA-LMS are most efficient in utilizing all the degrees of freedom of the adaptive filter. The formulations of the proposed algorithms are presented in the following sections.

6.1 Block implementation of the Complex LMS: Formulation

The following parameters are defined:

k : block iteration index

N: Length of the adaptive filter

L : Processing Block length

j : complex operator i.e. $\sqrt{-1}$

$e_l(k)$: l th complex error signal in the k th block

$W_i(k)$: the i th adaptive filter coefficient in the k th block

In the block implementation of the Complex LMS, the real and imaginary components of the complex weight vector W, namely W_R and W_I respectively, are updated by the following equations:

$$W_R(k+1) = W_R(k) - \mu_B \nabla_{BR}(k) \tag{6.1}$$

$$W_I(k+1) = W_I(k) - \mu_B \nabla_{BI}(k) \tag{6.2}$$

Where,

$$\nabla_{BR}(k) = \frac{1}{L} \frac{\partial\{\underline{e}^H(k)\underline{e}(k)\}}{\partial\{W_R(k)\}} \tag{6.3}$$

$$\nabla_{BI}(k) = \frac{1}{L} \frac{\partial\{\underline{e}^H(k)\underline{e}(k)\}}{\partial\{W_I(k)\}} \tag{6.4}$$

$$\underline{e}(k) = [e_1(k).....e_L(k)] \tag{6.5}$$

μ_B is the fixed convergence factor and H denotes the conjugate transpose or Hermitian transpose.

Evaluating (6.3) and (6.4) we obtain,

$$\nabla_{BR}(k) = \frac{1}{L}[-X_k{}^T \underline{e}^*(k) - X_k{}^H \underline{e}(k)] \tag{6.6}$$

$$\nabla_{BI}(k) = \frac{1}{L}[-jX_k{}^T \underline{e}^*(k) + jX_k{}^H \underline{e}(k)] \tag{6.7}$$

where, X_k is the $L\ X\ N$ matrix of input signal samples given as:

$$X_k = \begin{bmatrix} x_{11}(k).....x_{1N}(k) \\ . \\ . \\ x_{L1}(k).....x_{LN}(k) \end{bmatrix} \tag{6.8}$$

T and * represent transpose and complex conjugate respectively.

Since the complex weight vector is $W(k+1) = W_R(k+1) + jW_I(k+1)$, the Complex LMS weight update equation is given as:

$$W(k+1) = W(k) + 2\frac{\mu_B}{L} X_k^H \underline{e}(k) \tag{6.9}$$

6.2 Proposed Complex OBA-LMS: Formulation

As mentioned previously, the Complex OBA-LMS generates two time-varying convergence factors at each block iteration, for the real and imaginary components of the complex adaptive filter coefficients, in contrast to the constant μ_B of the Complex LMS [44, 45]. Let these time-varying convergence factors for the real and imaginary components be denoted as $\mu_{BR}(k)$ and $\mu_{BI}(k)$, respectively. Incorporating these convergence factors in the weight update equations (6.1) and (6.2), we get

$$W_R(k+1) = W_R(k) - \mu_{BR}(k)\nabla_{BR}(k) \tag{6.10}$$

$$W_I(k+1) = W_I(k) - \mu_{BI}(k)\nabla_{BI}(k) \tag{6.11}$$

The l th complex error signal $e_l(k+1)$ in the $(k+1)$ th block, can be expressed in terms of the l th complex error signal $e_l(k)$ in the k th block, and the present adaptive filter coefficients $W_R(k)$ and $W_I(k)$ by applying the Taylor's series as follows:

$$e_l(k+1) = e_l(k) + \sum_{i=1}^{N} \frac{\partial e_l(k)}{\partial w_{iR}(k)} \Delta W_{iR}(k) + \ldots$$

$$l = 1, 2 \ldots . L \tag{6.12}$$

$$e_l(k+1) = e_l(k) + \sum_{i=1}^{N} \frac{\partial e_l(k)}{\partial w_{iI}(k)} \Delta W_{iI}(k) + \ldots$$

$$l = 1, 2 \ldots . L \tag{6.13}$$

Where,

$$\Delta W_{iR}(k) = W_{iR}(k+1) - W_{iR}(k) \tag{6.14}$$

$$\Delta W_{iI}(k) = W_{iI}(k+1) - W_{iI}(k) \tag{6.15}$$

Due to linearity of the error function, higher order derivatives in the Taylor series expansion are ignored. Expanding (6.12) and (6.13) for all the L error signals, we obtain the expressions:

$$\underline{e}(k+1) = \underline{e}(k) - X_k \Delta W_R(k) \tag{6.16}$$

$$\underline{e}(k+1) = \underline{e}(k) - jX_k \Delta W_I(k) \tag{6.17}$$

From (6.10) and (6.11) we have,

$$\Delta W_R(k) = -\mu_{BR}(k)\nabla_{BR}(k) \tag{6.18}$$

$$\Delta W_I(k) = -\mu_{BI}(k)\nabla_{BI}(k) \tag{6.19}$$

Substituting (6.18) and (6.19) in (6.16) and (6.17), we obtain:

$$\underline{e}(k+1) = \underline{e}(k) + \mu_{BR}(k) X_k \nabla_{BR}(k) \tag{6.20}$$

$$\underline{e}(k+1) = \underline{e}(k) + j\mu_{BI}(k) X_k \nabla_{BI}(k) \tag{6.21}$$

The optimal convergence factors $\mu_{BR}(k)$ and $\mu_{BI}(k)$ should minimize the energy in the complex error signal $\underline{e}(k+1)$, i.e. the following conditions should be satisfied.

$$\frac{\partial\{\underline{e}^H(k+1)\underline{e}(k+1)\}}{\partial\mu_{BR}(k)} = 0 \tag{6.22}$$

$$\frac{\partial\{\underline{e}^H(k+1)\underline{e}(k+1)\}}{\partial\mu_{BI}(k)} = 0 \tag{6.23}$$

Evaluating (6.22) and (6.23), we obtain

$$\mu_{BR}(k) = \frac{-\underline{e}(k)^H X_k \nabla_{BR}(k) - \nabla_{BR}{}^H(k) X_k^H \underline{e}(k)}{2 * \nabla_{BR}{}^H(k) X_k{}^H X_k \nabla_{BR}(k)} \tag{6.24}$$

$$\mu_{BI}(k) = \frac{-\underline{e}(k)^H jX_k \nabla_{BI}(k) + \nabla_{BI}{}^H(k) jX_k^H \underline{e}(k)}{2 * \nabla_{BI}{}^H(k) X_k{}^H X_k \nabla_{BI}(k)} \tag{6.25}$$

By substituting (6.24) and (6.25) in (6.10) and (6.11), and applying $W(k+1) = W_R(k+1) + jW_I(k+1)$, the Complex OBA-LMS algorithm is obtained.

A sequential version of the Complex OBA-LMS called the Complex LMS with Homogeneous Adaptation (Complex HA-LMS) is presented in the following section.

6.3 Proposed Complex HA-LMS: Formulation

Since the Complex HA-LMS processes the input in samples, the error signal at the k th iteration, $e(k)$, is given as:

$$e(k) = d(k) - W^H X(k) \tag{6.26}$$

$d(k)$ and $X(k)$ are the desired signal sample and input signal vector, respectively.

In the Complex HA-LMS, the convergence factors $\mu_R(k)$ and $\mu_I(k)$ are optimally derived and updated at every sample iteration, as compared to every block iteration for the Complex OBA-LMS [73]. Hence, the expressions for $\nabla_{BR}(k)$ and $\nabla_{BI}(k)$ in (6.3) and (6.4) are modified as:

$$\nabla_{BR}(k) = \frac{\partial\{e^*(k)e(k)\}}{\partial\{W_R(k)\}} = -X(k)e^*(k) - X^*(k)e(k) \tag{6.27}$$

$$\nabla_{BI}(k) = \frac{\partial\{e^*(k)e(k)\}}{\partial\{W_I(k)\}} = e^*(k)jX(k) - e(k)jX^*(k) \tag{6.28}$$

Similar to (6.12) and (6.13), the Taylor's series expansion for the $(k+1)$ th complex error sample $e(k+1)$, in terms of the k th complex error sample $e(k)$,and the present adaptive filter coefficients $W_R(k)$ and $W_I(k)$ is expressed as:

$$e(k+1) = e(k) + \sum_{i=1}^{L} \frac{\partial e(k)}{\partial w_{iR}(k)} \Delta W_{iR}(k) + \ldots \tag{6.29}$$

$$e(k+1) = e(k) + \sum_{i=1}^{L} \frac{\partial e(k)}{\partial w_{iI}(k)} \Delta W_{iI}(k) + \ldots \tag{6.30}$$

Where,

$$\Delta W_{iR}(k) = W_{iR}(k+1) - W_{iR}(k) \tag{6.31}$$

$$\Delta W_{iI}(k) = W_{iI}(k+1) - W_{iI}(k) \tag{6.32}$$

Evaluating (6.29) and (6.30), and substituting (6.31) and (6.32) in the resulting expression, we obtain the following:

$$e(k+1) = e(k) - X^T(k)\Delta W_R(k) \tag{6.33}$$

$$e(k+1) = e(k) + jX^T(k)\Delta W_I(k) \tag{6.34}$$

Substituting (6.18) and (6.19) in (6.33) and (6.34), we have:

$$e(k+1) = e(k) + X^T(k)\mu_R(k)\nabla_{BR}(k) \tag{6.35}$$

$$e(k+1) = e(k) - jX^T(k)\mu_I(k)\nabla_{BI}(k) \tag{6.36}$$

The novel adaptation approach proposed in this research involves optimizing the error function with respect to μ_R and μ_I , independently, i.e.

$$\frac{\partial\{e^*(k+1)e(k+1)\}}{\partial\mu_R(k)} = 0 \tag{6.37}$$

$$\frac{\partial\{e^*(k+1)e(k+1)\}}{\partial\mu_I(k)} = 0 \tag{6.38}$$

Evaluating (6.37) and (6.38) , we obtain

$$\mu_R(k) = \frac{-e(k)^* X^T(k)\nabla_{BR}(k) - \nabla_{BR}{}^H(k)X^*(k)e(k)}{2*\nabla_{BR}{}^H(k)X(k)X^H(k)\nabla_{BR}(k)} \tag{6.39}$$

$$\mu_I(k) = \frac{-e(k)^* jX^T(k)\nabla_{BI}(k) + \nabla_{BI}{}^H(k)jX^*(k)e(k)}{2*\nabla_{BI}{}^H(k)X(k)X^H(k)\nabla_{BI}(k)} \tag{6.40}$$

In this manner, the Complex HA-LMS is formulated.

6.4 Proposed Complex OBAI-LMS: Formulation

The Complex OBAI-LMS is a block adaptive algorithm that derives a unique convergence factor for each component of each complex adaptive filter coefficient [43, 46]. In addition, the real and imaginary components of the complex filter weights are updated independently. Consequently, for a complex weight vector W of length N , $2N$ convergence factors are optimally derived for the real and imaginary components of W . Hence, the real and imaginary components of the complex weight vector W , namely W_R and W_I respectively, are updated by the following equations:

$$w_R(k+1) = w_R(k) - [MU]_{Rk} \nabla_{BR}(k) \tag{6.41}$$

$$w_I(k+1) = w_I(k) - [MU]_{Ik} \nabla_{BI}(k) \tag{6.42}$$

$[MU]_{Rk}$ and $[MU]_{Ik}$ are diagonal matrices of order N, whose elements are the convergence factors for the real and imaginary components of W, i.e.

$$[MU]_{Rk} = \begin{bmatrix} \mu_{R1}(k) & \dots & 0 \\ \dots & \dots & \dots \\ 0 & \dots & \mu_{RN}(k) \end{bmatrix} \tag{6.43}$$

$$[MU]_{Ik} = \begin{bmatrix} \mu_{I1}(k) & \dots & 0 \\ \dots & \dots & \dots \\ 0 & \dots & \mu_{IN}(k) \end{bmatrix} \tag{6.44}$$

Expanding the L complex error signals in a Taylor series expansion similar to (6.12) and (6.13), we obtain the error expression in a matrix-vector form as :

$$\underline{e}(k+1) = \underline{e}(k) - X_k \Delta W_R(k) \tag{6.45}$$

$$\underline{e}(k+1) = \underline{e}(k) - jX_k \Delta W_I(k) \tag{6.46}$$

From (6.41) and (6.42), we have

$$\Delta W_R(k) = -[MU]_{Rk} \nabla_{BR}(k) \tag{6.47}$$

$$\Delta W_I(k) = -[MU]_{Ik} \nabla_{BI}(k) \tag{6.48}$$

Substituting (6.47) and (6.48) in (6.45) and (6.46), we obtain:

$$\underline{e}(k+1) = \underline{e}(k) + X_k [MU]_{Rk} \nabla_{BR}(k) \tag{6.49}$$

$$\underline{e}(k+1) = \underline{e}(k) + jX_k [MU]_{Ik} \nabla_{BI}(k) \tag{6.50}$$

The $2N$ convergence factors are chosen such that the sum of the squares of the magnitudes of the complex error signals is minimized in the next iteration, i.e.

$$\frac{\partial\{\underline{e}^H(k+1)\underline{e}(k+1)\}}{\partial\mu_{Ri}(k)}=0 \qquad i=1.2,.....,N \quad (6.51)$$

$$\frac{\partial\{\underline{e}^H(k+1)\underline{e}(k+1)\}}{\partial\mu_{Ii}(k)}=0 \qquad i=1.2,.....,N \quad (6.52)$$

For simplicity, we define the following parameters:

$$z_R(k)=\mathrm{Re}\{X_k^H\,\underline{e(k)}\}=[z_{R1}(k)\,z_{R2}(k)\quad .....\quad z_{RN}(k)]^T \quad (6.53)$$

$$z_I(k)=\mathrm{Im}\{X_k^H\,\underline{e(k)}\}=[z_{I1}(k)\,z_{I2}(k)\quad .....\quad z_{IN}(k)]^T \quad (6.54)$$

$$[R]_k=X_k^H X_k=[R_{mn}(k)] \qquad 1\le m,n\le N \quad (6.55)$$

$\underline{e}^H(k+1)\underline{e}(k+1)$ can be rewritten as:

$$\underline{e}^H(k+1)\underline{e}(k+1)=S_1+S_2+S_3+S_4 \quad (6.56)$$

Where,

$$S_1=\underline{e}^H(k)\underline{e}(k) \quad (6.57)$$

$$S_2=\underline{e}^H(k)X_k[MU]_{Rk}\nabla_{BR}(k) \quad (6.58)$$

$$S_3=\nabla_{BR}{}^H(k)[MU]_{Rk}X_k{}^H\underline{e}(k) \quad (6.59)$$

$$S_4=\nabla_{BR}{}^H(k)[MU]_{Rk}[R]_k[MU]_{Rk}\nabla_{BR}(k) \quad (6.60)$$

It is worth mentioning that since the gradient vectors are real, $\nabla_{BR}{}^H(k)=\nabla_{BR}{}^T(k)$.

Expressing equations (6.57) to (6.60) in summation form we obtain:

$$S_1=\sum_{i=1}^{L}e_i^2(k) \quad (6.61)$$

$$S_2=\sum_{i=1}^{N}[e^H(k)X_k]_i\,\mu_{Ri}(k)\nabla_{BRi}(k) \quad (6.62)$$

$$S_3 = \sum_{i=1}^{N} \mu_{Ri}(k) \nabla_{BRi}(k) [X_k{}^H e(k)]_i \tag{6.63}$$

$$S_4 = \sum_{m=1}^{N} [\sum_{n=1}^{N} \mu_{Rn}(k) \nabla_{BRn}(k) R_{mn}(k)] \mu_{Rm}(k) \nabla_{BRm}(k) \tag{6.64}$$

Combining (6.62) and (6.63) yields the following:

$$\begin{aligned} S_2 + S_3 &= \sum_{i=1}^{N} \mu_{Ri}(k) \nabla_{BRi}(k) \{[e^H(k) X_k]_i + [X_k{}^H e(k)]_i\} \\ &= 2 \sum_{i=1}^{N} \mu_{Ri}(k) \nabla_{BRi}(k) \operatorname{Re}\{[X_k{}^H e(k)]_i\} \\ &= 2 \sum_{i=1}^{N} \mu_{Ri}(k) \nabla_{BRi}(k) z_{Ri}(k) \end{aligned} \tag{6.65}$$

Substituting (6.56) in (6.51) gives the following:

$$\frac{\partial S_1}{\partial \mu_{Ri}(k)} + \frac{\partial (S_2 + S_3)}{\partial \mu_{Ri}(k)} + \frac{\partial S_4}{\partial \mu_{Ri}(k)} = 0 \qquad i = 1.2, ..., N \tag{6.66}$$

Substituting (6.61) in (6.65), and (6.64) in (6.66), and using the symmetry of $[R]_k$ given by (6.55), the following result is obtained:

$$[MU]_{Rk} \nabla_{BR}(k) = -[R]_k^{-1} z_R(k) \tag{6.67}$$

In order to compute $[MU]_{Ik}$,a similar procedure is followed in evaluating (6.52). As a result, we obtain the following expression:

$$[MU]_{Ik} \nabla_{BI}(k) = -[R]_k^{-1} z_I(k) \tag{6.68}$$

Substituting (6.67) and (6.68) in (6.41) and (6.42), we obtain the following update equations for the real and imaginary components of *W* as follows:

$$w_R(k+1) = w_R(k) + [R]_k^{-1} z_R(k) \tag{6.69}$$

$$w_I(k+1) = w_I(k) + [R]_k^{-1} z_I(k)) \tag{6.70}$$

In this manner, the Complex OBAI-LMS algorithm is obtained.

6.5 Computational Complexity of the Complex OBAI-LMS algorithm

From (6.69) and (6.70), it can be seen that the weight update equations for the Complex OBAI-LMS algorithm requires matrix inversion. This is a computationally intensive operation, especially for high-order adaptive systems. The matrix inversion operation can be eliminated by processing the signals in overlapping blocks as opposed to disjoint blocks. This means that in a data block of length L, the K oldest signals are replaced with new ones with $(L-K)$ signals overlapping between the previous and present blocks. In this manner, only the most recent information is retained as the adaptive filter moves to a new block. Furthermore, incorporating the block shifting technique results in a recursive relation between the correlation matrices $[R]_k$ and $[R]_{k-1}$ in the present and previous blocks, respectively. This in turn, allows the application of a matrix inversion lemma for recursively computing $[R]_k^{-1}$ which leads to a considerable saving in computations. The detailed description of the matrix inversion lemma is given in the Appendix.

Using the matrix inversion lemma, the Complex OBAI-LMS requires only one matrix inversion at $k=1$, with the subsequent inverses computed recursively. The first inversion can be further eliminated by replacing the correlation matrix in the first iteration, $[R]_1$ with a matrix containing only its diagonal elements. In this manner, the computational complexity significantly reduces from $O(N^3)$ to $O(N)$.

Hence, the Complex OBAI-LMS can be implemented in two ways. In the first method called Complex OBAI(1), the inverse of $[R]_k$ is computed directly in the first iteration, and the lemma is applied for $k > 1$. In Complex OBAI (2), at the first iteration, $[R]_k$ is estimated with a matrix containing its diagonal elements, and the lemma is applied in subsequent iterations. Thus, only in the first iteration, the Complex OBAI(1) requires more computations than Complex OBAI(2). However, it converges much faster than the Complex OBAI(2), as will be shown subsequently in Chapter 7.

6.6 Proposed Complex IA-LMS: Formulation

The Complex IA-LMS is the sequential version of the Complex OBAI-LMS. Hence, (6.49) and (6.50) are reduced to sample form:

$$e(k+1) = e(k) + X^T(k)[MU]_{Rk}\nabla_R(k) \tag{6.71}$$

$$e(k+1) = e(k) - jX^T(k)[MU]_{Ik}\nabla_I(k) \tag{6.72}$$

Similar to Complex OBAI, the $2N$ convergence factors are optimally derived such that the square of the magnitude of the error sample is minimized in the subsequent iteration, i.e.

$$\frac{\partial\{e^*(k+1)e(k+1)\}}{\partial\mu_{Ri}(k)} = 0 \qquad i = 1.2,....., N \tag{6.73}$$

$$\frac{\partial\{e^*(k+1)e(k+1)\}}{\partial\mu_{Ii}(k)} = 0 \qquad i = 1.2,....., N \tag{6.74}$$

From (6.71), the expression $e^*(k+1)e(k+1)$ can be written in summation form as follows:

$$e^*(k+1)e(k+1) = 2*[\sum_{i=1}^{N} \mu_{Ri}(k)\nabla_{Ri}(k)\,\mathrm{Re}\{x_i^*(k)e(k)\}] + (\sum_{n=1}^{N} |x_i(k)|\mu_{Ri}(k)\nabla_{Ri}(k))^2 \tag{6.75}$$

Applying (6.73) for all i, we obtain the following equation in matrix form:

$$\begin{bmatrix} \mathrm{Re}\{x_1^*(k)e(k)\} \\ \cdot \\ \cdot \\ \cdot \\ \cdot \\ \mathrm{Re}\{x_N^*(k)e(k)\} \end{bmatrix}^T = \begin{bmatrix} |x_1(k)|[\mathrm{Re}\{x_1^*(k)e(k)\}] \\ \cdot \\ \cdot \\ \cdot \\ \cdot \\ |x_N(k)|[\mathrm{Re}\{x_N^*(k)e(k)\}] \end{bmatrix}^T \begin{bmatrix} \mu_{R1} \\ \cdot \\ \cdot \\ \cdot \\ \cdot \\ \mu_{RN} \end{bmatrix} \begin{bmatrix} |x_1(k)| \\ \cdot \\ \cdot \\ \cdot \\ \cdot \\ |x_N(k)| \end{bmatrix}^T \tag{6.76}$$

Defining the following parameters:

$$Y_{Rk} = \begin{bmatrix} \mathrm{Re}\{x_1^*(k)e(k)\} \\ \cdot \\ \cdot \\ \cdot \\ \cdot \\ \mathrm{Re}\{x_N^*(k)e(k)\} \end{bmatrix}^T, \; Z_{Rk} = \begin{bmatrix} |x_1(k)|[\mathrm{Re}\{x_1^*(k)e(k)\}] \\ \cdot \\ \cdot \\ \cdot \\ \cdot \\ |x_N(k)|[\mathrm{Re}\{x_N^*(k)e(k)\}] \end{bmatrix}^T \text{ and } S_k = \begin{bmatrix} |x_1(k)| \\ \cdot \\ \cdot \\ \cdot \\ \cdot \\ |x_N(k)| \end{bmatrix}^T$$

(6.76) becomes:

$$Y_{Rk} = Z_{Rk} \begin{bmatrix} \mu_{R1} \\ \cdot \\ \cdot \\ \cdot \\ \cdot \\ \mu_{RN} \end{bmatrix} S_k \tag{6.77}$$

In this manner, the individual convergence factors for the updating the real component of the weight vector are obtained as:

$$\begin{bmatrix} \mu_{R1} \\ . \\ . \\ . \\ . \\ \mu_{RN} \end{bmatrix} = Z_{Rk}^{\#} Y_{Rk} S_k^{\#} \tag{6.78}$$

Where, $Z_{Rk}^{\#}$ and $S_k^{\#}$ denote the pseudo-inverses of Z_{Rk} and S_k, respectively.

Following a similar approach with (6.72), the convergence factors for the imaginary component of the weight vector are derived as:

$$\begin{bmatrix} \mu_{I1} \\ . \\ . \\ . \\ . \\ \mu_{IN} \end{bmatrix} = Z_{Ik}^{\#} Y_{Ik} S_k^{\#} \tag{6.79}$$

Where,

$$Y_{Ik} = \begin{bmatrix} \mathrm{Im}\{x_1^*(k)e(k) \\ . \\ . \\ . \\ . \\ \mathrm{Im}\{x_N^*(k)e(k) \end{bmatrix}^T \tag{6.80}$$

$$Z_{Ik} = \begin{bmatrix} -|x_1(k)|[\mathrm{Im}\{x_1^*(k)e(k)] \\ . \\ . \\ . \\ . \\ -|x_N(k)|[\mathrm{Im}\{x_N^*(k)e(k)] \end{bmatrix}^T \tag{6.81}$$

Incorporating these convergence factors in the weight update equations, the Complex IA-LMS algorithm is obtained.

6.7 Conclusions

In this chapter, novel complex block adaptive algorithms employing optimally derived convergence factors, Complex OBA-LMS and Complex OBAI-LMS and their respective sequential versions, Complex HA-LMS and Complex IA-LMS, were presented. Similar to the Complex LMS, these algorithms are based on the LMS approach to find the minimum of the complex error function. However, the time-varying convergence factors are automatically derived at each iteration, in contrast to the constant manually chosen convergence factor of the Complex LMS. In this regard, the Complex OBA-LMS and Complex HA-LMS derive a separate convergence factor, updated at every block and sample iteration respectively, for the real and imaginary components of the complex adaptive filter coefficients. The Complex OBAI-LMS and Complex IA-LMS derive a unique convergence factor for each component of each adaptive filter coefficient, at every block and sample iteration, respectively. As a result, they are most effective in utilizing the degrees of freedom of the adaptive system. In addition, the inverse of the matrices in the Complex OBAI-LMS weight update equations were recursively computed using a matrix inversion lemma. The details of the lemma are presented in the Appendix. In this manner, the computational complexity of the Complex OBAI-LMS is significantly reduced. The application of the lemma lends itself to two versions of the Complex OBAI-LMS, namely, Complex OBAI(1) and Complex OBAI(2). In Complex OBAI(1), the inverse of the autocorrelation matrix $[R]_k$ is computed directly in the first iteration, and the lemma is applied in subsequent iterations. The Complex OBAI(2) approximates $[R]_k$ in the first iteration with a matrix containing only its diagonal elements, and the lemma is applied in the following iterations. Hence,

the computational complexity of the Complex OBAI(2) reduces to $O(N)$ in the first iteration. In subsequent iterations, the Complex OBAI(2) has the same computational complexity as the Complex OBAI(1). In the following chapters, the performance of the presented algorithms will be compared to the Complex LMS algorithm through extensive simulations, in channel estimation and adaptive beamforming applications.

CHAPTER SEVEN: APPLICATION OF PROPOSED COMPLEX OBA-LMS AND COMPLEX OBAI-LMS ALGORITHMS TO CHANNEL ESTIMATION

The Complex LMS algorithm has been widely used both in block and sequential mode for various adaptive filtering applications, e.g. in the wireless communications, biomedical fields, due to its computational simplicity and relative ease of implementation. However, the main drawback of the Complex LMS algorithm is its slow convergence. In addition, the performance is highly dependent on the choice of the convergence factor or learning rate which is constant and has to be manually selected by trial and error depending on the type of application. Furthermore, an incorrect choice of convergence factor could even result in divergence. In the previous chapter, block and sequential algorithms employing time-varying and optimally derived convergence factors were presented. In this chapter, the proposed optimum block algorithms, namely Complex OBA-LMS and Complex OBAI-LMS are applied to system identification for wireless communication applications. Through extensive simulation results, their performance is compared to the block Complex LMS algorithm. The convergence speed and accuracy are used as a measure of performance. Simulation results confirm the significant improvement in convergence properties yielded by the proposed techniques over the block Complex LMS. In addition, it is shown that this improvement is achieved without having to manually select a convergence factor for different inputs.

7.1 System identification of a complex Finite Impulse Response (FIR) filter

System identification and modeling is a very essential application in the wireless communications, control systems, and signal processing fields. In this regard, an adaptive

filter can be used for modeling or duplicating the response or behavior of an unknown system. To perform system identification, the same input is applied to both the adaptive filter and the unknown system. The adaptive filter adjusts its coefficients till a suitable least squares fit to the response of the unknown system is achieved [15]. The accuracy of this fit depends on the flexibility or the "degrees of freedom" of the adaptive system and also on the statistical and spectral properties of the input signal.

In wireless communications, convolution of the transmitted signal with the channel induces undesirable effects in the received signal such as frequency selective fading and dispersion. As a result, channel estimation form an integral part of any wireless receiver design. Estimation of the wireless channel involves obtaining an approximation of the impulse response of the channel which is modeled as an FIR filter. Typically, this is done by transmitting a known training sequence through the channel and observing the corresponding channel output at the receiver. Employing the same training sequence, the adaptive filter adjusts itself to minimize the mean square error, the error being the difference between the channel output or desired response and the adaptive filter output. For proper estimation and convergence, it is imperative that there is no frequency offset between the transmitter and receiver clocks.

7.2 Simulation Results

In the simulations, the convergence properties of the Complex OBA-LMS and Complex OBAI-LMS are compared to the block Complex LMS in channel estimation. In this regard, the two algorithms are applied to the adaptive system shown in Fig. 33, to determine the parameters of the unknown channel modeled as a complex FIR filter F (z). Normalized Error Energy (NEE) is used as a measure of performance and is defined as:

$$\text{NEE} = \int_{\omega=0}^{\omega=\pi} \left|F(e^{j\omega}) - T(e^{j\omega})\right|^2 d\omega \Big/ \int_{\omega=0}^{\omega=\pi} \left|F(e^{j\omega})\right|^2 d\omega \qquad (7.1)$$

Where, $F(e^{j\omega})$ and $T(e^{j\omega})$ are the transfer functions of the unknown complex FIR filter and the adaptive filter, respectively.

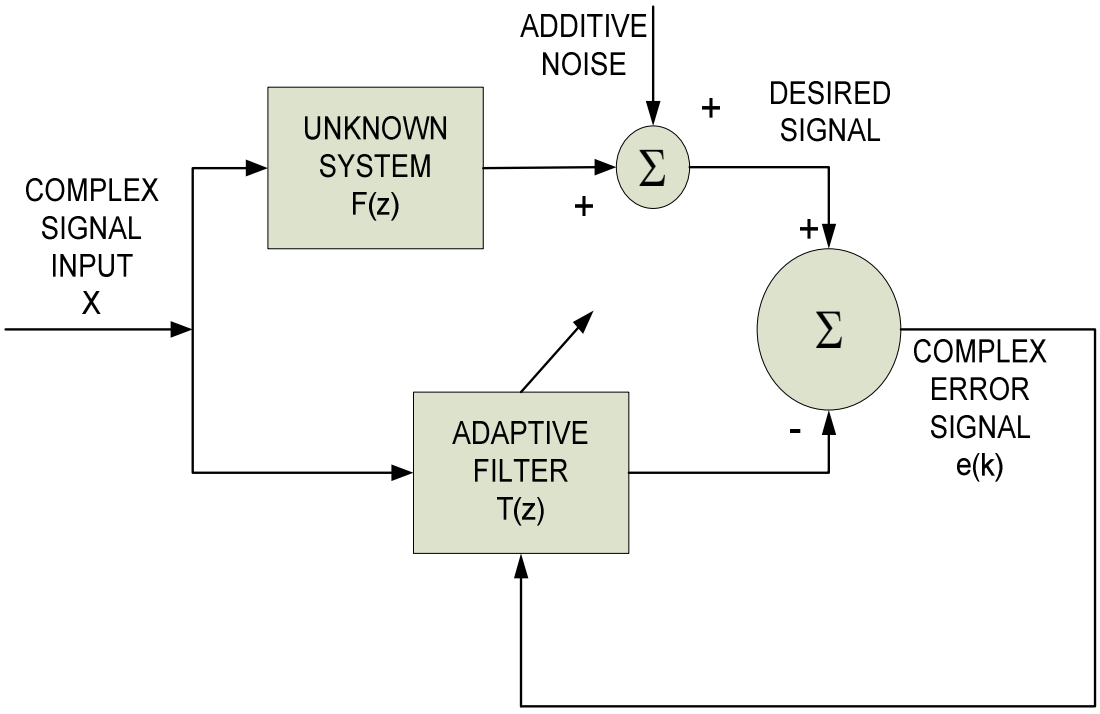

Figure 33: Signal Model for estimating an unknown complex FIR filter

The unknown complex FIR filters $F_1(z)$ and $F_2(z)$ used in the simulations are 9th order and 19th order, respectively and are given as follows:

$$F_1(z) = (.0883+.234j)+(.3895+.1123j)\,z^{-1}+(.4823+.6574)\,z^{-2}+(-.3132-.1645j)\,z^{-3}$$
$$+(.6007+.3245j)\,z^{-4}+(.2538+0.4356j)\,z^{-5}+(-.5267+.2156j)\,z^{-6}+$$
$$(-.0552+.0123j)\;z^{-7}+(.5530+.5612j)\;z^{-8}+(-.4720-.1209j)\;z^{-9} \qquad (7.2)$$

$$F_2(z) = (0.976+.145j)+(0.5873+.1123j)\,z^{-1}+(0.3360+.6574j)\,z^{-2}+(.6563+.8965j)\,z^{-3}+$$

$(.1231+.4352j)\,z^{-4}+(\ .1883+.3895j)\,z^{-5}+(.4823-.3132j)\,z^{-6}+(\ .6007+.2538j)\,z^{-7}+$

$(-.5267-.0552j)\ z^{-8}+(\ .5530-.4720j)\ z^{-9}+(.5162-.4668j)\ z^{-10}+(.5089+.3455j)\ z^{-11}+$

$(.3560+.3428j)\ z^{-12}+(-.6737+.0781j)\ z^{-13}+(.8235-.2836j)\ z^{-14}+(-.5267+.2156j)\ z^{-15}+$

$(.3428+.376j)\ z^{-16}+(-.2836-.187j)\ z^{-17}+(-.3132-.1645j)\ z^{-18}+(-.0552+.0123j)\ z^{-19}$ (7.3)

All the simulations are averaged over 100 Monte Carlo simulation runs, with the initial weights of the adaptive filter set to zero. In the first set of simulations, the performance of the proposed Complex OBA-LMS is compared to the block Complex LMS. In the second set of simulations, the developed Complex OBAI-LMS technique is applied to channel estimation.

7.2.1 Comparison of the proposed Complex OBA-LMS and Block Complex LMS

In this scenario, the Complex OBA-LMS and Block Complex LMS are applied to estimate $F_1(z)$ and $F_2(z)$ for both the noise free case and noisy cases. In the noisy case, AWGN is added to simulate an SNR of 30 dB. Furthermore, the performance is tested for white gaussian noise input, colored noise or band-limited noise, and a Pseudo Random (PN) sequence input signals. The colored noise is generated by passing complex gaussian noise through a band pass filter $F_{BP}(z)$ given by the following specifications:

$$F_{BP}(z)=1-0.4375\,z^{-2}+0.3281\,z^{-4}+0.0244\,z^{-6} \qquad (7.4)$$

In the estimation of $F_1(z)$, the adaptive filter length N and the block length L are chosen to be 15 and 30, respectively. With white gaussian noise input processed in overlapping blocks, the NEE (dB) achieved by both the algorithms vs. the number of samples for the noise free case is illustrated in Fig. 34. The corresponding simulation results with 30 dB SNR is shown in Fig. 35. In the second case, the simulations are

performed with colored noise input. For the noise free and 30 dB SNR cases, the NEE (dB) vs. the number of samples are plotted in Figs. 36 and 37, respectively. In Figs.38 and 39, simulation results are shown when the PN training sequence uniformly distributed in [0, 1] is employed as training input.

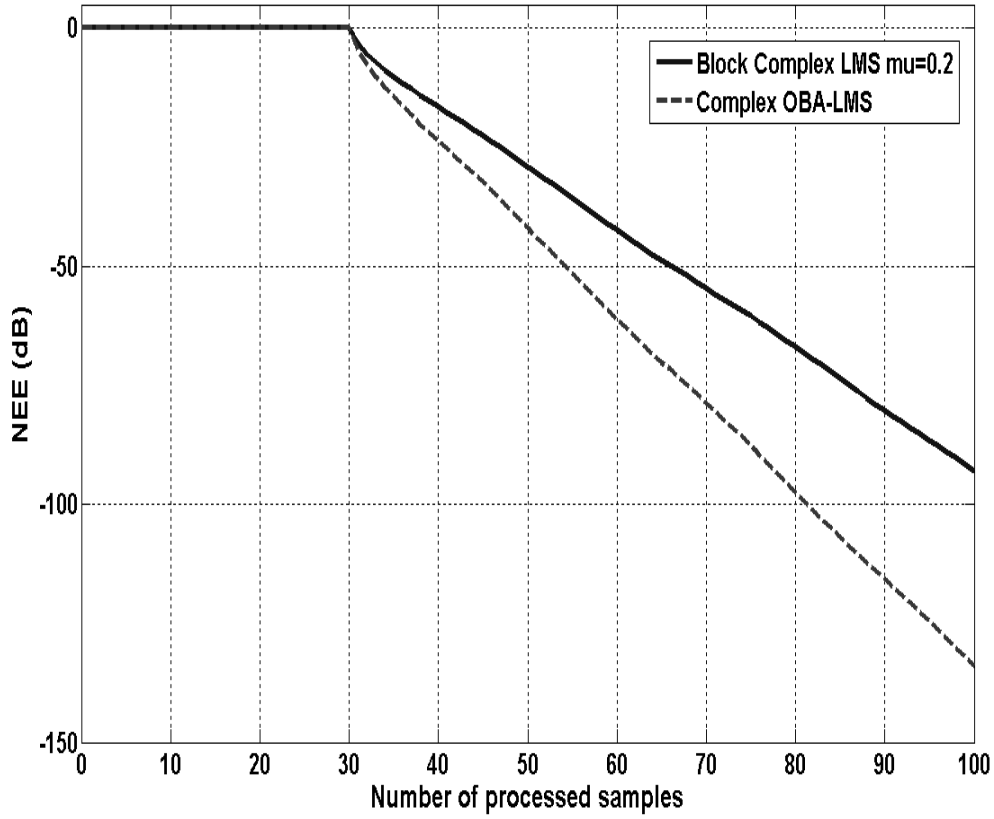

Figure 34: NEE (dB) vs. the number of samples in the estimation of $F_1(z)$ using Complex OBA-LMS with complex gaussian noise input and zero additive noise

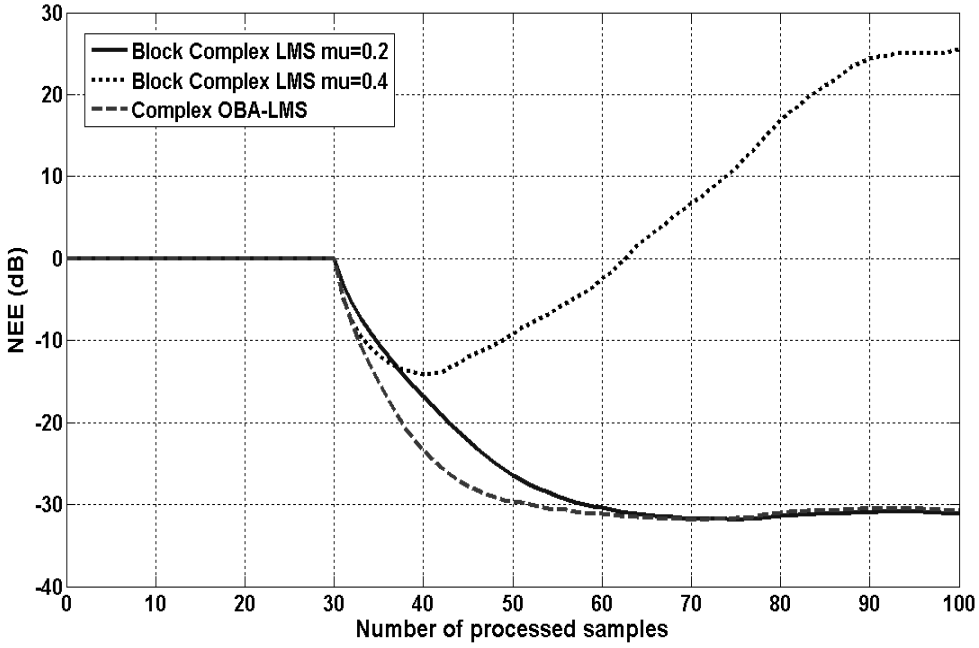

Figure 35: NEE (dB) vs. number of samples in the estimation of $F_1(z)$ using Complex OBA-LMS with complex gaussian noise input and 30 dB SNR

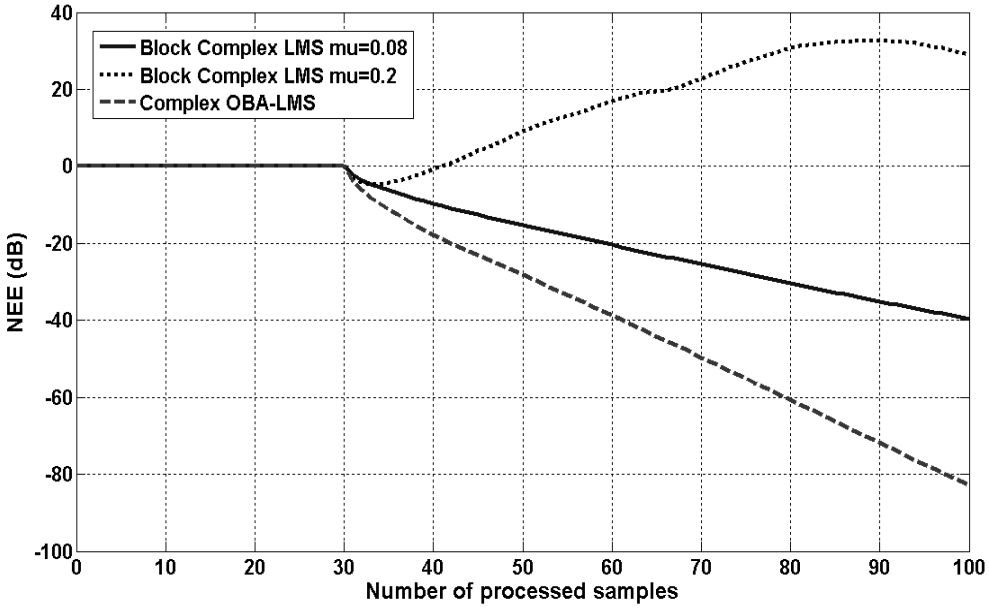

Figure 36: NEE (dB) vs. number of samples in the estimation of $F_1(z)$ using Complex OBA-LMS with colored noise input and zero additive noise

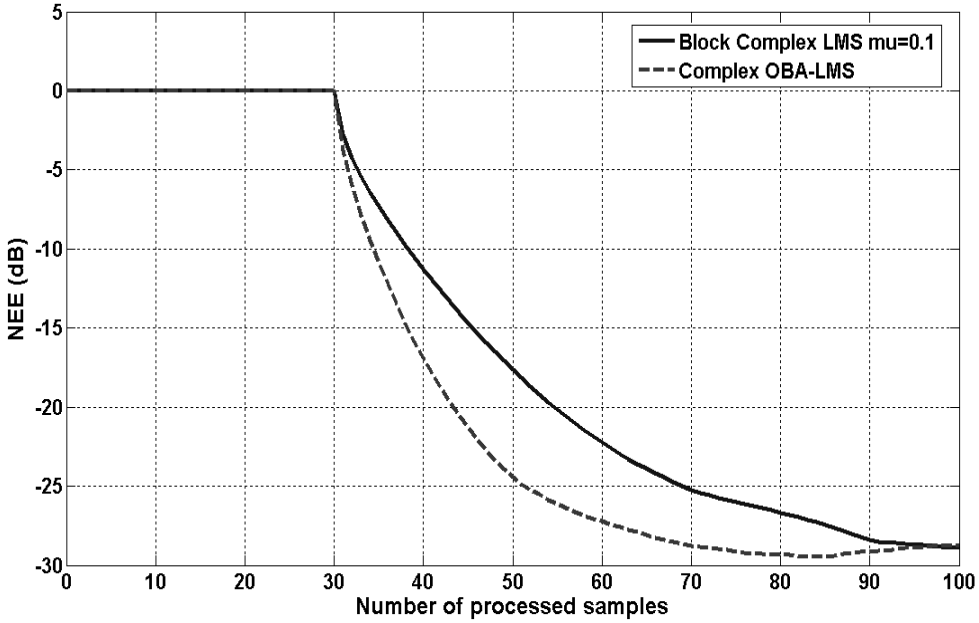

Figure 37: NEE (dB) vs. number of samples in the estimation of $F_1(z)$ using Complex OBA-LMS with colored noise input and 30 dB SNR

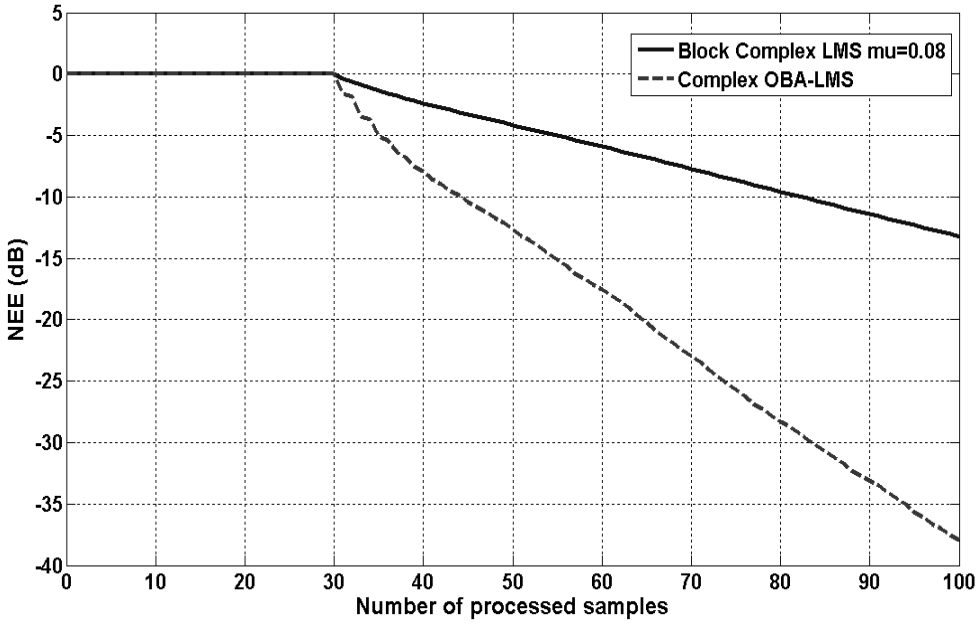

Figure 38: NEE (dB) vs. number of samples in the estimation of $F_1(z)$ using Complex OBA-LMS with PN sequence input and zero additive noise

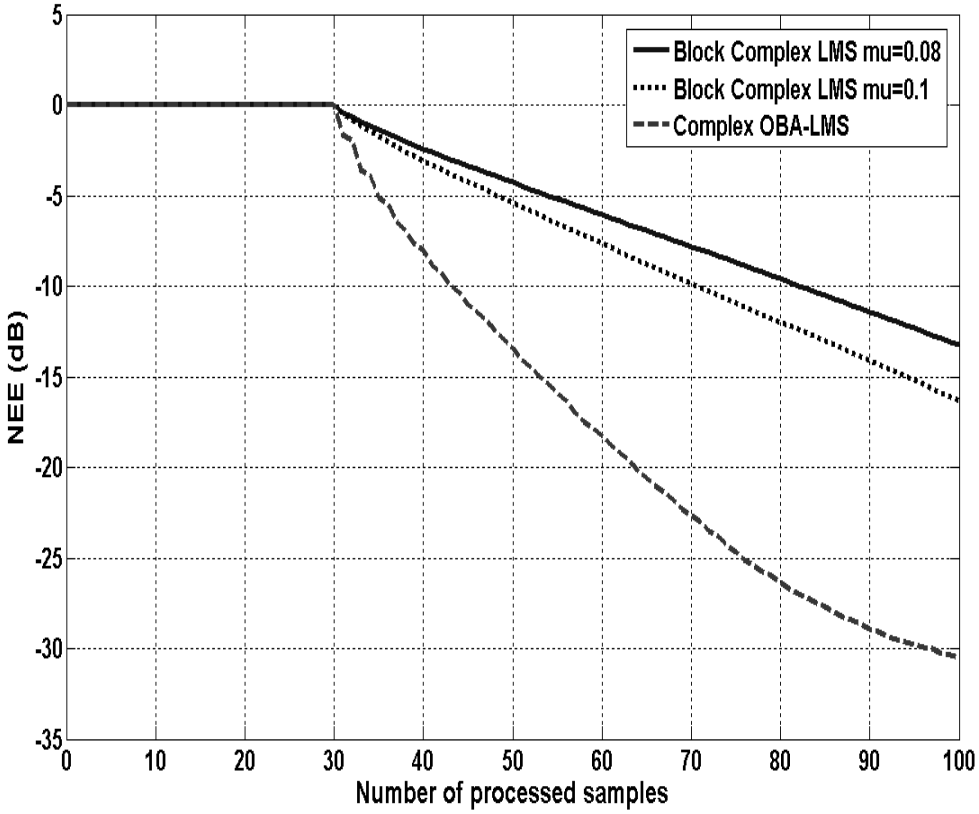

Figure 39: NEE (dB) vs. number of samples in the estimation of $F_1(z)$ using Complex OBA-LMS with PN sequence input and 30 dB SNR

The algorithms are then tested in the estimation of a 19th order complex FIR filter $F_2(z)$. In this regard, the values of N and L are chosen to be 25 and 50, respectively. The simulation results for complex gaussian noise, colored noise and PN sequence inputs in the presence of AWGN are presented in Figs. 40-42.

When data is processed in disjoint blocks, the performance yielded by the Complex OBA-LMS and block Complex LMS algorithms in the estimation of $F_2(z)$ using a PN sequence input is illustrated in Fig 43.

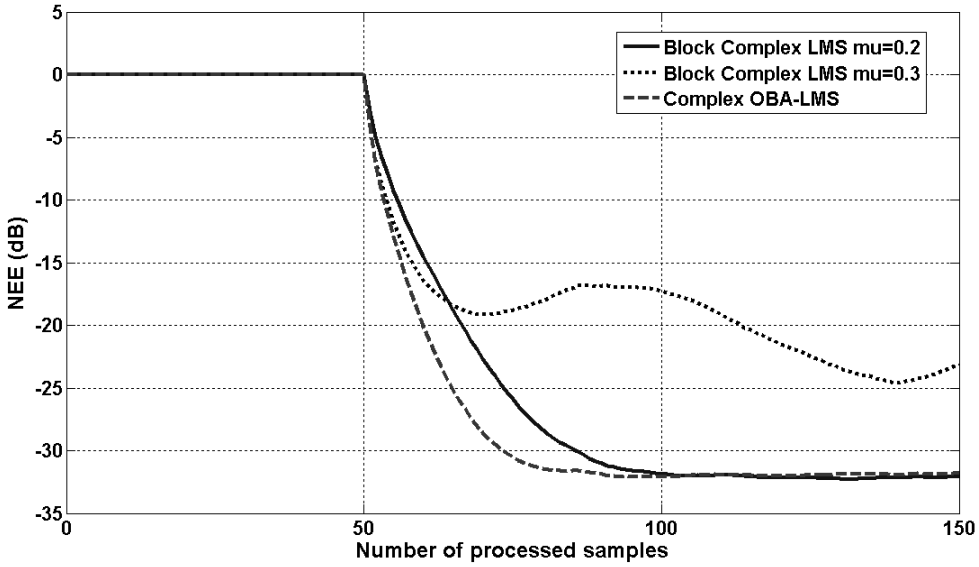

Figure 40: NEE (dB) vs. number of samples in the estimation of $F_2(z)$ using Complex OBA-LMS with complex gaussian noise input and 30 dB SNR

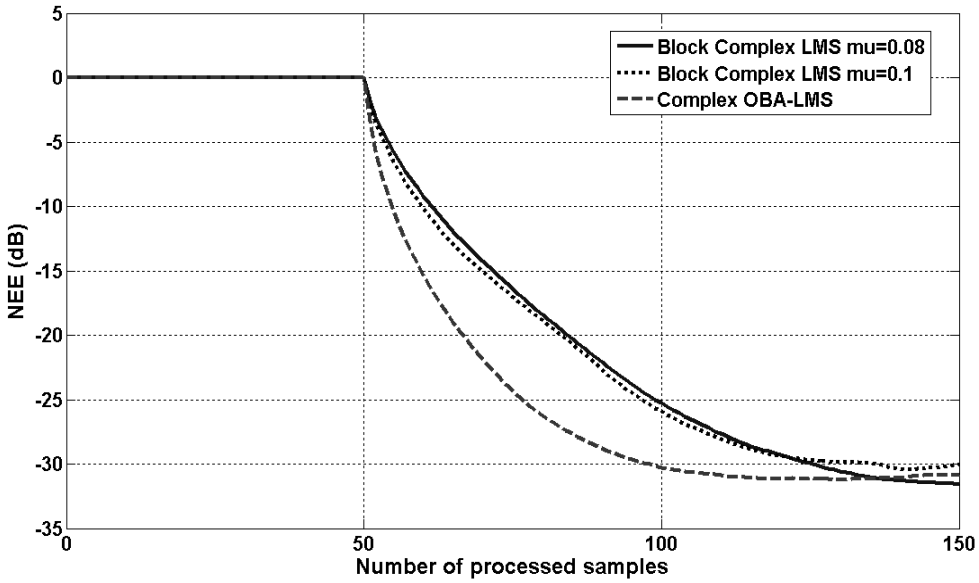

Figure 41: NEE (dB) vs. number of samples in the estimation of $F_2(z)$ using Complex OBA-LMS with colored noise input and 30 dB SNR

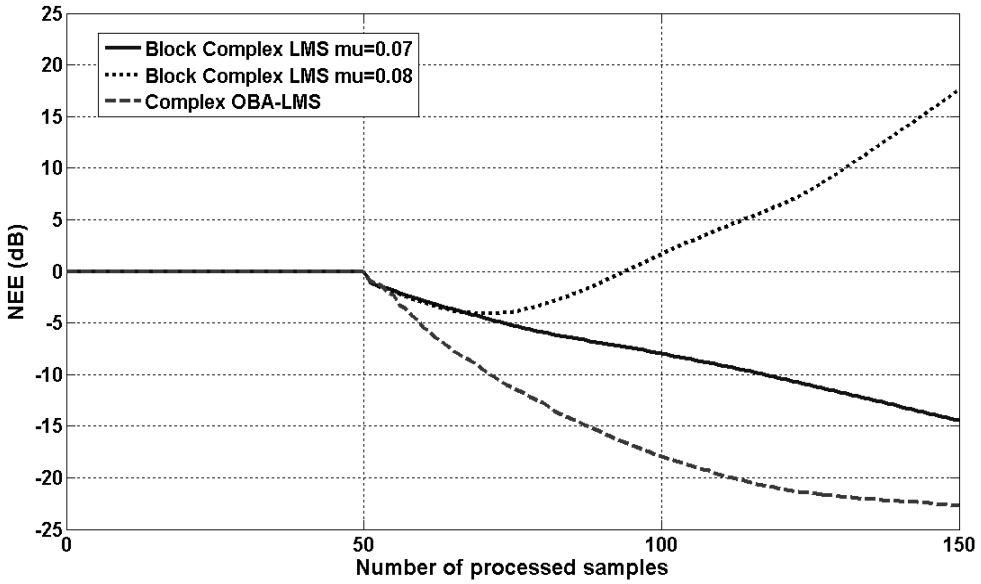

Figure 42: NEE (dB) vs. number of samples in the estimation of $F_2(z)$ using Complex OBA-LMS with PN sequence input and 30 dB SNR

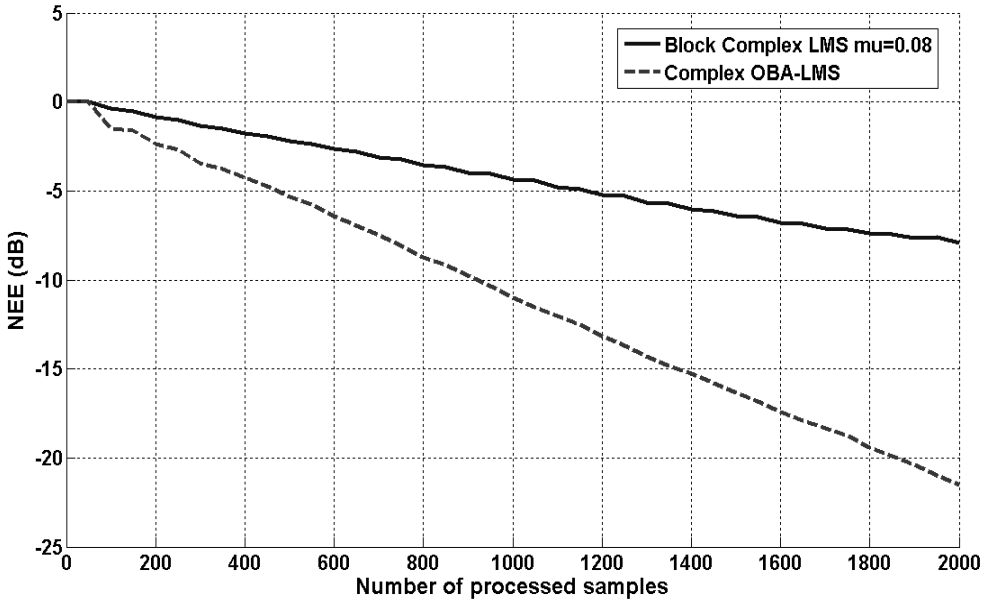

Figure 43: NEE (dB) vs. number of samples in the estimation of $F_2(z)$ using Complex OBA-LMS with PN sequence input processed in disjoint blocks and 30 dB SNR

7.2.2 Comparison of the proposed Complex OBAI-LMS and Block Complex LMS

In this section, the proposed Complex OBAI-LMS is compared to the block Complex LMS. As mentioned previously, the Complex OBAI-LMS can be operated in two modes, Complex OBAI(1) and Complex OBAI (2), depending on whether direct matrix inversion is applied in the first iteration or not. However, both the modes apply the matrix inversion lemma in subsequent iterations to reduce computational complexity. As the matrix inversion lemma is a recursive algorithm, the input signal is always processed in overlapping blocks.

In the simulations, the performance of the Complex OBAI (1) and Complex OBAI (2) algorithms is tested in the estimation of $F_2(z)$. For the Complex OBAI (1), N and L are set as 25 and 50, respectively. Similar to the simulation setup in 7.2.1, the performance is compared for different training inputs in 30 dB SNR. The NEE (dB) achieved by the Complex OBAI (1) vs. the number of processed samples for complex gaussian noise, colored noise, and PN sequence inputs, is illustrated in Figs. 44, 45, and 46, respectively.

With regard to the Complex OBAI (2), L is set as 3*N, i.e. 75. The NEE (dB) achieved by Complex OBAI (2) for complex gaussian noise and colored noise inputs is illustrated in Figs. 47, and 48, respectively.

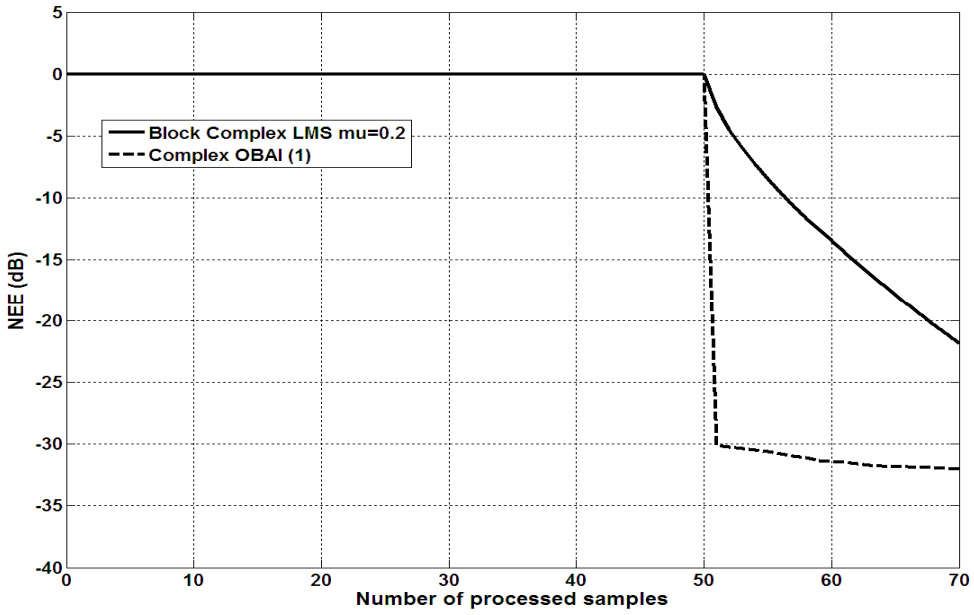

Figure 44: NEE (dB) vs. number of samples in the estimation of $F_2(z)$ using Complex OBAI (1) with complex gaussian noise input and 30 dB SNR

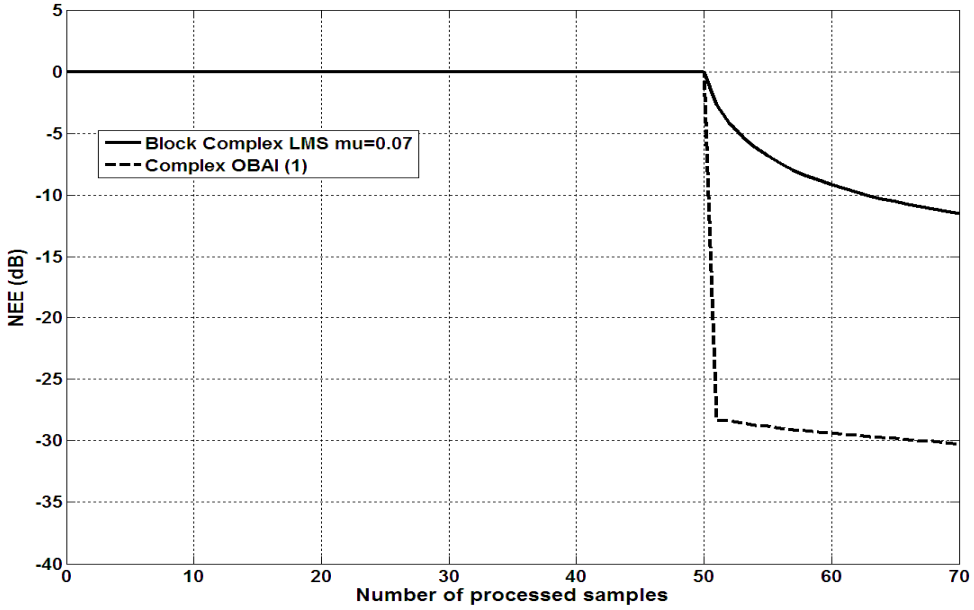

Figure 45: NEE (dB) vs. number of samples in the estimation of $F_2(z)$ using Complex OBAI (1) with colored noise input and 30 dB SNR

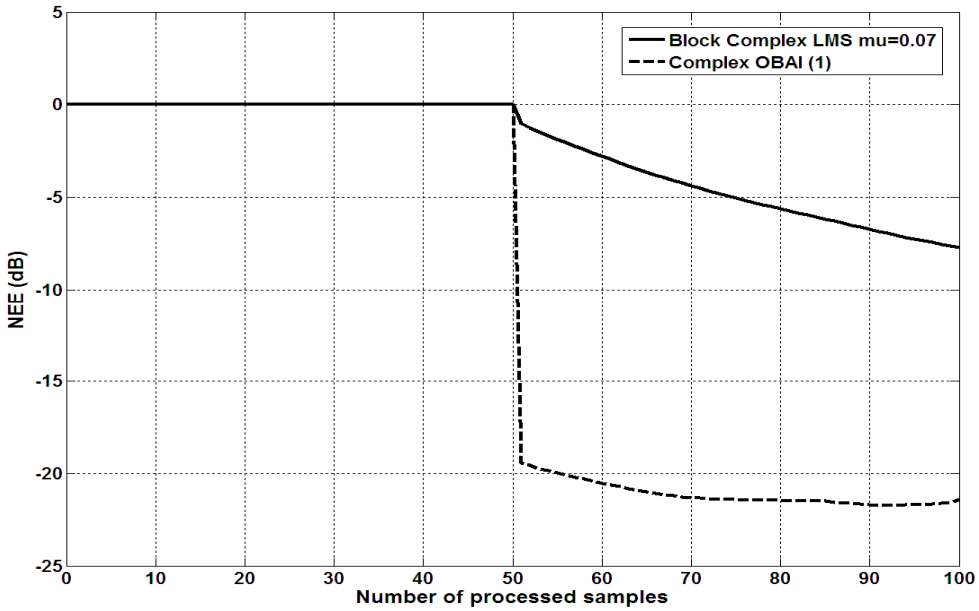

Figure 46: NEE (dB) vs. number of samples in the estimation of $F_2(z)$ using Complex OBAI (1) with PN sequence input and 30 dB SNR

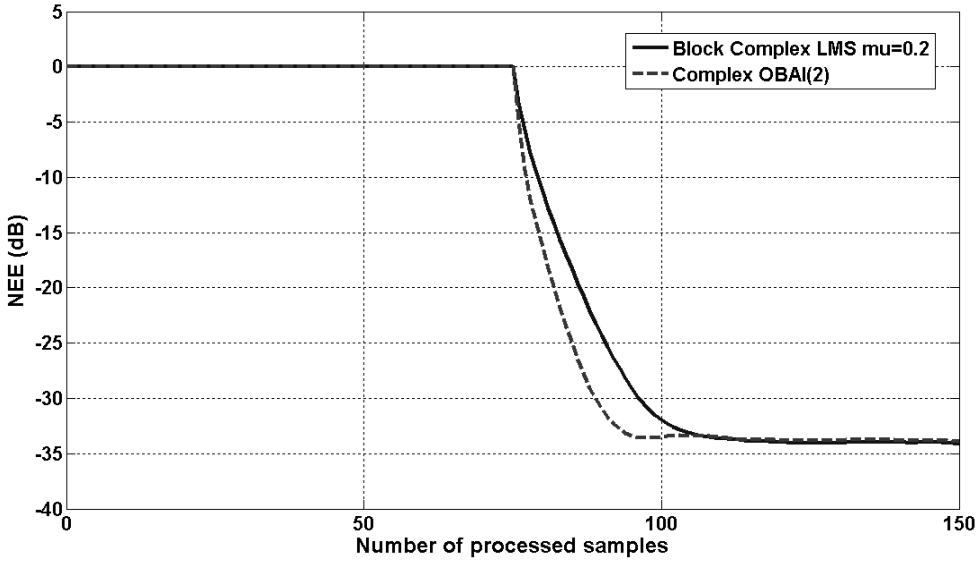

Figure 47: NEE (dB) vs. number of samples in the estimation of $F_2(z)$ using Complex OBAI (2) with complex gaussian noise input and 30 dB SNR

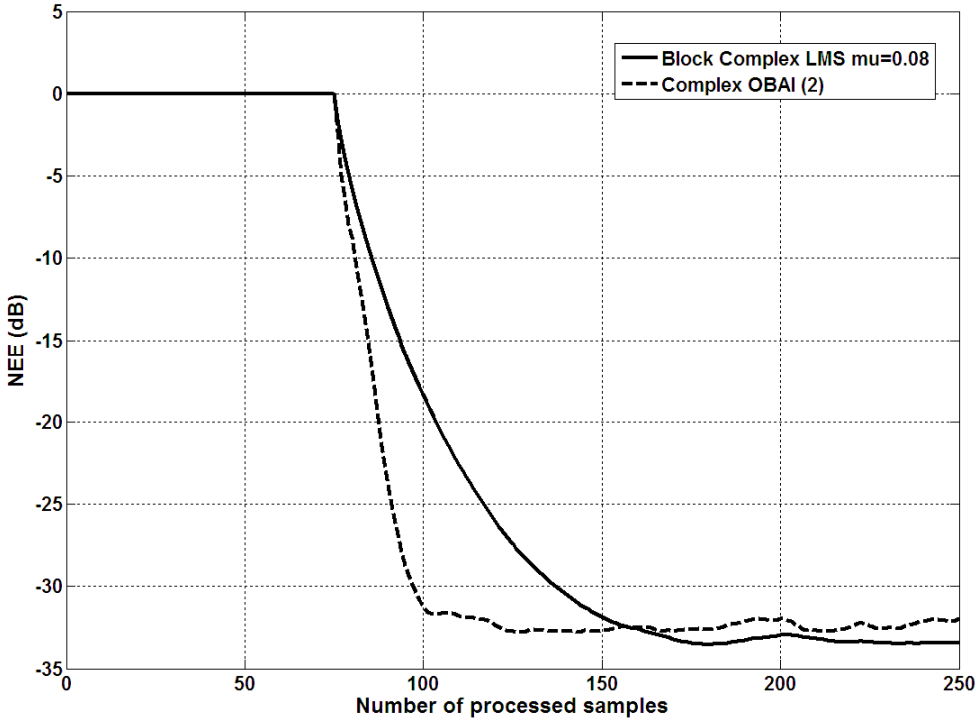

Figure 48: NEE (dB) vs. number of samples in the estimation of $F_2(z)$ using Complex OBAI (2) with colored noise input and 30 dB SNR

7.3 Conclusions

In this Chapter, the proposed Complex OBA-LMS and Complex OBAI-LMS algorithms were applied to the identification of a wireless channel modeled as a complex FIR filter. The simulation results clearly indicate that the novel techniques, especially Complex OBAI (1), exhibit a considerable improvement in convergence speed, in comparison to the traditional block Complex LMS. In addition, it was observed that the performance of the block Complex LMS depended on the choice of the convergence factor, which had to be manually selected each time a different input signal was used for training. In contrast, the proposed methods employing optimally derived convergence factors at each block iteration, exhibit consistent performance in all the simulated

scenarios. Furthermore, being block based, the computational complexity of the Complex OBA-LMS and Complex OBAI-LMS can be further reduced by employing transform domain implementations like the Fast Fourier Transform (FFT).

CHAPTER EIGHT: ADAPTIVE BEAMFORMING

Adaptive beamforming is a spatial form of adaptive filtering in which an array of antennas are employed to achieve maximum reception in a particular direction. This is achieved by estimating the signal arrival from a desired direction (in the presence of noise) while co-channel signals from other directions are suppressed [74, 75]. The individual outputs of the array of sensors or antenna elements are modified so as to produce a desired radiation pattern that optimizes, in some statistical sense, the reception of a target signal along the desired direction [14]. Using the typical adaptive filtering approach, this optimization is achieved by adjusting the weights of each of the sensors used in the array. In this manner, the spatial separation of the signals originating from different transmitters is exploited to retrieve the desired signal from the interfering signals. The technique of adaptive beamforming is widely used for various applications, such as interference suppression in wireless communications [76-78], and in microphone arrays [79, 80].

In this chapter, the previously proposed complex least mean square algorithms employing time-varying convergence factors are applied to adaptive beamforming [73, 81]. The Complex OBA-LMS and Complex OBAI-LMS are applied when the signal is processed in blocks, and the Complex HA-LMS and Complex IA-LMS are employed when sequential processing is adopted at the beamforming receiver. The performance of these techniques is compared to the block and sequential versions of the Complex LMS algorithm. In contrast to the Complex LMS, simulation results will show that the proposed methods exhibit improved convergence speed and accuracy, irrespective of the

flat fading channel parameters, number of antenna elements, and type of modulation employed by the users.

8.1 Beamforming Receiver Structure

An adaptive antenna or adaptive beamforming receiver consists of a set of spatially disposed sensors or antenna elements connected to a single channel or multi-channel adaptive signal processor. The simplest form of adaptive antenna is the sidelobe canceller [15] shown in Fig. 49.

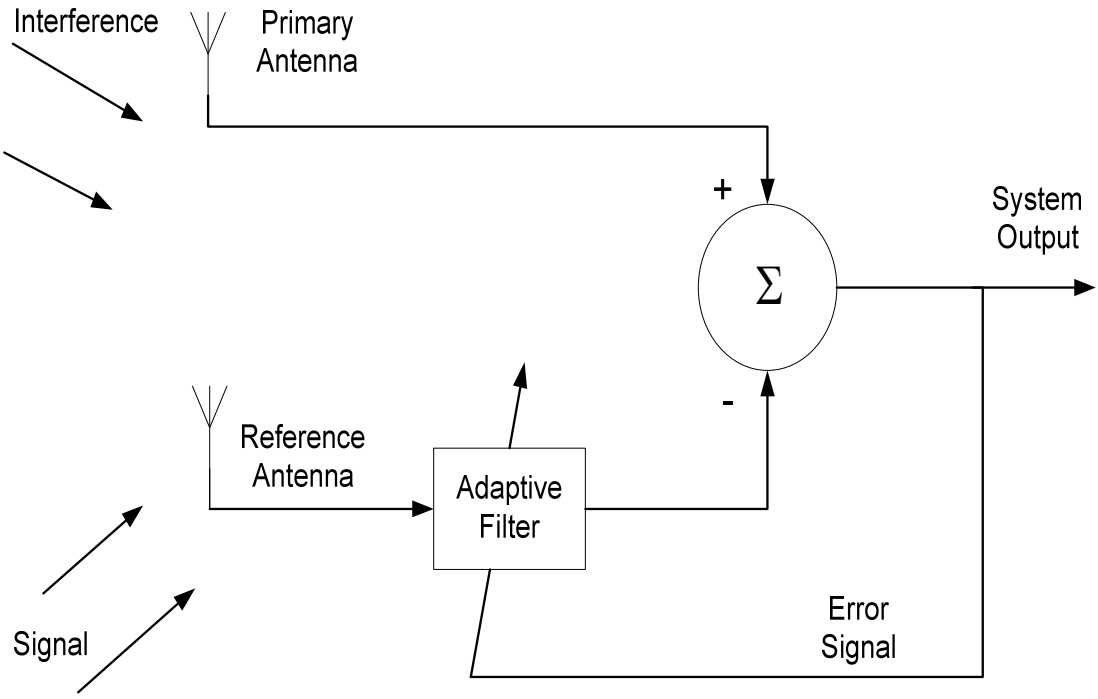

Figure 49: Adaptive Sidelobe cancellation with two antenna array elements

In Fig. 49, two omnidirectional antenna elements are employed, one called the "primary", and the other the "reference". Both the antenna elements receive the signal and interference transmissions at the same time. However, since the elements are spatially separated their outputs are different at any instant of time.

When the interferer is stronger than the signal, the adaptive filter adjusts its weights to produce an output which is identical to the interference component of the primary antenna. As a result, in the system output the interferer is completely cancelled and the signal is successfully recovered.

The interference cancellation mechanism in Fig. 49 can be extended to a beamforming receiver employing a larger number of antenna elements in an environment where many users are transmitting on the same frequency, but originate from spatially separated sources. Hence, the user signals at the receiver arrive from different directions. The structure of the receiver is illustrated in Fig. 50.

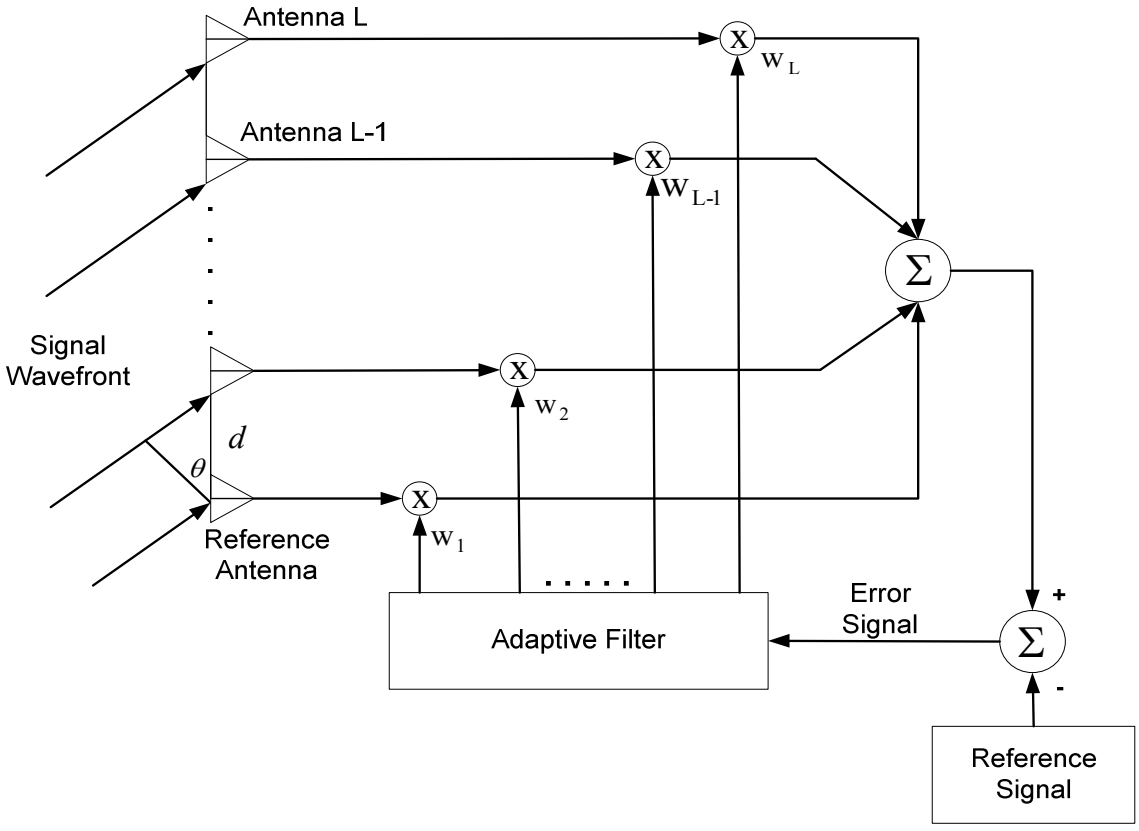

Figure 50: Adaptive Beamformer

8.2 Signal Representation

In Fig. 50, an adaptive beamformer with L antenna elements is shown, with d being the spacing between the elements. Let θ be the direction of arrival or the incidence angle of the wavefronts of a particular user, and λ be the wavelength. Considering the sensor or antenna at the bottom end of the antenna array as the reference, the steering vector $\mathrm{s}(\phi)$ is defined by:

$$\mathrm{s}(\phi) = [1,\, e^{-j\phi},\ldots\ldots,\, e^{-j(L-1)\phi}]^T \tag{8.1}$$

Where, ϕ is the phase of the incident wave relative to the reference antenna given by:

$$\phi = \frac{2\pi d}{\lambda}\sin\theta \tag{8.2}$$

Considering M users, the output of each array element is given by:

$$x_l(k) = \sum_{i=1}^{M} A_i s_i(k) e^{j\omega t_l(\theta_i)} + n_l(k)$$

$$= \quad r_l(k) + n_l(k) \qquad 1 \le l \le L \tag{8.3}$$

Where, $s_i(k)$ is the user symbol for source i at time index k, $r_l(k)$ is the received signal at element l, and $n_l(k)$ is additive white complex gaussian noise. Furthermore, $t_l(\theta_i)$ is the time delay at element l for user i, with direction of arrival θ_i. Assuming a flat fading channel, A_i is the complex fading channel parameter.

Expressing (8.3) in vector form for all the L elements, we obtain

$$X(k) = R(k) + N(k) \tag{8.4}$$

Source 1 is considered to be the desired user and the remaining sources are the interferers. Hence, the Signal to Interference Ratio (SIR), for interferer i is given by

$$\mathrm{SIR}_i = |A_1|^2 / |A_i|^2$$

$$2 \le i \le M \quad (8.5)$$

The output of the beamformer is given by

$$y(k) = W^H X(k) \quad (8.6)$$

Where $W = [w_1(k) \quad w_2(k) \quad ..... \quad w_L(k)]$ is the complex weight vector of the adaptive beamformer and H denotes the conjugate transpose. The beamformer iteratively tries to compute the optimal W that minimizes the MSE between the desired user symbol $s_1(k)$ and $y(k)$, i.e.

$$e(k) = s_1(k) - y(k) \quad (8.7)$$

8.3 Simulation Results

8.3.1 Application of the proposed Complex HA-LMS and Complex IA-LMS

In Sections 6.3 and 6.6, the formulations of the Complex HA-LMS and Complex IA-LMS were presented. In this section, the performance of these algorithms is compared to the Complex LMS in an adaptive beamforming application.

In the simulations, the performance of the beamforming techniques is compared for different number of array elements (L). The elements are separated half a wavelength apart and support 6 users. Furthermore, the performance is compared for both QAM and QPSK modulated user signaling. As mentioned previously, the performance of

the Complex LMS was highly sensitive to the choice of convergence factor. In the simulations, the convergence factor for the Complex LMS had to be chosen by trial and error, depending on the type of modulation of the user signals. Furthermore, the performance of the Complex LMS was inconsistent with variation in L, and signal strengths of the interfering users. The corresponding Angles of Arrival (AOA) of the user signals are shown in Table 1.

User *i*	1	2	3	4	5	6
AOA (degrees)	0	-45	30	-20	-10	18

Table 1: AOA simulated for the different users in degrees

Assuming flat fading, the complex channel parameters A_i in (8.3) were randomly generated for each simulation run to ensure a thorough performance evaluation under diverse channel conditions. The SNR realized was 25 dB, and the μ for Complex LMS was set as 0.0005 for QAM signaling and 0.01 for QPSK modulations. For higher values of μ, the Complex LMS failed to converge.

In the first case, the randomly generated A_i for each run, was set the same for all users, making SIR_i = 0 dB, for all i. In addition, L was varied between 10 and 15 elements. For each L, the performance was averaged over 100 independent simulation runs. The SER (dB) vs. L achieved by the Complex LMS and proposed Complex HA-LMS and Complex IA-LMS algorithms for QPSK and QAM signaling is illustrated in **Figs**. 51 and 52, respectively. The corresponding SER (dB) vs. Number of processed samples for L=10 is shown in **Figs**. 53 and 54, respectively.

In the second scenario, the SIR_i = 0 dB for i =1 to 5, and SIR_6 = -6 dB. The corresponding SER (dB) vs. L for QPSK and QAM user modulations is illustrated in **Figs.** 55 and 56, respectively. The corresponding SER (dB) vs. Number of processed samples for L =10 is shown in **Figs.** 57 and 58, respectively**.**

In the third case, the performance is tested in the presence of strong interferers, i.e. SIR_i = 0 dB for i =1 to 4, and SIR_5 = SIR_6 = -6 dB. The achieved SER (dB) vs. L is illustrated in **Figs**.59 and 60. The corresponding SER (dB) vs. Number of processed samples for L =10 is shown in **Figs**.61 and 62.

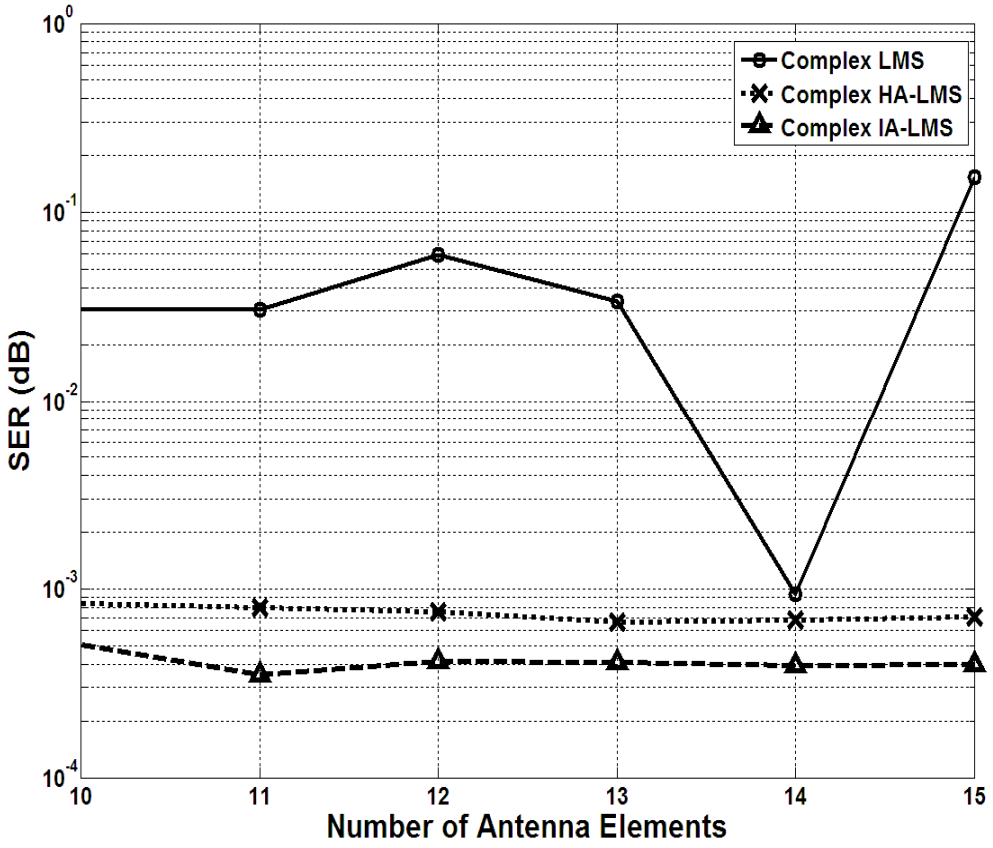

Figure 51: SER (dB) vs. L for QPSK user signaling with SIR_i = 0 dB for all *i*

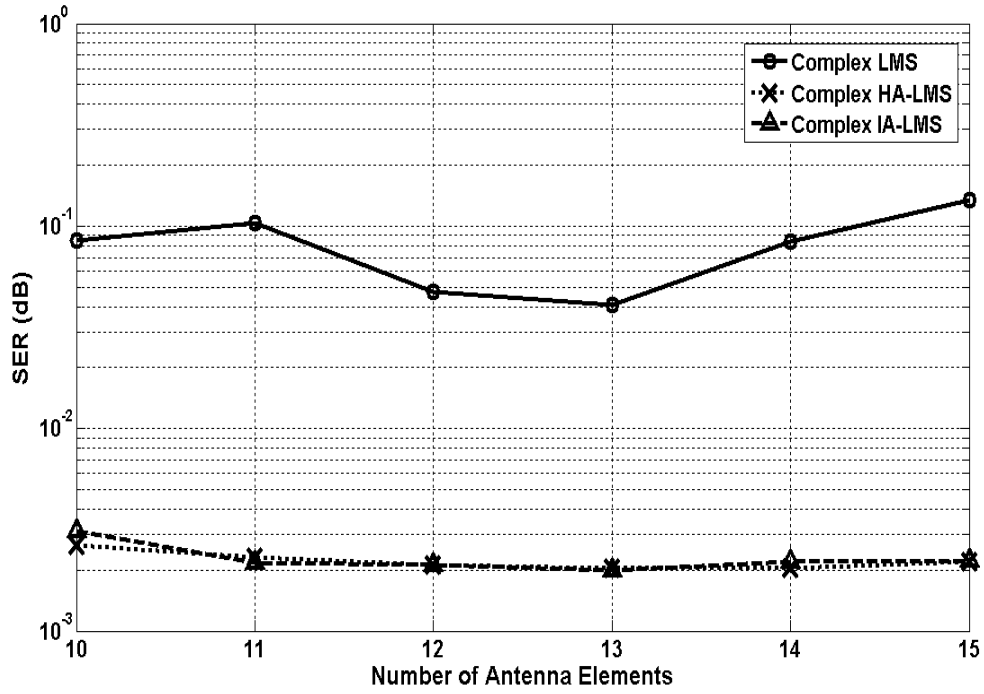

Figure 52: SER (dB) vs. L for QAM user signaling with SIR_i = 0 dB for all *i*

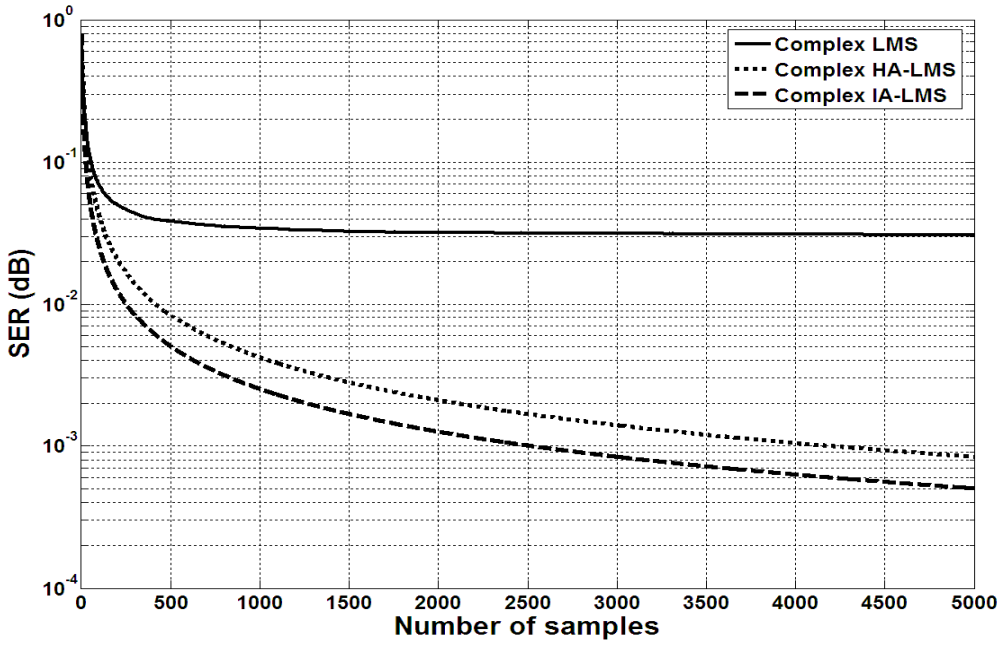

Figure 53: SER (dB) vs. Number of processed samples for QPSK user signaling with L=10, SIR_i = 0 dB for all *i*

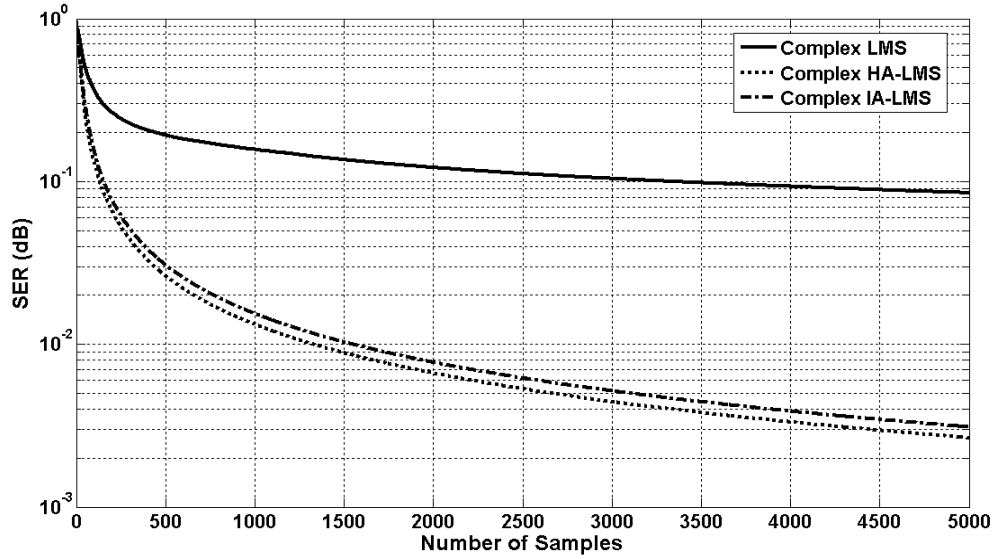

Figure 54: SER (dB) vs. Number of processed samples for QAM user signaling with L=10, SIR_i = 0 dB for all *i*

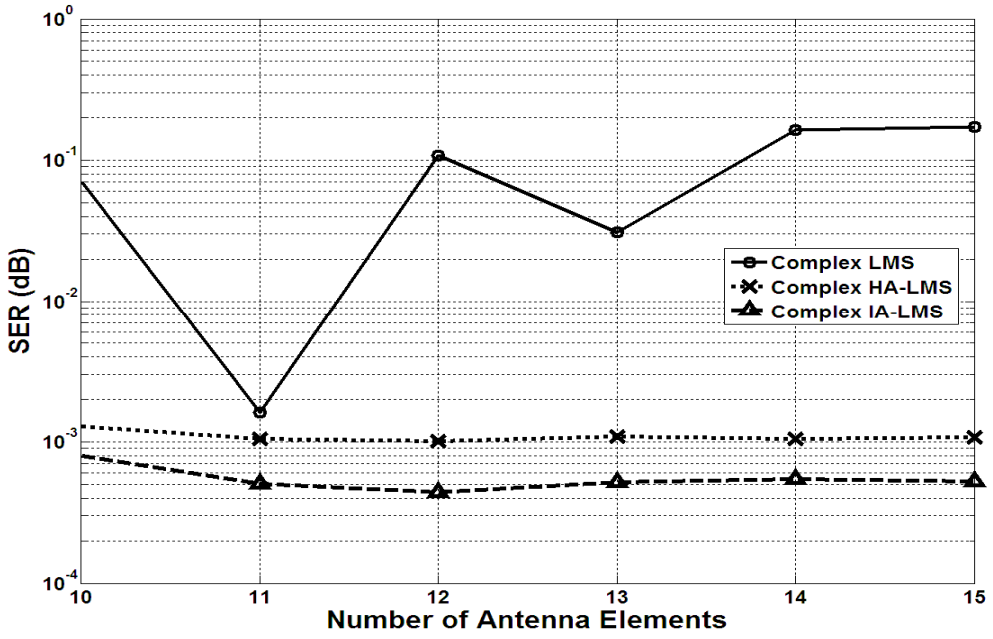

Figure 55: SER (dB) vs. L for QPSK user signaling with SIR_i = 0 dB for *i* =1 to 5, and SIR_6 = -6 dB

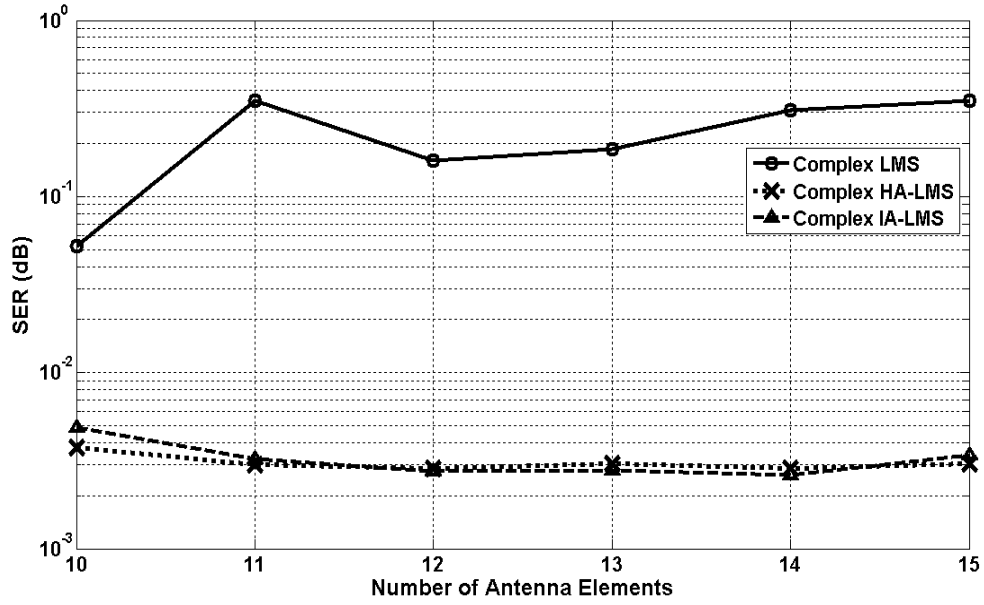

Figure 56: SER (dB) vs. L for QAM user signaling with SIR_i = 0 dB for *i* =1 to 5, and SIR_6 = -6 dB

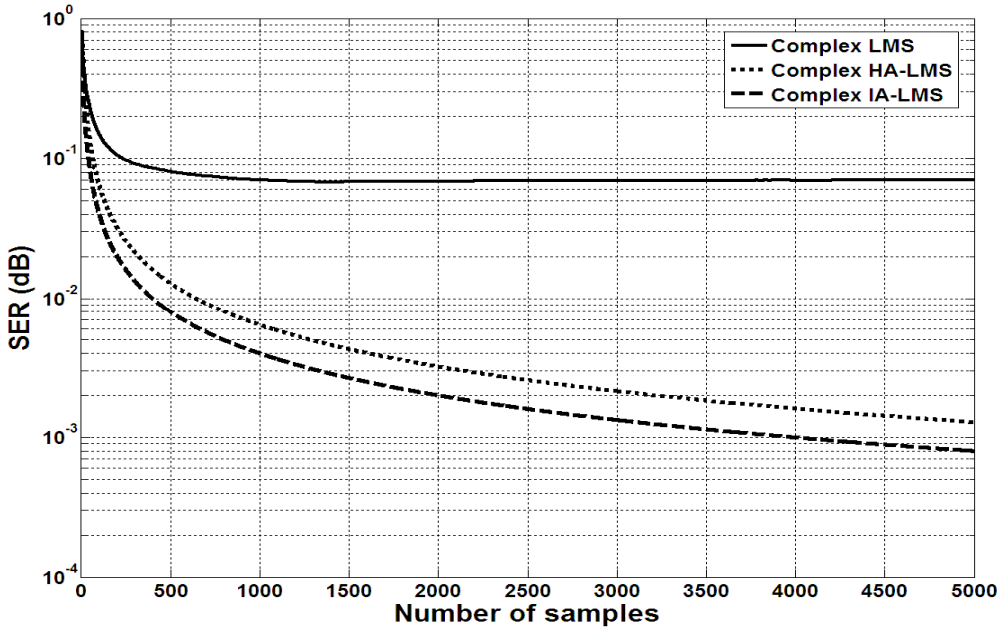

Figure 57: SER (dB) vs. Number of Samples for QPSK user signaling with L=10, SIR_i = 0 dB for *i* =1 to 5, SIR_6 = -6 dB

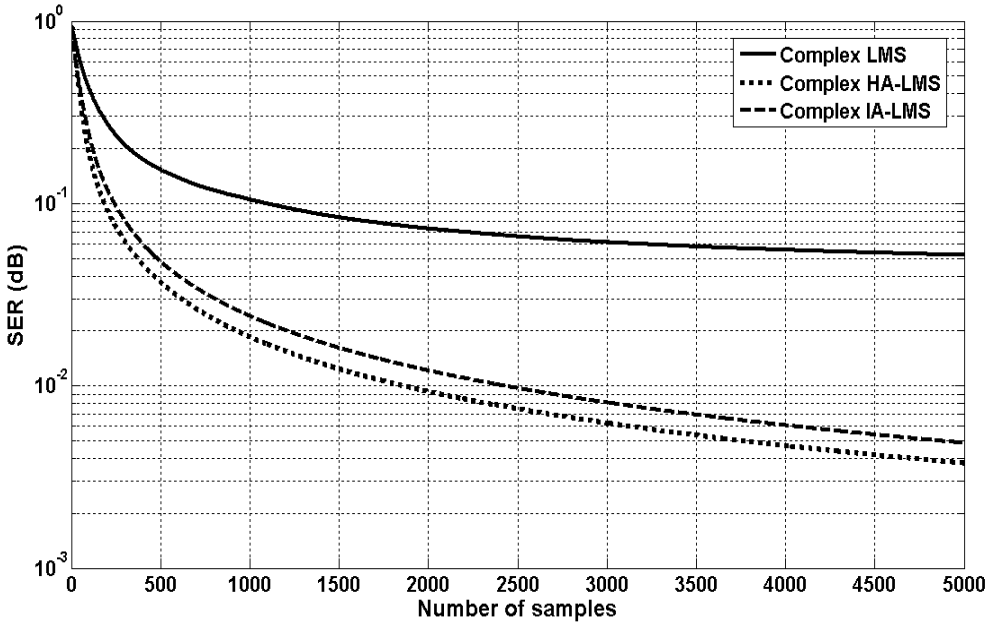

Figure 58: SER (dB) vs. Number of Samples for QAM user signaling with L=10,

SIR_i **= 0 dB for** ***i*** **=1 to 5,** SIR_6 **= -6 dB**

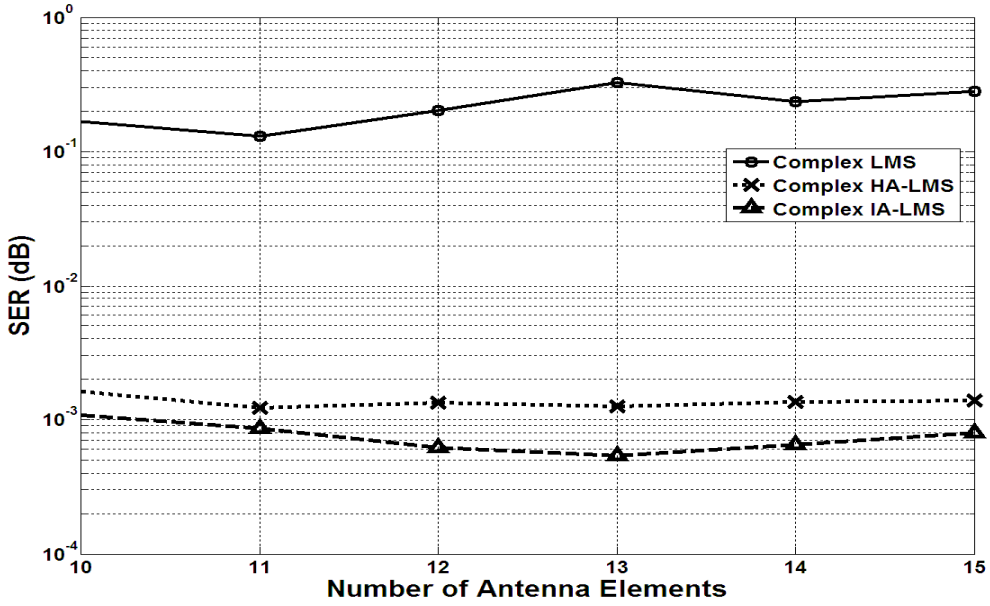

Figure 59: SER (dB) vs. L **for QPSK user signaling with** SIR_i **= 0 dB for** ***i*** **=1 to 4,**

and $\mathrm{SIR}_5 = \mathrm{SIR}_6$ **= -6 dB**

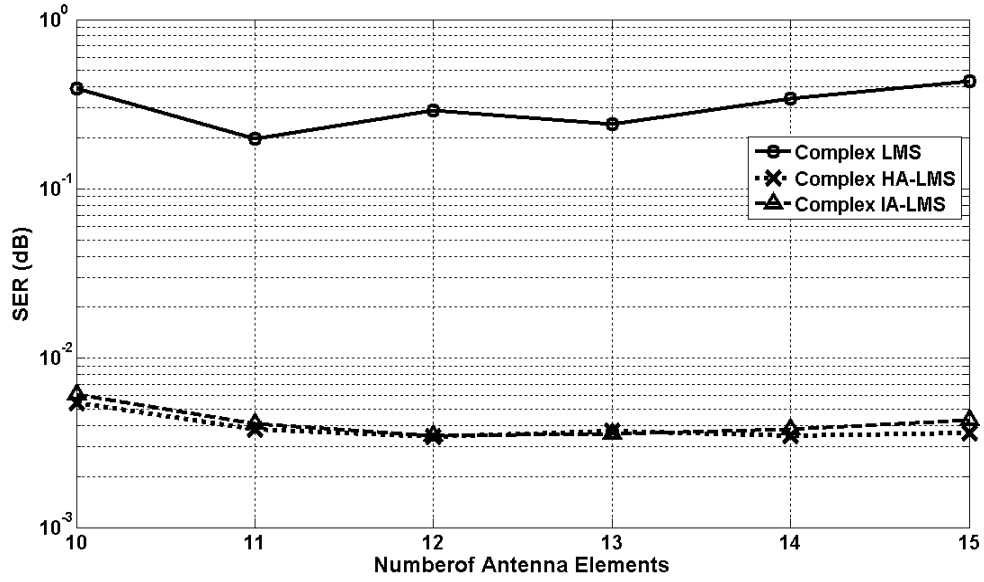

Figure 60: SER (dB) vs. L for QAM user signaling with SIR_i = 0 dB for *i* =1 to 4, and $\mathrm{SIR}_5 = \mathrm{SIR}_6$ = -6 dB

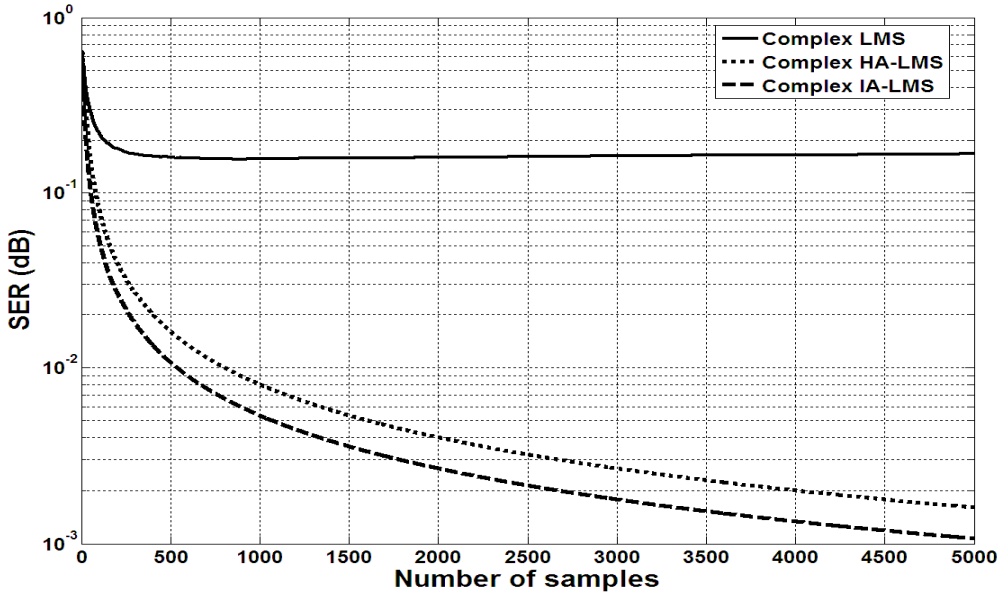

Figure 61: SER (dB) vs. Number of Samples for QPSK user signaling with SIR_i = 0 dB for *i* =1 to 4, $\mathrm{SIR}_5 = \mathrm{SIR}_6$ = -6 dB, and L =10

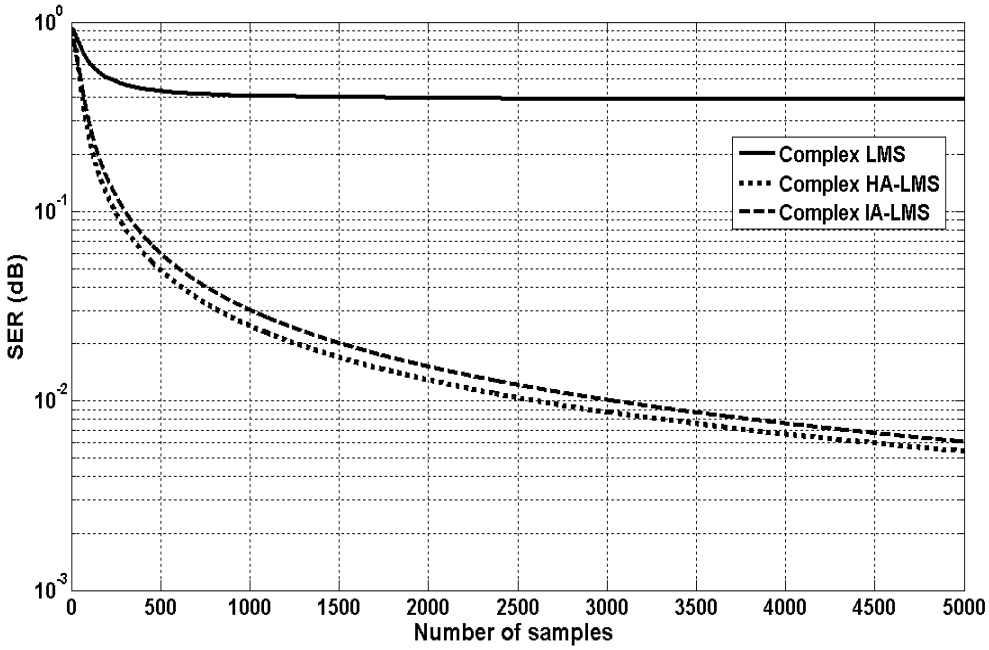

Figure 62: SER (dB) vs. Number of Samples for QAM user signaling with SIR_i = 0 dB for *i* =1 to 4, $\mathrm{SIR}_5 = \mathrm{SIR}_6$ = -6 dB, and L =10

8.3.2 Application of the proposed Complex OBA-LMS and Complex OBAI-LMS

In this section, the novel block algorithms, Complex OBA-LMS and Complex OBAI-LMS, proposed in Chapter 6, are applied to the adaptive beamforming problem for QPSK and QAM modulated users. Similar to the simulation setup in 8.3.1, the performance of the Complex OBA-LMS and Complex OBAI-LMS are compared to the block Complex LMS for different number of antenna elements and varied strengths of the interfering signals. In addition, the processing block length is set as $2L$ in all the simulations.

In this regard, for a SIR_i = 0 dB, for all i, the SER (dB) vs. L achieved by the Block Complex LMS and proposed Complex OBA-LMS and Complex OBAI-LMS algorithms for QPSK and QAM signaling is shown in Figs. 63 and 64, respectively. The

corresponding SER (dB) vs. Number of processed samples for L =10 is shown in Figs. 65 and 66, respectively. In Fig.63, the performance curves for the Complex OBA-LMS and Complex OBAI-LMS algorithms almost overlap each other, since they achieve similar SER.

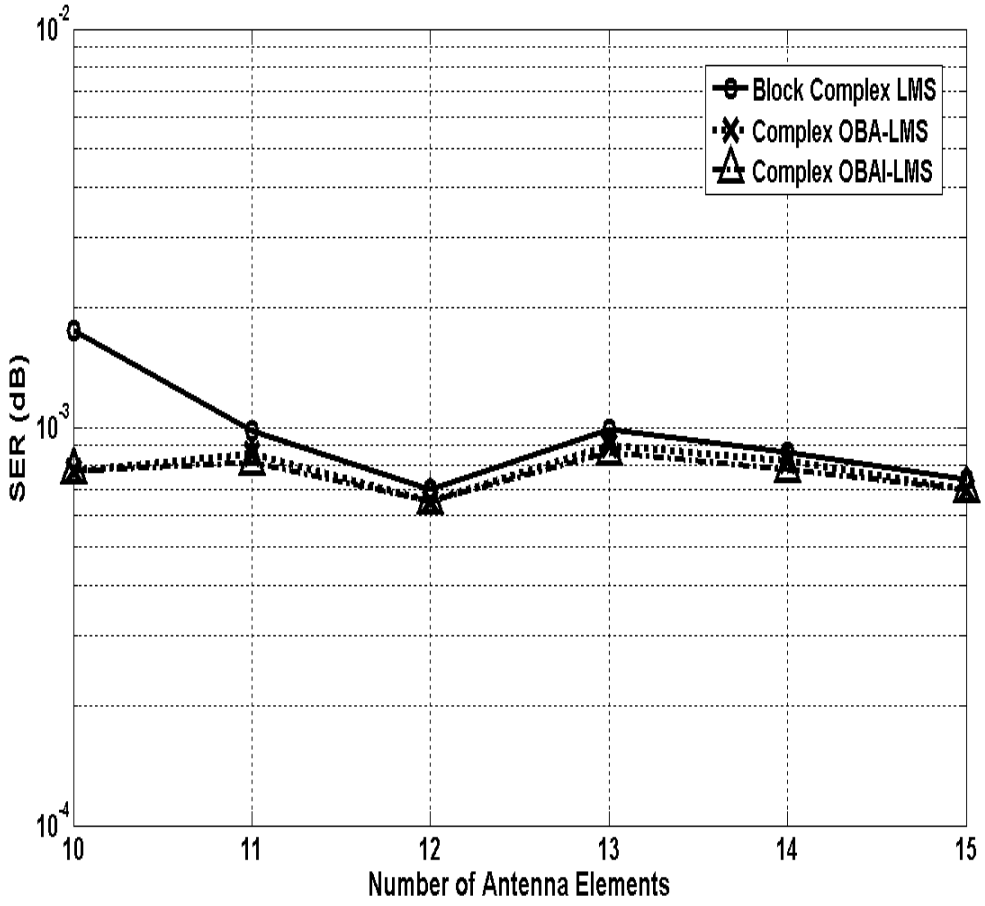

Figure 63: SER (dB) vs. L for QPSK user signaling with SIR_i = 0 dB for all *i*

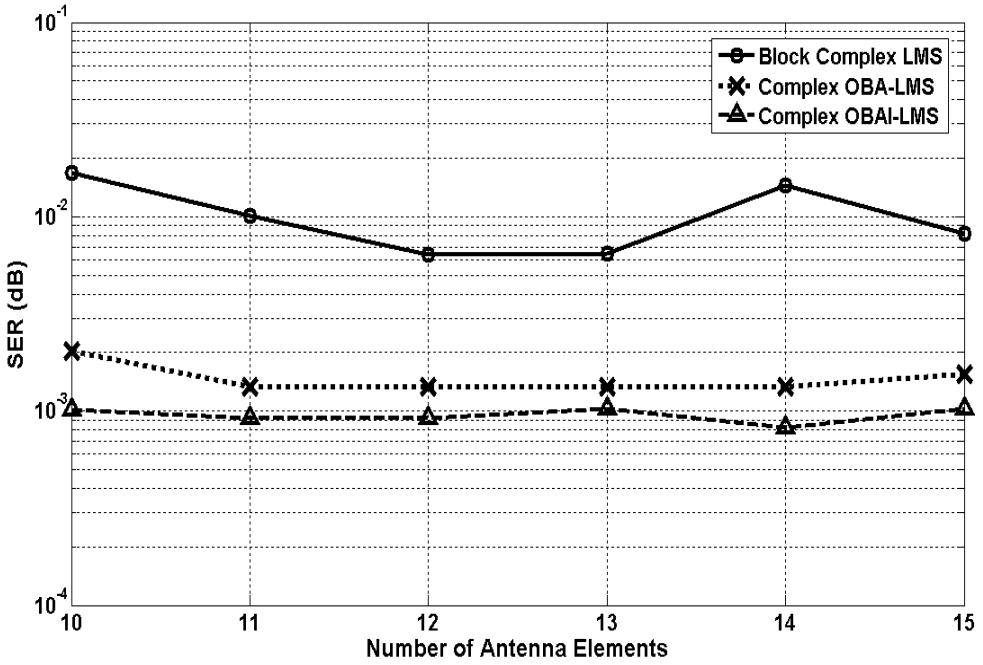

Figure 64: SER (dB) vs. L for QAM user signaling with SIR_i = 0 dB for all *i*

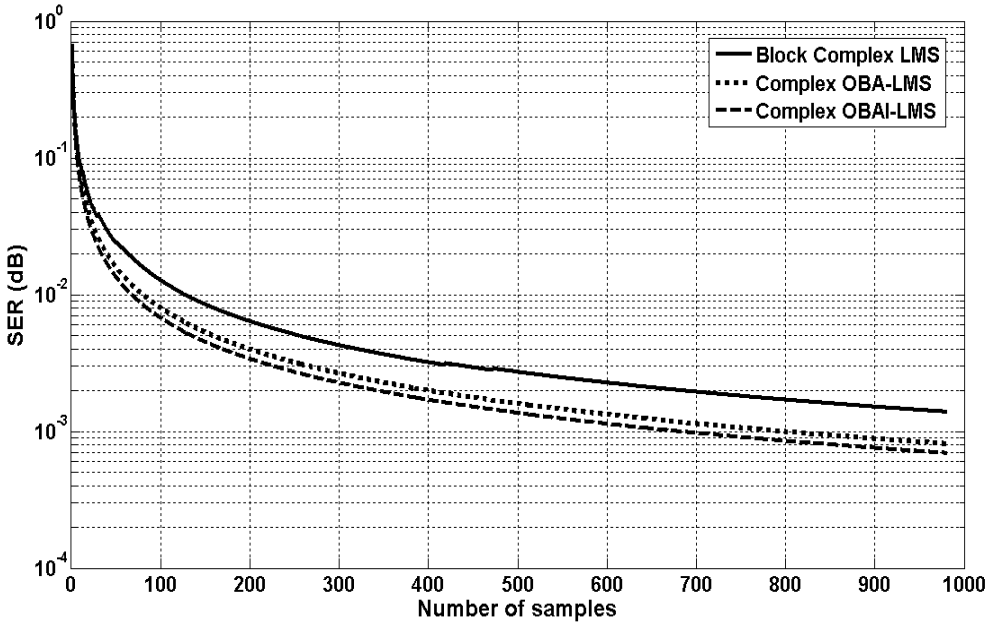

Figure 65: SER (dB) vs. Number of processed samples for QPSK user signaling with SIR_i = 0 dB for all *i*

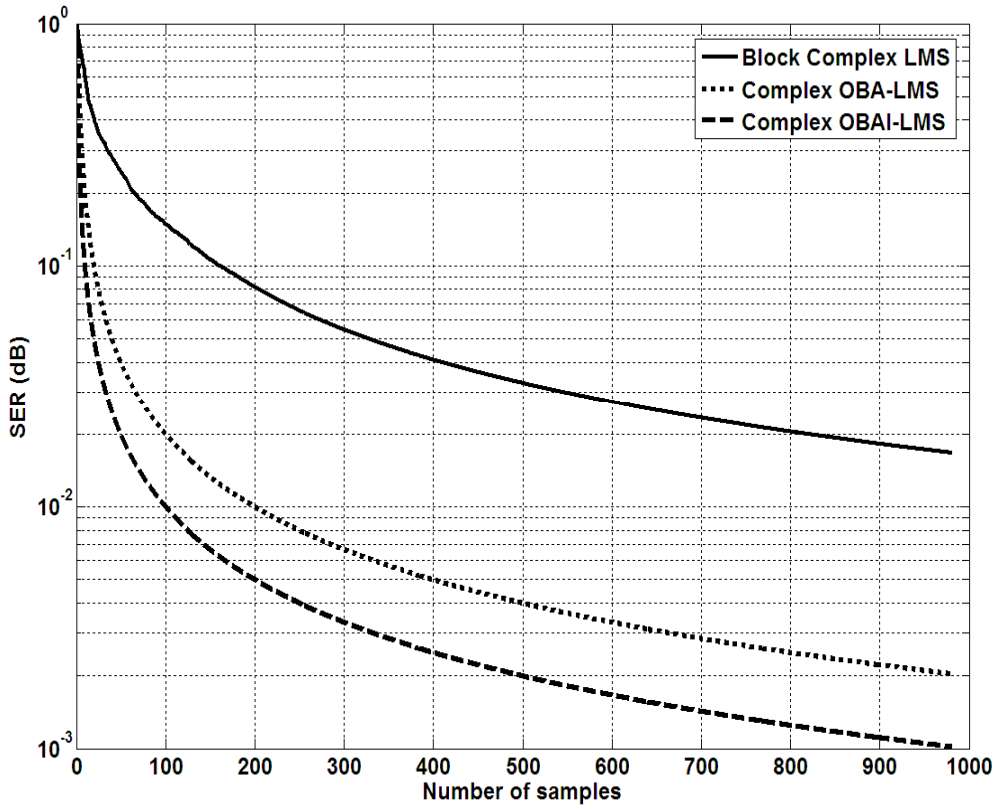

Figure 66: SER (dB) vs. Number of processed samples for QAM user signaling with SIR_i = 0 dB for all *i*

In the second case, the SIR_i = 0 dB for i =1 to 5, and SIR_6 = -6 dB. The corresponding SER (dB) vs. L for QPSK and QAM user modulations is illustrated in **Figs.** 67 and 68, respectively. The corresponding SER (dB) vs. Number of processed samples for L =10 is shown in **Figs.** 69 and 70, respectively**.**

In the third case, the performance is tested in the presence of strong interferers, i.e. SIR_i = 0 dB for i =1 to 4, and SIR_5 = SIR_6 = -6 dB. The achieved SER (dB) vs. L is illustrated in **Figs**.71 and 72. The corresponding SER (dB) vs. Number of processed samples for L =10 is shown in **Figs**.73 and 74.

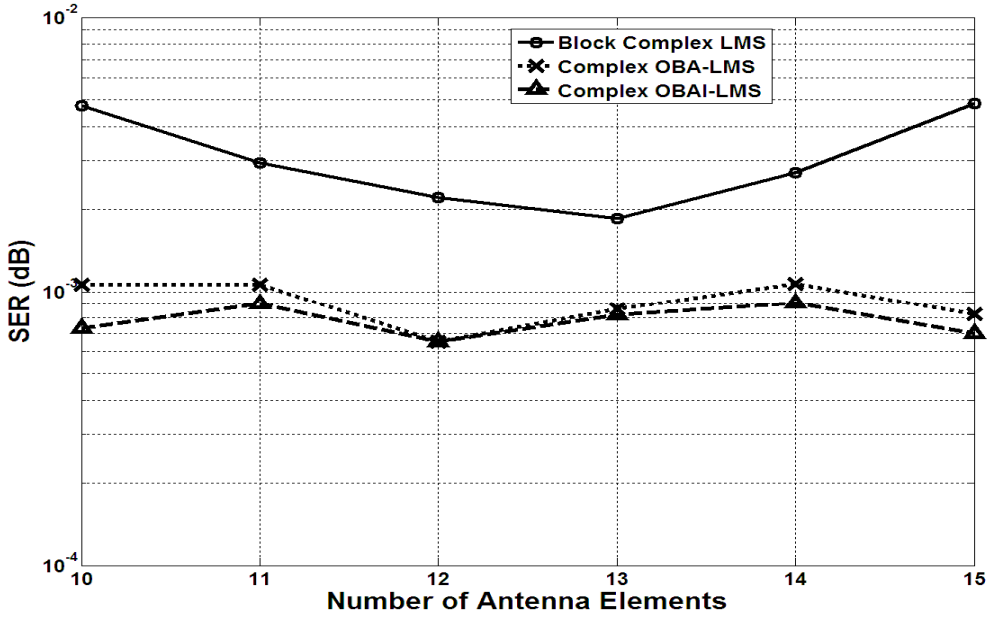

Figure 67: SER (dB) vs. L for QPSK user signaling with SIR_i = 0 dB for *i* =1 to 5, and SIR_6 = -6 dB

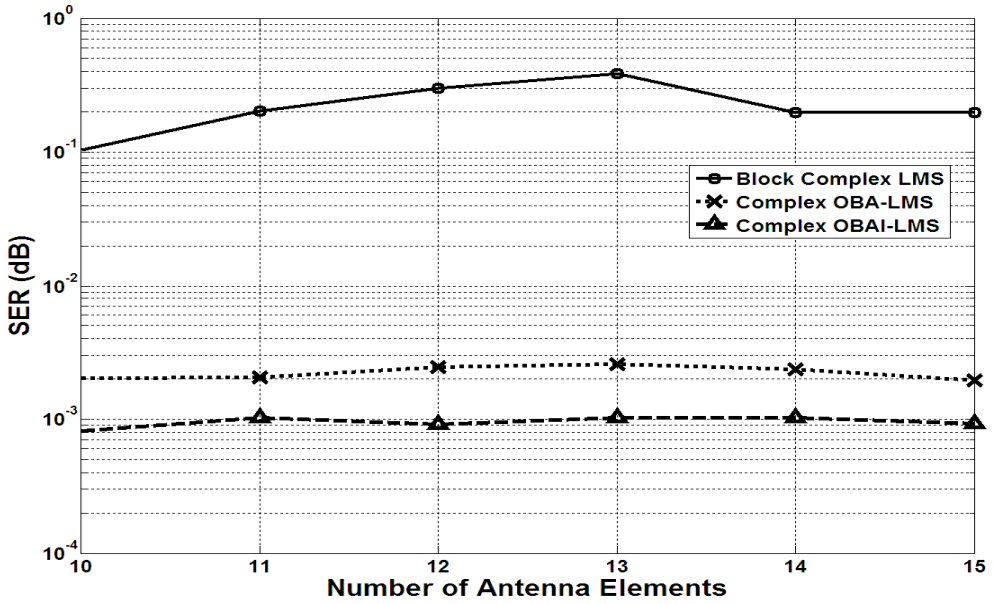

Figure 68: SER (dB) vs. L for QAM user signaling with SIR_i = 0 dB for *i* =1 to 5, and SIR_6 = -6 dB

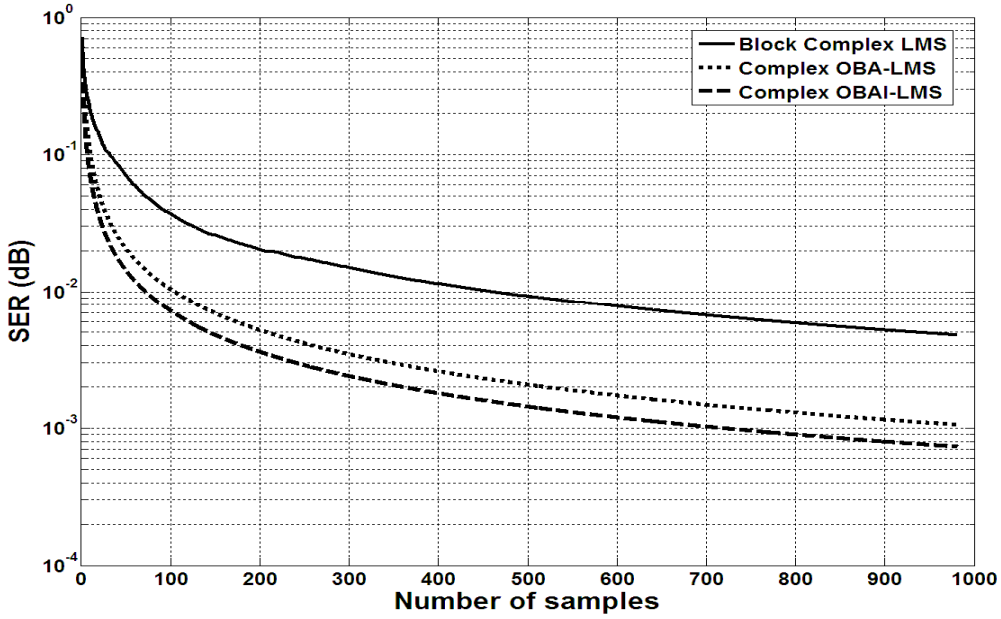

Figure 69: SER (dB) vs. Number of Samples for QPSK user signaling with L=10,

SIR_i = 0 dB for *i* =1 to 5, SIR_6 = -6 dB

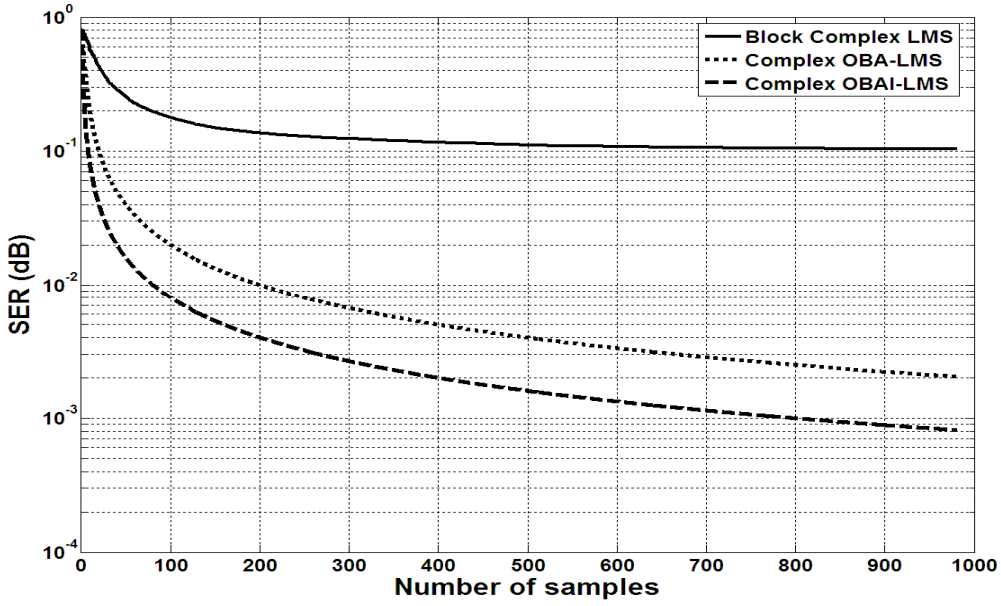

Figure 70: SER (dB) vs. Number of Samples for QAM user signaling with L=10,

SIR_i = 0 dB for *i* =1 to 5, SIR_6 = -6 dB

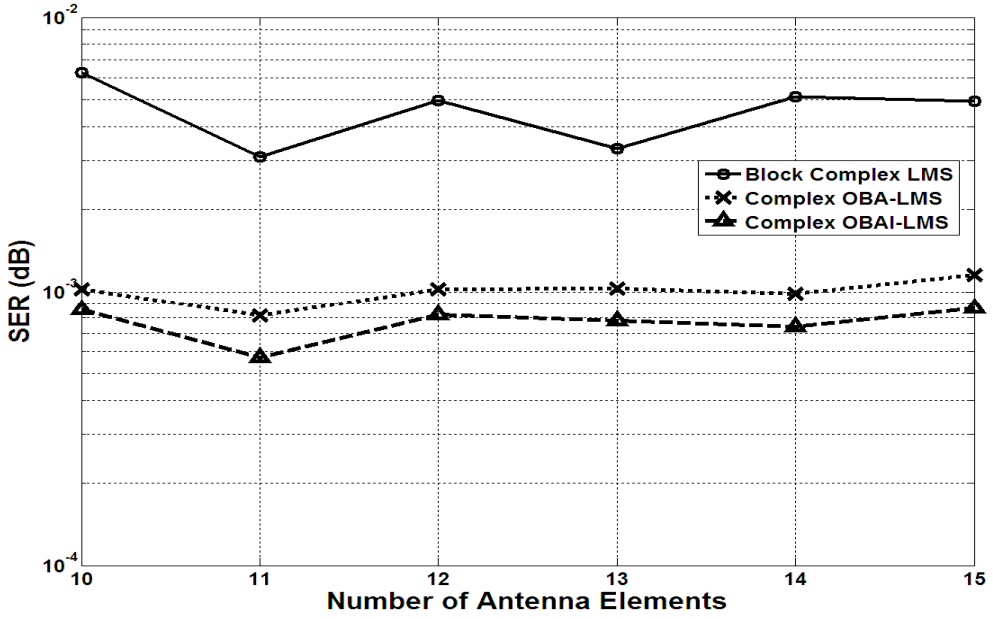

Figure 71: SER (dB) vs. L for QPSK user signaling with SIR_i = 0 dB for *i* =1 to 4, and $\mathrm{SIR}_5 = \mathrm{SIR}_6$ = -6 dB

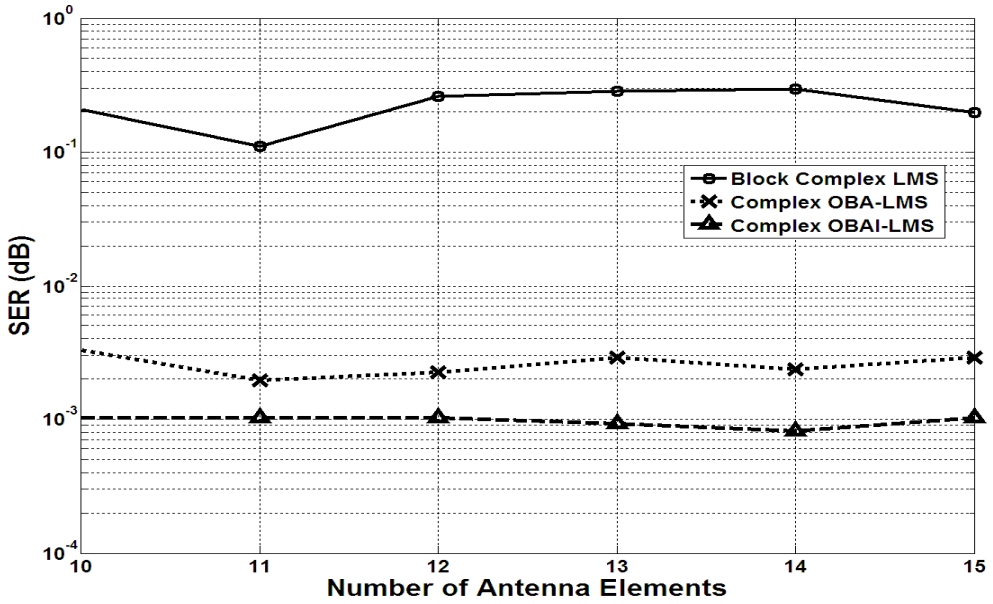

Figure 72: SER (dB) vs. L for QAM user signaling with SIR_i = 0 dB for *i* =1 to 4, and $\mathrm{SIR}_5 = \mathrm{SIR}_6$ = -6 dB

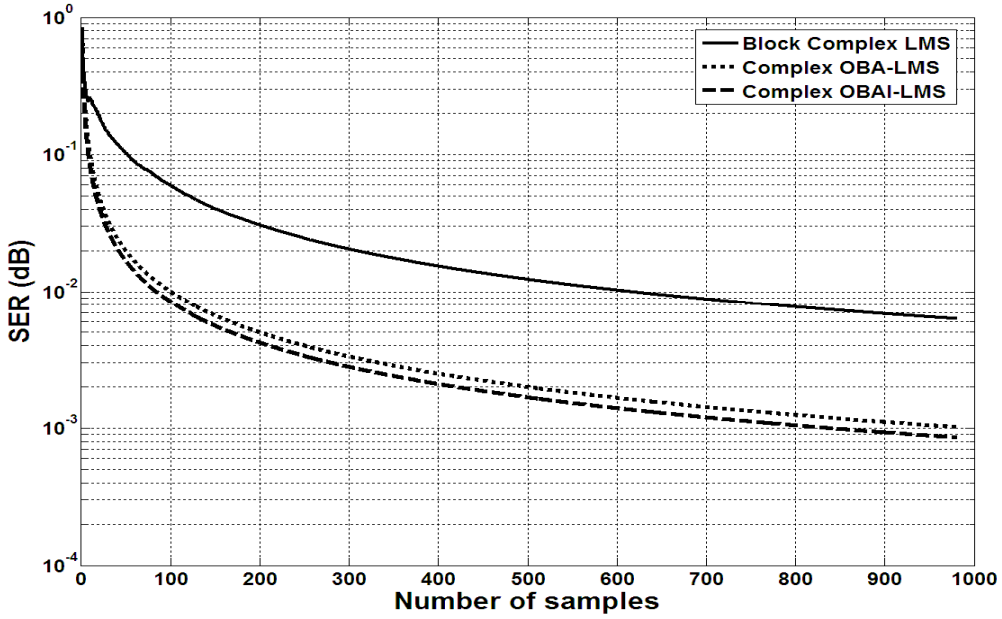

Figure 73: SER (dB) vs. Number of Samples for QPSK user signaling with SIR_i = 0 dB for *i* =1 to 4, $\mathrm{SIR}_5 = \mathrm{SIR}_6$ = -6 dB, and L =10

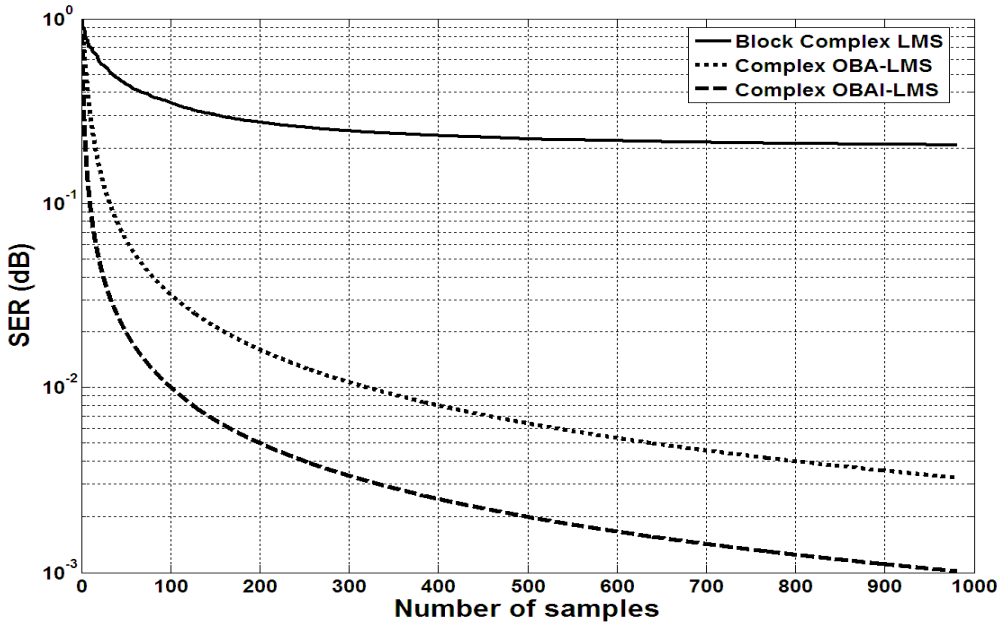

Figure 74: SER (dB) vs. Number of Samples for QAM user signaling with SIR_i = 0 dB for *i* =1 to 4, $\mathrm{SIR}_5 = \mathrm{SIR}_6$ = -6 dB, and L =10

8.4 Conclusions

In this chapter, the proposed complex least mean square algorithms with optimally and automatically derived convergence factors were applied in an adaptive beamforming application. In this regard, the performance of the Complex HA-LMS and Complex IA-LMS were compared to the Complex LMS algorithm when the received signals were processed sequentially. For block processing, the Complex OBA-LMS and Complex OBAI-LMS were employed and their convergence properties compared to the Block Complex LMS. In addition, the performance of the novel techniques were tested for varied number of receiver antenna elements, SIR' s and user signal modulations. The extensive simulation results and illustrations presented clearly show that in all conditions, the proposed techniques exhibit a considerable improvement in accuracy and convergence speed, as compared to the Complex LMS and Block Complex LMS.

CHAPTER NINE: BLIND INTERCARRIER INTERFERENCE MITIGATION AND MULTI-USER DETECTION FOR MIMO-OFDM SYSTEMS IN TIME VARIANT CHANNELS

Orthogonal Frequency Division Multiplexing (OFDM) is a widely applied scheme in modern wireless communication systems that effectively operate in frequency selective fading channels. The combination of OFDM and the Multiple-Input-Multiple-Output (MIMO) technique represents a promising candidate for future broadband wireless systems. This chapter addresses the Intercarrier Interference (ICI) issue in multi-user MIMO-OFDM systems operating in time-varying frequency selective channel environments. ICI, which is caused by Carrier Frequency Offset (CFO) between local oscillators in the transmitter and the receiver, can lead to severe system performance degradation. In our proposed method, the previously proposed Independent Component Analysis (ICA) technique called Complex Optimum Block Adaptive ICA (Complex OBA-ICA) is employed to recover user signals in the presence of ICI and channel induced mixing. Simulation results indicate that the new technique significantly reduces Inter Symbol Interference (ISI) and Symbol Error Rate (SER) in multi-user MIMO-OFDM systems in dynamic channel environments.

9.1 ICI in OFDM systems

OFDM has been adopted in several important wireless standards, including Digital Audio Broadcasting (DAB), Digital Video Broadcasting (DVB-T), the IEEE 802.11a Local Area Network (LAN) and the IEEE 802.16a Metropolitan Area Network (MAN). As a promising technique for high data rate communications, OFDM is also a candidate for the fourth-generation (4G) mobile systems. If OFDM is combined with

antenna arrays at the receiver and/or the transmitter, the resulting MIMO-OFDM system capacity in frequency selective channels can be substantially enhanced [82-84].

In OFDM, a wideband source signal is partitioned into a number of narrowband signals, which are transmitted simultaneously through orthogonal sub-carriers. A major issue in most applications is the crosstalk between the sub-carriers, namely ICI, due to frequency offsets between local oscillators in the transmitter and the receiver [85, 86].
To combat the adverse effect of ICI, most OFDM systems employ a data-aided approach, i.e., a preamble consisting of one or more training sequences [87-89]. These approaches reduce bandwidth efficiency and introduce delay in the detection process. Several blind ICI cancellation techniques that do not require training sequences have also been proposed [90-92], but they pose additional constraints on air interface design or sampling frequency.

In [93], a blind ICI cancellation technique for OFDM systems based on maximum likelihood estimation is proposed. In this paper, we present an ICI cancellation method for multi-user MIMO-OFDM systems adopting our recently proposed Complex Optimum Block Adaptive ICA (Complex OBA-ICA) algorithm for Quadrature Phase Shift Keying (QPSK) user signaling. The new technique is especially suitable for time-variant environments in which the well-known Complex FastICA often has difficulty in convergence [39]. The effectiveness of the new approach in performing ICI mitigation and signal separation is tested for various values of CFO, time variation parameter and Signal to Noise Ratio (SNR) [104].

9.2 MIMO-OFDM Transmitter/Receiver Structure and Signal Model

For illustrative purposes, we consider a MIMO-OFDM system that employs two transmit and two receive antennas. The transmitter section is given in Fig.75.

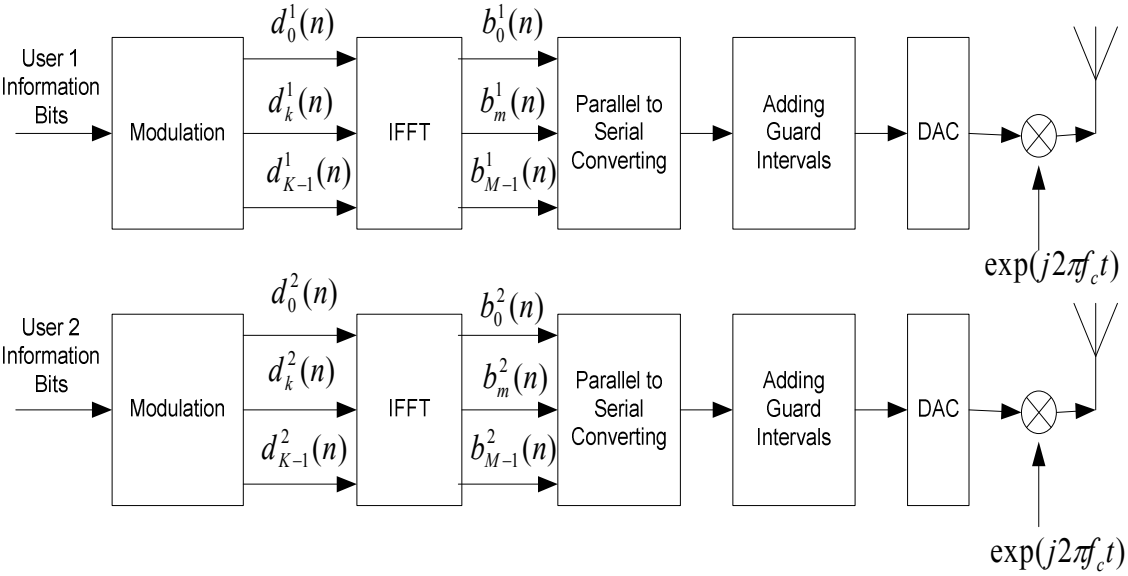

Figure 75: Multi-User MIMO-OFDM Transmitter

In each transmit path, K parallel modulated symbols of user i at time index n, i.e. $d_k^i(n)$'s , $k = 0,...,K-1$, are mapped onto orthogonal subcarriers by a M-point IFFT operation. Without loss of generality, in the simulation results presented in Section 9.4, K and i are assumed to be 4 and 2, respectively, and $M = K$.

In practice, there are frequency offsets between the local oscillators of the transmitter and the receiver, resulting in ICI. Furthermore, the wireless channel induces mixing of the OFDM modulated user symbols causing decoding errors at the receiver.

The block diagram of the diversity receiver structure employing two antennas and suffering from CFO's $f_{\Delta 1}$ and $f_{\Delta 2}$ is shown in Fig.76.

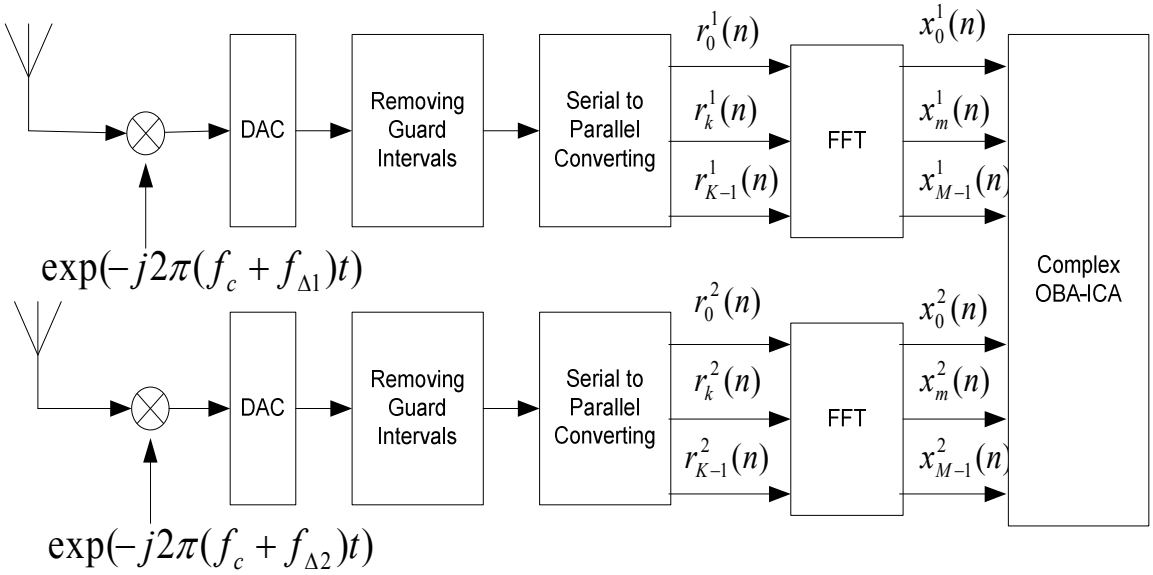

Figure 76: Multi-User MIMO-OFDM Receiver

The normalized frequency errors e_1 and e_2 due to frequency offsets $f_{\Delta 1}$ and $f_{\Delta 2}$, respectively, are defined by

$$e_1 = f_{\Delta 1} T \tag{9.1}$$

$$e_2 = f_{\Delta 2} T \tag{9.2}$$

where T is the OFDM symbol duration.

The baseband received signal at each antenna prior to sampling by the Analog to Digital Converter (ADC) is given by

$$r^i(t) = \exp(-j * 2 * \pi * e_i)(b^i(t) \otimes h_{ab}(t)) \tag{9.3}$$

Where, $h_{ab}(t)$ is the multipath fading channel between transmitter antenna a and receiver antenna b ($a, b = 1, 2$), modeled as

$$h_{ab}(t) = \sum_{p=0}^{P-1} \sigma_{ab,p} \delta(t - pT) \tag{9.4}$$

P is the total number of fading paths, and $\sigma_{ab,p}$ are the Rayleigh distributed fading parameters. In the simulation results presented in Section 9.4, P is assumed to be 3.

The corresponding channel transfer factors are defined as:

$$h_{ab,k} = \sum_{p=0}^{P-1} \sigma_{ab,p} \exp(-\frac{j2\pi k}{M} p) \tag{9.5}$$

The received signals $x_m^i(n)$ in the frequency domain after ADC and applying FFT is expressed as

$$x_m^i(n) = \frac{1}{\sqrt{K}} \sum_{k=0}^{K-1} r_k^i(n) \exp(\frac{-j2\pi k}{K} m) \tag{9.6}$$

From [94], the ICI coefficients $a_{i,m,k}$ are defined as

$$a_{i,m,k} = \frac{1}{K} \sum_{k=0}^{K-1} \exp(\frac{j2\pi k}{K}(k-m-e_i)) \tag{9.7}$$

Hence, (9.6) becomes

$$x_m^i(n) = \sum_{k=0}^{K-1} a_{i,m,k} h_{ab,k} d_k^i(n) \tag{9.8}$$

(9.7) can also be written as

$$a_{i,m,k} = \frac{\sin(\pi(k-m+e_i))}{K \sin\left(\pi \frac{k-m+e_i}{K}\right)} \exp\left(j\pi(\frac{K-1}{K})(k-m+e_i)\right)$$

$$m = 0,...,M-1 \tag{9.9}$$

In the absence of CFO, $e_i = 0$, and ICI coefficients satisfy the following properties

$$a_{i,m,k} = 1, \quad m = k \tag{9.10}$$

$$a_{i,m,k} = 0, \quad m \neq k \tag{9.11}$$

Thus, no ICI occurs. On the other hand, if $e_i \neq 0$,

$$\left|a_{i,m,k}\right| \leq 1, \quad m = k \tag{9.12}$$

$$a_{i,m,k} \neq 0, \quad m \neq k \tag{9.13}$$

The corresponding ICI matrices A_i for $i = 1, 2$ are given as:

$$A_i = \begin{bmatrix} a_{i,0,0} & \cdots & a_{i,0,M-1} \\ \vdots & \ddots & \vdots \\ a_{i,M-1,0} & \cdots & a_{i,M-1,M-1} \end{bmatrix} \tag{9.14}$$

The transmitted signal vectors $D_1(n)$ and $D_2(n)$ of source signal matrix D are expressed as:

$$D_1(n) = \left[d_0^1(n),\ldots\ldots,d_k^1(n),\ldots\ldots,d_{K-1}^1(n)\right]^T \tag{9.15}$$

$$D_2(n) = \left[d_0^2(n),\ldots\ldots,d_k^2(n),\ldots\ldots,d_{K-1}^2(n)\right]^T \tag{9.16}$$

The baseband signal vectors $X_1(n)$ and $X_2(n)$ of observation matrix X, from the two receive antennas are given as:

$$X_1(n) = \left[x_0^1(n),\ldots\ldots,x_m^1(n),\ldots\ldots,x_{M-1}^1(n)\right]^T \tag{9.17}$$

$$X_2(n) = \left[x_0^2(n),\ldots\ldots,x_m^2(n),\ldots\ldots,x_{M-1}^2(n)\right]^T \tag{9.18}$$

The received signal vectors $X_1(n)$ and $X_2(n)$ can be expressed in terms of the transmitted source vectors $D_1(n)$ and $D_2(n)$ as follows:

$$X_1(n) = A_1 H_{11} D_1(n) + A_1 H_{21} D_2(n) \tag{9.19}$$

$$X_2(n) = A_2 H_{12} D_1(n) + A_2 H_{22} D_2(n) \tag{9.20}$$

where H_{ab} is a K x K diagonal matrix given by

$$H_{ab} = \begin{bmatrix} h_{ab,0} & 0 & ..... & 0 \\ 0 & ..... & 0 & 0 \\ ..... & ..... & h_{ab,k} & ..... \\ 0 & 0 & 0 & h_{ab,K-1} \end{bmatrix} \tag{9.21}$$

(9.21) represents a static channel whose fading characteristics are stationary over time. In the presented research, a time-variant scenario is modeled, in which the fading parameters of the channel change over the processing block. Hence, (9.21) becomes

$$H_{ab}(n) = \begin{bmatrix} h_{ab,0}(1+n\Delta) & 0 & ..... & 0 \\ 0 & ..... & 0 & 0 \\ ..... & ..... & h_{ab,k}(1+n\Delta) & ..... \\ 0 & 0 & 0 & h_{ab,K-1}(1+n\Delta) \end{bmatrix} \tag{9.22}$$

where Δ represents the speed of variation of the channel.

Accordingly, (9.19) and (9.20) become as follows:

$$X_1(n) = A_1 H_{11}(n) D_1(n) + A_1 H_{21}(n) D_2(n) \tag{9.23}$$

$$X_2(n) = A_2 H_{12}(n) D_1(n) + A_2 H_{22}(n) D_2(n) \tag{9.24}$$

Thus, the ICA signal model in matrix form is expressed as:

$$\begin{bmatrix} X_1(n) \\ X_2(n) \end{bmatrix} = \begin{bmatrix} A_1 H_{11}(n) & A_1 H_{21}(n) \\ A_2 H_{12}(n) & A_2 H_{22}(n) \end{bmatrix} \begin{bmatrix} D_1(n) \\ D_2(n) \end{bmatrix} \tag{9.25}$$

or

$$X = YD \tag{9.26}$$

9.3 Outline of the Complex OBA-ICA algorithm

The observation matrix X, as expressed in (9.26), is processed by the proposed Complex OBA-ICA algorithm, which will recover the source signals in *D*. The Complex OBA-ICA independently updates the real and imaginary components of the complex

separating weight matrix W [39, 66]. In order to retrieve independent source components from X, the non-gaussianity or the absolute value of the kurtosis of the projection $W^H X$ has to be maximized, where H denotes the Hermitian operator. In most wireless communication applications, the modulation scheme of the user source signals is known. As a result, their corresponding kurtosis values can be easily calculated. Hence, for QPSK source symbols having values $\pm 0.707 \pm 0.707\text{j}$, the kurtosis of the source signal distribution is -1. The Complex OBA-ICA algorithm follows a Newton's type iteration to update the real and imaginary parts of the weights such that each element of the kurtosis vector becomes -1 after adaptation. The outline of the algorithm is given below:

Step 1: Set p =1. The observation matrix X is whitened using Eigenvalue Decomposition (EVD).

Step 2: The p^{th} column of W, namely w_p, is normalized to a random vector of unit length and iteration index k is set to 0.

Step 3: The update equations for the real and imaginary parts of w_p, namely $w_{pR}(k)$ and $w_{pI}(k)$, respectively, are given as follows:

$$w_{pR}(k+1) = w_{pR}(k) - [R]_R^{\#}(k)(kurt(k) + K) \tag{9.27}$$

$$w_{pI}(k+1) = w_{pI}(k) - [R]_I^{\#}(k)(kurt(k) + K) \tag{9.28}$$

Where $-K = [\text{-1 -1}.....\text{-1}]^{\text{T}}$ is a vector of length L (L is the processing block size).

$$[R]_R^{\#}(k) = \begin{cases} [R]_R^T(k)([R]_R(k)[R]_R^T(k))^{-1} & L < N \\ ([R]_R^T(k)[R]_R(k))^{-1}[R]_R^T(k) & L \geq N \end{cases} \tag{9.29}$$

$$[R]_I^{\#}(k) = \begin{cases} [R]_I^T(k)([R]_I(k)[R]_I^T(k))^{-1} & L < N \\ ([R]_I^T(k)[R]_I(k))^{-1}[R]_I^T(k) & L \geq N \end{cases} \tag{9.30}$$

$[R]_R^{\#}(k)$ and $[R]_I^{\#}(k)$ are the pseudo-inverses of the matrices $[R]_R(k)$ and $[R]_I(k)$, respectively, where,

$$[R]_R(k) = [\mathrm{Re}\{[C]_k[G]_k\}] \tag{9.31}$$

$$[R]_I(k) = [\mathrm{Im}\{[C]_k[G]_k\}] \tag{9.32}$$

$[G]_k = [X_1(k)\ X_2(k).....X_L(k)]^T$ is the observation matrix for the *k*th iteration. Re{.} and Im{.} represent the real and imaginary component of {.}, respectively. $kurt(k)$ is a column vector containing the kurtosis values of $w_p(k)X$, given by:

$$kurt(k) = \left| w_p(k)^H X \right|^4 \tag{9.33}$$

and

$$[C]_k = diag[\{w_p(k)^H X\}^* \left| w_p(k)^H X \right|^2] \tag{9.34}$$

is a diagonal matrix, with * representing the complex conjugate. After $w_{pR}(k)$ and $w_{pI}(k)$ are updated, the new complex weight vector is obtained as:

$$w_p(k+1) = w_{pR}(k+1) + jw_{pI}(k+1) \tag{9.35}$$

Step 4: If $p > 1$, the previously extracted columns of W, i.e., w_1,....., w_{p-1} are decorrelated using Gram-Schmidt like decorrelation as follows:

$$w_p = w_p - \sum_{k=1}^{p-1}(w_p^H w_k w_k) \tag{9.36}$$

Step 5: $w_p(k+1)$ is normalized to unit length.

Step 6: Check the convergence of $w_p(k+1)$. If the required convergence accuracy of 10^{-6} has not been reached, go back to Step 3; otherwise proceed to Step 7.

Step 7: Set $p = p + 1$. If $p \le N$ (N is the dimension of the mixing matrix), go to Step 2.

9.4 Simulation Results

In our simulations, the proposed method is applied to perform CFO compensation and multi-user detection simultaneously.

In the first set of experiments, the performance of the Complex OBA-ICA is tested for different SNR's between 5 and 30 dB and $\Delta = 1.15\times10^{-6}$. The Carrier Frequency Offsets e_1 and e_2 are set as 0.3 and 0.35, respectively. The performance is measured by Inter Symbol Interference (ISI) [37], convergence speed (number of iterations required for convergence), and Symbol Error Rate (SER). The ISI is given by the following expression:

$$\mathrm{ISI} = \frac{1}{2\mathrm{N}}\sum_{m}\left(\sum_{n}\frac{|p_{mn}|^2}{(\max|\mathrm{P_m}|)^2}-1\right)+\frac{1}{2\mathrm{N}}\sum_{n}\left(\sum_{m}\frac{|p_{mn}|^2}{(\max|\mathrm{P_n}|)^2}-1\right) \qquad (9.37)$$

Where, N is the length of the weight vector w, $\mathrm{P} = w^H VA$ is the permutation matrix with coefficients p_{mn}, max $|\mathrm{P_m}|$ and max $|\mathrm{P_n}|$ are the absolute maximum values of the *m*th row and *n*th columns of P respectively. In all the simulations, the performance is averaged over 100 montecarlo runs for a processing block length L of 1000 symbols.

The ISI measured in dB, number of iterations required for convergence, and SER achieved by the Complex OBA-ICA are illustrated in **Figs**. 77, 78, and 79, respectively.

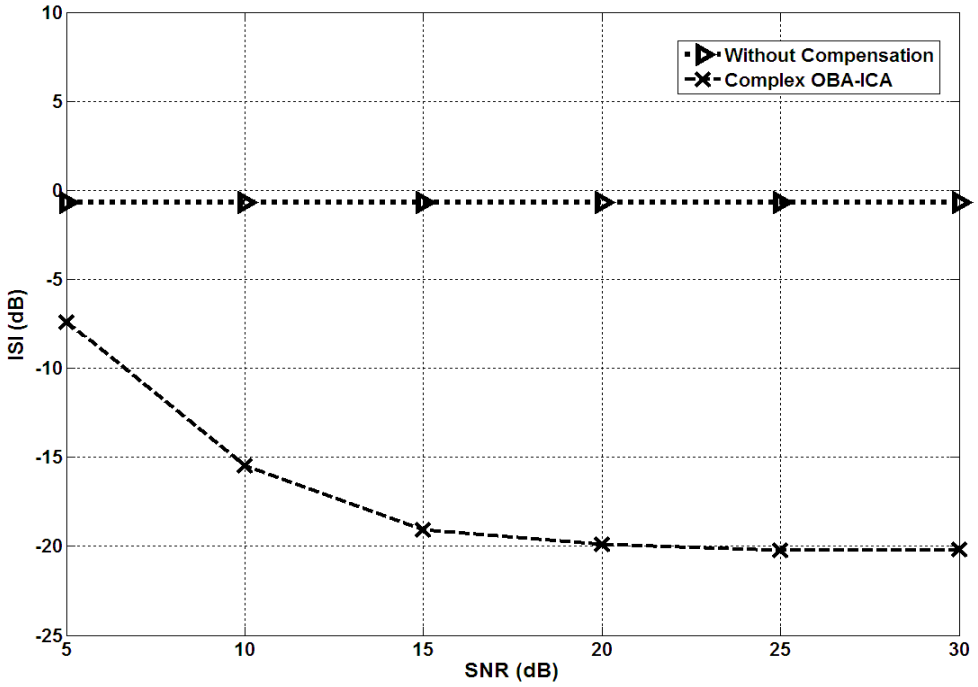

Figure 77: ISI (dB) vs. SNR (Δ =1.15×10^{-6}, e_1 = 0.3, e_2 = 0.35)

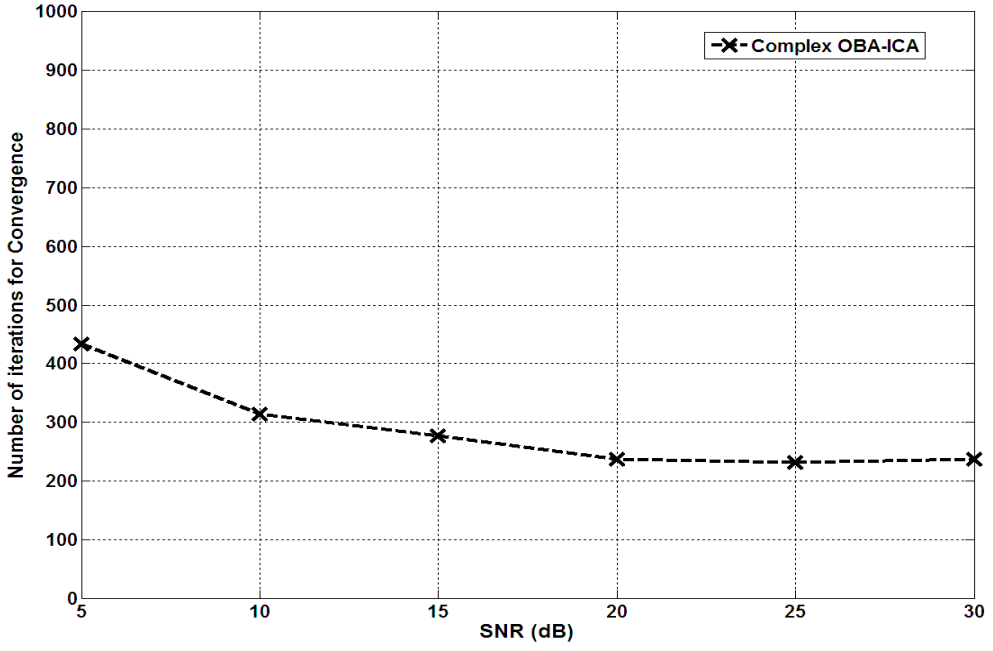

Figure 78: Convergence speed vs. SNR (Δ =1.15×10^{-6}, e_1 = 0.3, e_2 = 0.35)

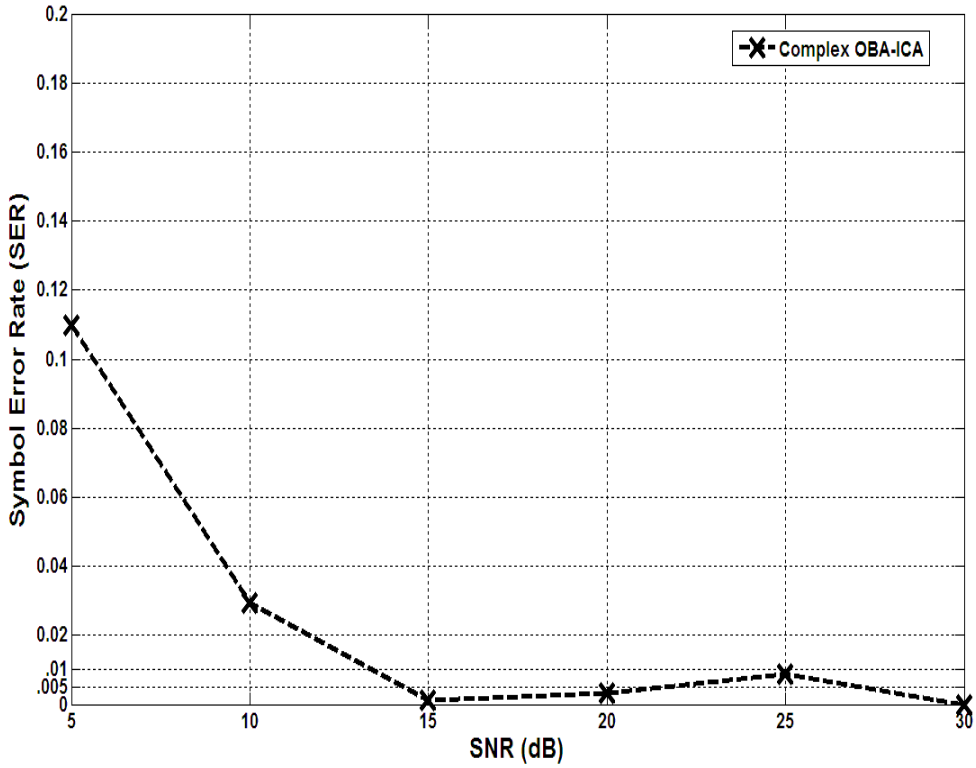

Figure 79: SER vs. SNR (Δ =1.15×10^{-6}, e_1 = 0.3, e_2 = 0.35)

In the second set of experiments, the performance is obtained for different channel variation parameters. Here, Δ is varied between 1.1×10^{-6} and 1.15×10^{-6}, with a step size of 1×10^{-8}. e_1 and e_2 are set as 0.3 and 0.35, respectively, and the SNR simulated is 20 dB. The ISI (dB), the speed of convergence and SER achieved are shown in **Figs**. 80, 81 and 82, respectively.

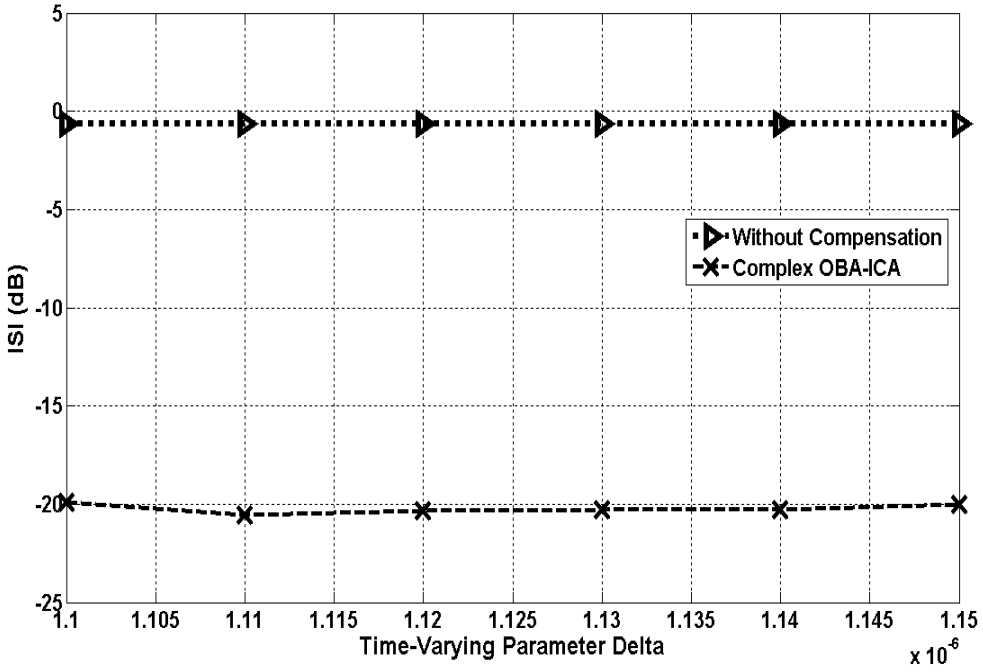

Figure 80: ISI (dB) vs. Δ (SNR=20 dB, $e_1 = 0.3$, $e_2 = 0.35$)

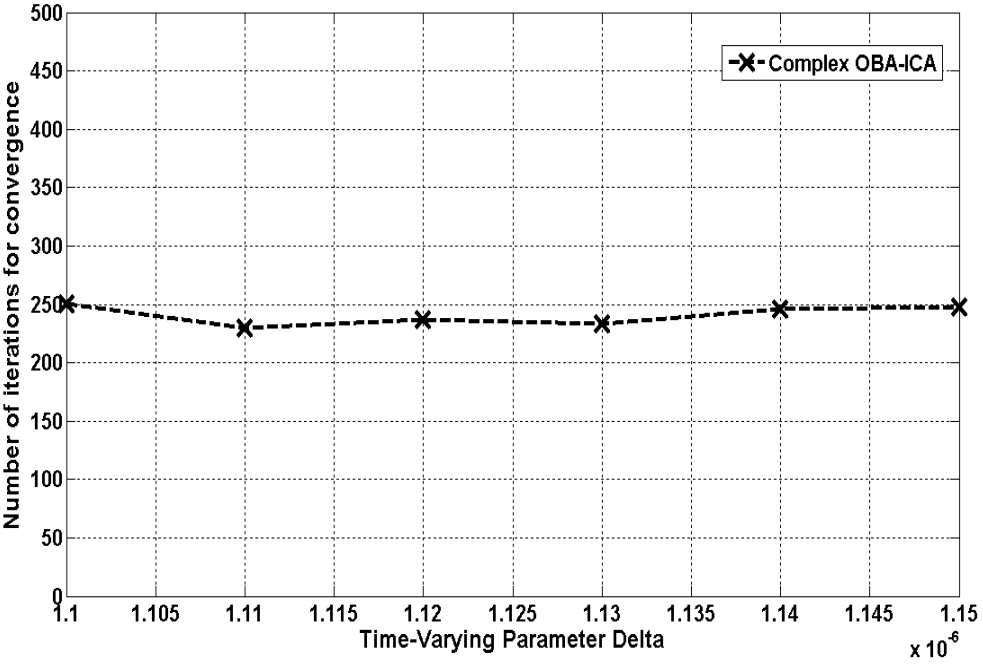

Figure 81: Convergence speed vs. Δ (SNR=20 dB, $e_1 = 0.3$, $e_2 = 0.35$)

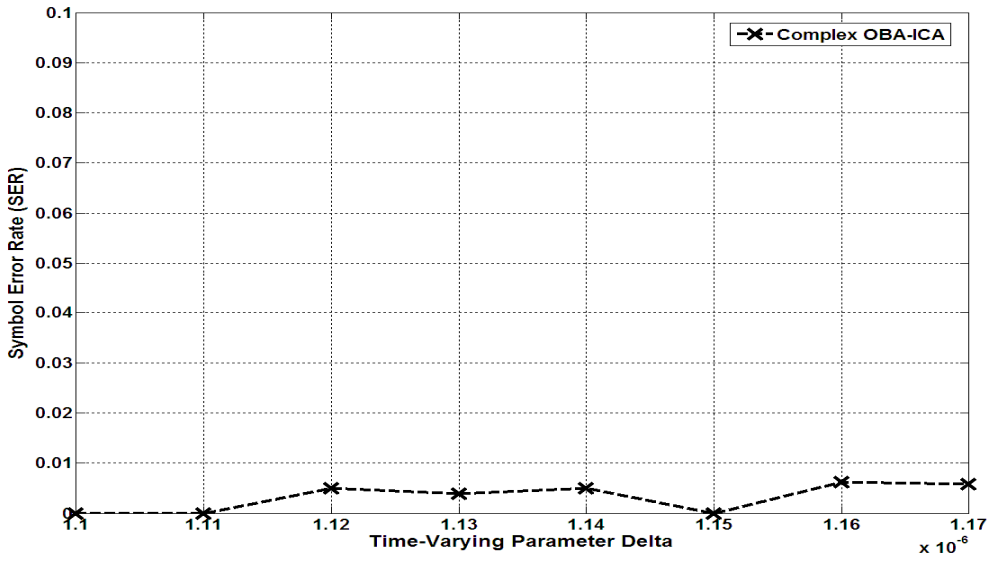

Figure 82: SER vs. Δ (SNR=20 dB, $e_1 = 0.3$, $e_2 = 0.35$)

e_1	e_2
-0.4	-0.45
-0.3	-0.35
-0.2	-0.25
-0.1	-0.15
-0.05	-0.1
0	0
0.05	0.1
0.1	0.15
0.2	0.25
0.3	0.35
0.4	0.45

Table 2: CFO's simulated between the transmitter and receiver

In the third set of experiments, different CFO's are simulated with $\Delta = 1.14\times10^{-6}$ and SNR =20 dB. The values of e_1 and e_2 used in the simulations are shown above in **Table** 2. The resulting ISI (dB), convergence speed in iterations, and SER achieved, are shown in **Figs.** 83, 84 and 85, respectively.

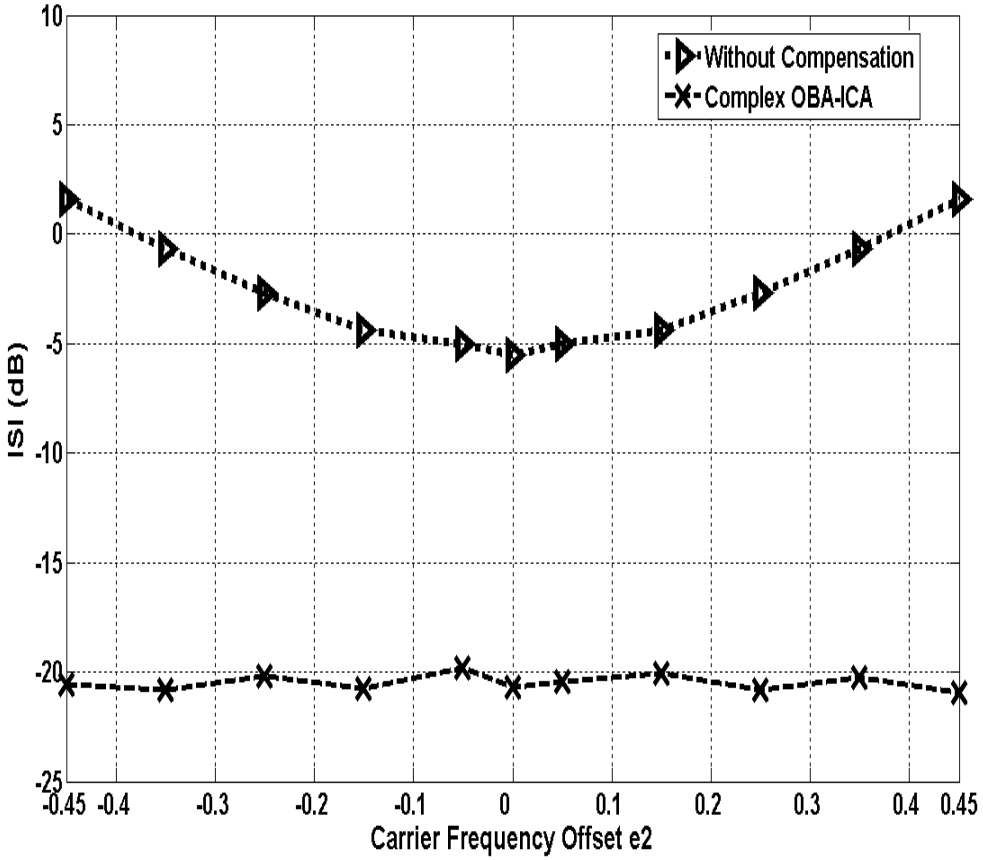

Figure 83: ISI (dB) vs. e_1 and e_2 (Table. 1) with SNR=20 dB, $\Delta = 1.14\times10^{-6}$

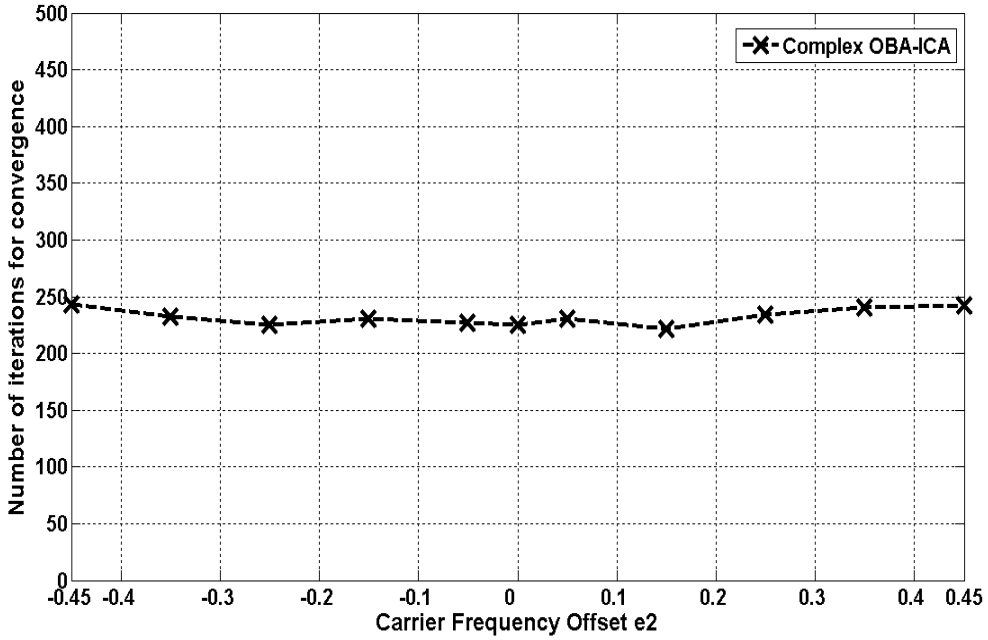

Figure 84: Convergence speed vs. e_1 and e_2 (Table. 1) with SNR = 20 dB, $\Delta = 1.14\times10^{-6}$

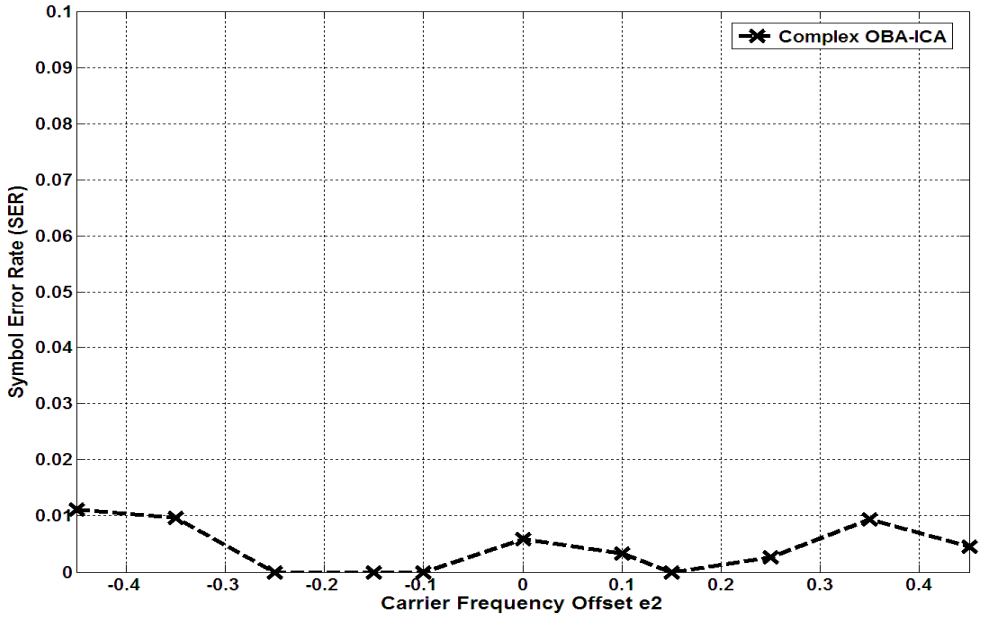

Figure 85: SER(dB) vs. e_1 and e_2 (Table. 1) with SNR=20 dB, $\Delta = 1.14\times10^{-6}$

The simulation results clearly show that the Complex OBA-ICA is able to successfully recover the user symbols in time-varying channels, with the presence of CFO.

9.5 Conclusions

In this chapter, a novel approach is proposed to perform CFO mitigation and multi-user detection simultaneously in MIMO-OFDM systems operating in a time-variant environment. The recently proposed Complex OBA-ICA is adopted as the leading technique. The performance of the proposed method is tested for different values of SNR, CFO, and channel time-varying parameter. Simulation results indicate that the new technique is highly effective in reducing ISI and achieving satisfying SER with reasonable computational requirement under various conditions.

CHAPTER TEN: CONTRIBUTIONS AND FUTURE RESEARCH DIRECTIONS

The research presented in this dissertation describes novel adaptive digital signal processing techniques for processing complex-valued signals. The developed techniques treat the complex-valued adaptive system coefficients as a combination of two independent real quantities. As a result, the real and imaginary components of the adaptive system parameters are independently updated at each iteration by employing optimally derived step-sizes or convergence factors. In this chapter, the major contributions of the research are given, and future research directions are outlined.

10.1 Major Contributions

As a result of increased demands for bandwidth, complex modulation schemes like QPSK, QAM are frequently adopted in wireless communications. Furthermore, signal processing operations such as equalization, channel estimation, and interference suppression are efficiently performed in the digital domain at the receiver. Hence, it necessitates the need for accurate and fast-converging complex digital signal processing algorithms. In this research, novel complex adaptive digital signal processing algorithms for interference suppression, channel estimation and beamforming were proposed that satisfy this requirement. An outline of the contributions is given below.

In Chapter Three, a novel Complex ICA algorithm with Individual Adaptation (Complex IA-ICA) was proposed. The Complex IA-ICA independently updated each real and imaginary component of the complex adaptive filter weight using separate convergence factors. The cost function used was the absolute value of the kurtosis, which

is maximized to achieve separation of the desired signal from an interfering signal. Simulation results showed that the Complex IA-ICA achieved excellent accuracy and fast convergence, even in dynamic flat fading channel conditions, in contrast to the existing Complex FastICA algorithm.

In Chapter Four, the formulation of the Complex OBA-ICA algorithm was presented which had reduced computational complexity as compared to the Complex IA-ICA. This was achieved by deriving only two optimal convergence factors, one for all the real components, and the other for all the imaginary components of the weights, as opposed to the Complex IA-ICA, which employed one convergence factor for each part of each weight.

In reality, the wireless receiver has prior information about the modulation scheme of the desired signal. Hence, the corresponding kurtosis value which has to be achieved is readily known. Using this information, a modification of the Complex OBA-ICA algorithm was proposed for separating complex-valued signals with known source distributions. In dynamic environments for diversity QPSK receivers, the proposed methods exhibited much better convergence properties, as compared to the Complex FastICA.

Chapter Five described the principle of conjugate gradients and its application to Complex Adaptive ICA for maximization of the kurtosis function. The resulting novel technique was called Complex Block Conjugate Independent Component Analysis (CBC-ICA). The CBC-ICA derived independent conjugate-gradient search directions for the real and imaginary components of the weight vector. In addition, by using the Taylor's series approximation, an optimal update or step size was generated separately

along each conjugate direction for the real and imaginary components. In dynamic flat fading conditions, the CBC-ICA demonstrated excellent convergence speed, even for large processing block sizes, while maintaining satisfactory SER.

Chapter Six presented the formulations for novel complex adaptive LMS algorithms that independently update the real and imaginary parts of the adaptive filter coefficients at each block iteration. In addition, the optimal convergence factors were automatically derived at each iteration, for the real and imaginary components of the complex adaptive filter coefficients. For block processing of input signal samples, the algorithms were called Complex Optimum Block Adaptive LMS (Complex OBA-LMS) and Complex Optimum Block Adaptive LMS with Individual Adaptation (Complex OBAI-LMS). For sequential processing, the developed techniques were called Complex LMS with Homogeneous Adaptation (Complex HA-LMS), and Complex LMS with Individual Adaptation (Complex IA-LMS). In the Complex OBA-LMS and Complex HA-LMS, two optimal convergence factors were separately derived at each iteration, one for all the real components, and one for the imaginary components of the complex adaptive filter coefficients. On the other hand, the Complex OBAI-LMS and Complex IA-LMS derived a unique convergence factor for each component of each complex adaptive filter weight. As a result, they efficiently utilized all the degrees of freedom of the adaptive filter at the cost of a modest increase in computational complexity. Furthermore, a matrix inversion lemma was utilized that significantly reduced the computational complexity of the Complex OBAI-LMS, resulting in two modifications called the Complex OBAI (1), and Complex OBAI (2) algorithms.

In Chapter Seven, the proposed optimum block algorithms, namely Complex OBA-LMS and Complex OBAI-LMS, were applied to system identification for wireless communications. Simulation results confirmed that a significant improvement in convergence speed and accuracy was achieved by the proposed techniques over the block Complex LMS. In addition, this improvement was achieved without having to manually select the convergence factor for different inputs, in contrast to the block Complex LMS which easily diverged for an incorrect choice of the convergence factor.

In Chapter Eight, the previously proposed complex least mean square algorithms employing time-varying convergence factors were applied to adaptive beamforming. The Complex OBA-LMS and Complex OBAI-LMS were applied when the signal is processed in blocks, and the Complex HA-LMS and Complex IA-LMS were employed when sequential processing is adopted at the beamforming receiver. The performance of these techniques was compared to the block and sequential versions of the Complex LMS algorithm. In contrast to the Complex LMS, simulation results showed that the proposed methods exhibit improved convergence speed and accuracy, irrespective of the flat fading channel parameters, number of antenna elements, and type of modulation employed by the users.

Chapter Nine addressed the InterCarrier Interference (ICI) problem caused by Carrier Frequency Offset (CFO) between local oscillators in the transmitter and the receiver in multi-user MIMO-OFDM systems. In this regard, the previously proposed Independent Component Analysis (ICA) technique called Complex Optimum Block Adaptive ICA (Complex OBA-ICA) was employed to recover user signals in the presence of ICI, and channel induced mixing in time-varying frequency selective channel

environments. The presented simulation results indicated that the new technique significantly reduces Inter Symbol Interference (ISI) and Symbol Error Rate (SER) in multi-user MIMO-OFDM systems in dynamic channel environments.

10.2 Future Research Directions

The research work described in this dissertation can be extended in several directions.

10.2.1 Hybrid ICA-LMS algorithm using Lagrange Multipliers

The integration of voice and high-speed data services has led to increased demands for wireless systems that offer higher data rates, and basestations with higher capacity to support more users. Smart antennas technology in conjunction with adaptive beamforming offers a promising solution to reduce interference levels and improve the system capacity [75, 95]. Through adaptive beamforming, the basestation can form narrower beams towards the desired user and nulls towards interfering users, considerably improving the signal-to-interference-plus-noise ratio.

In this dissertation, novel block and sequential LMS algorithms with improved convergence speed and accuracy were developed for adaptive beamforming. However, the performance of any beamforming algorithm starts deteriorating when the number of interfering users is much larger than the number of antenna elements at the receiver. In order to remove this limitation, the concept of Lagrange Multipliers [96] may be applied to develop a hybrid ICA-LMS algorithm that employs both the kurtosis and mean square error cost functions. The hybrid ICA-LMS may have faster convergence and accuracy

than existing methods, even in a high interference scenario. This would significantly help improve system capacity and reduce network costs.

10.2.2: Natural-Gradient ICA algorithm for Dynamic Frequency Selective Fading Channels

The Natural-Gradient algorithm is a highly accurate algorithm to perform ICA of signals in convolutive mixing scenarios [97-99]. However, the main drawback of the Natural-Gradient technique is its slow convergence. Furthermore, ICA of signals in time-varying frequency-selective channels continues to be a challenging area of research. A possible solution to this problem could be to develop an improved Natural-Gradient algorithm that utilizes the techniques of optimal and independent convergence factors developed in this dissertation. The new algorithm may exhibit improved convergence speed, even in dynamic frequency selective fading channels, while retaining the accuracy of the Natural-Gradient method.

10.2.3: Conjugate Gradient LMS algorithm with optimal convergence factors

The conjugate gradient method [67, 68] continues to be a versatile tool in various adaptive filtering and wireless communication applications [100,101], due its unique tradeoff between convergence speed and computational complexity. In Chapter Five, the CBC-ICA algorithm was developed which employs the conjugate gradient method for maximization of the kurtosis function. A similar approach can be used to develop a Conjugate Gradient LMS algorithm with optimally derived step-sizes along each conjugate direction, to achieve faster convergence.

APPENDIX: MATRIX INVERSION LEMMA

In [102, 103], it has been shown that the matrix inversion lemma can be applied to invert an N x N matrix $[R]_k$ in the k th iteration, provided it contains the $(N-1)$ x $(N-1)$ section of the matrix in the $(k-1)$ th iteration, i.e. $[R]_{k-1}$. The description of the lemma proceeds as follows:

The N x N matrix $[R]_k$ is partitioned into sub-matrices as

$$[R]_k = \left[\begin{array}{c|c} \overline{R}_{11}(k) & \overline{R}_{12}(k) \\ \hline \overline{R}_{12}^{T}(k) & \overline{R} \end{array}\right] \tag{A.1}$$

where, $\overline{R}_{11}(k)$ is a scalar, $\overline{R}_{12}(k)$ is a 1 x $(N-1)$ row vector, and $\overline{R}$ is a $(N-1)$ x $(N-1)$ square matrix. Since, $[R]_{k-1}$ is also known, it is partitioned in the following manner.

$$[R]_{k-1} = \left[\begin{array}{c|c} \overline{R} & \hat{R}_{12}(k-1) \\ \hline \hat{R}_{12}^{T}(k-1) & \hat{R}_{22}(k-1) \end{array}\right] \tag{A.2}$$

where, $\hat{R}_{12}(k-1)$ is a $(N-1)$ x 1 column vector, $\hat{R}_{22}(k-1)$ is a scalar, and $\overline{R}$ is a matrix defined in A.1.

Since the lemma recursively computes the matrix inverse, it is applied to find $[R]_k^{-1}$, knowing $[R]_{k-1}^{-1}$ which is expressed as

$$[R]_{k-1}^{-1} = \left[\begin{array}{c|c} \alpha_{11} & \alpha_{12} \\ \hline \alpha_{12}^{T} & \alpha_{22} \end{array}\right] \tag{A.3}$$

Where, α_{22} is a scalar, α_{12} is a $(N-1)$ x 1 vector, and α_{11} is a $(N-1)$ x $(N-1)$ matrix.

Since $[R]_k$, $[R]_{k-1}$, and $[R]_{k-1}^{-1}$ in (A.1), (A.2), and (A.3), respectively are already known, the matrix inversion lemma uses this information to compute $[R]_k^{-1}$, which can be expressed as

$$[R]_k^{-1} = \left[\begin{array}{c|c} \beta_{11} & \beta_{12} \\ \hline \beta_{12}^T & F \end{array}\right] \tag{A.4}$$

where,

$$\beta_{11} = \frac{1}{\overline{R}_{11}(k)} + \frac{1}{\overline{R}_{11}^2(k)} \overline{R}_{12}(k) F \overline{R}_{12}^T(k) \tag{A.5}$$

$$\beta_{12} = - \frac{1}{\overline{R}_{11}(k)} \overline{R}_{12}(k) F \tag{A.6}$$

and

$$F = [\overline{R} - \frac{1}{\overline{R}_{11}(k)} \overline{R}_{12}^T(k) \overline{R}_{12}(k)] \tag{A.7}$$

The inverse of the $(N-1)$ x $(N-1)$ matrix F is computed using the following lemma

$$F = \overline{R}^{-1} - \overline{R}^{-1} \overline{R}_{12}^T(k) C \overline{R}_{12}(k) \overline{R}^{-1} \tag{A.8}$$

where,

$$C = [\overline{R}_{12}(k) \overline{R}\, \overline{R}_{12}^T(k) - \overline{R}_{11}(k)]^{-1} \tag{A.9}$$

and

$$\overline{R}^{-1} = \alpha_{11} [I - \hat{R}_{12}(k-1) \alpha_{12}^T]^{-1} \tag{A.10}$$

I being the identity matrix. Applying another matrix inversion lemma the inverse in (A.10) can be obtained as follows

$$\overline{R}^{-1} = \alpha_{11}\{I + \hat{R}_{12}(k-1)\alpha_{12}^{T} / [1 - \alpha_{12}^{T}\hat{R}_{12}(k-1)]\} \qquad \text{(A.11)}$$

From (A.11), it can be easily seen that $\overline{R}^{-1}$ can be calculated using only matrix algebra. In this manner, (A.4)-(A.11) can be used to find the inverse of the matrix $[R]_k$, with reduced computational complexity.

LIST OF REFERENCES

[1] Ken Martin, “Complex signal processing is not-complex," in *Proc. of the 29th European Solid-State Circuits Conference (ESSCIRC '03)*, pp. 3-14, 16-18 Sept. 2003.

[2] J. Crols and M. Steyaert, “Low-IF Topologies for High-Performance Analog Front Ends of Fully Integrated Receivers,” *IEEE Transactions on Circuits and Systems-II*, Vol. 45, No. 3, pp. 269-282, Mar. 1998.

[3] G. R. Lang and P.O. Brackett, “Complex Analogue Filters,” in *Proc. of the European Conference on Circuit Theory and Design*, pp. 412-419, 1981.

[4] A. Sedra, W. Snelgrove, and R. Allen, “Complex Analog Bandpass Filters Designed by Linearly Shifting Real Low-Pass Prototypes,” in *Proc. of Int. Symp. on Circuits and Systems (ISCAS’ 85)*, Vol. III, pp. 1223-1226, 1985.

[5] W.M. Snelgrove, A.S. Sedra, G.R. Lang, and P.O. Brackett, “Complex Analog Filters,”1981, Tech. Report in Electrical Engineering Dept., Univ. Toronto.

[6] C. Cuypers, N. Voo, M. Teplechuk, and J. Sewell, “The General Synthesis of Complex Analogue Filters,” in *Proc. of the 9’th Intl. Conference on Electronics., Circuits, and Systems*, Vol. 1, pp. 153-156, 2002.

[7] P. Kong-pang, J.E. Franca, C. Azeredo-Leme, “A Quadrature Sampling Scheme with Improved Image Rejection for Complex-IF Receivers,” in *Proc. IEEE Intl. Symp. on Circuits and Systems (ISCAS)*, pp. 45-48, May 2001.

[8] S. Jantzi, K. Martin, and A.S. Sedra, "The effects of Mismatch in Complex Bandpass $\sum\Delta$ Modulators," in *Proc. IEEE Intl. Symp. on Circuits and Systems (ISCAS)*, pp. 227-230, May 1996.

[9] E. Buracchini, "The Software Radio Concept", *IEEE Communications Magazine*, September 2000.

[10] R. Boite and H. Leich, "On Digital Filters with Complex Coefficients," in *Network and Signal Theory* (edited by J.K. Skwirzynski and J.O. Scanlan), pp. 344-351, Peter Peregrinus, London, 1973.

[11] A.V. Oppenheim and R.W. Schafer, *Digital Signal Processing*, Prentice-Hall, 1975.

[12] L. Yu and W.M. Snelgrove, "A Novel Adaptive Mismatch Cancellation System for Quadrature IF Radio Receivers", in *IEEE Transactions on Circuits and Systems-II*, Vol. 46, No. 6, pp. 789-801, Jun. 1999.

[13] M. Valkama and M. Renfors, "Advanced Methods for I/Q Imbalance Compensation in Communication Receivers," in *IEEE Transactions. on Signal Processing*., Vol. 49, No. 10., pp. 2335-2334, Oct. 2001.

[14] Simon Haykin, *Adaptive Filter Theory*, Prentice-Hall, 2001.

[15] Bernard Widrow and Samuel Stearns, *Adaptive Signal Processing*, Prentice-Hall, 1985.

[16] A.J Paulraj, D.A Gore, R.U Nabar, H.Bolcskei, "An Overview of MIMO Communications—A Key to Gigabit Wireless," in *Proc. of the IEEE*, Vol. 92, No. 2, pp. 198-218, Feb. 2004.

[17] A. Goldsmith, A.S. Jafar, N. Jindal, S. Vishwanath, "Capacity limits of MIMO channels", in *IEEE Journal on Selected Areas in Communications*, Vol. 21, No.5, pp. 684-702, June 2003.

[18] D. Gesbert, M. Shafi, D. Shiu, P.J. Smith, A. Naguib, "From Theory to Practice: An overview of MIMO space-time coded wireless systems", in *IEEE Journal on Selected Areas in Communications*, Vol. 21, No.3, pp. 281-302, April 2003.

[19] Ezio Biglieri, Robert Calderbank, Anthony Constantinides, Andrea Goldsmith, Arogyaswami Paulraj, and H. Vincent Poor, *MIMO Wireless Communications*, Cambridge University Press, 2007.

[20] G.L. Stuber, J.R. Barry, S.W. Mclaughlin, Y.G. Li, M.A. Ingram, T.G. Pratt, "Broadband MIMO-OFDM wireless communications", in *Proc. of the IEEE*, Vol. 92, No. 2, pp. 271-294, Feb. 2004.

[21] Sanjiv Nanda, Rod Walton, John Ketchum, Mark Wallace, and Steven Howard, "A High-Performance MIMO OFDM Wireless LAN", *IEEE Communications Magazine*, Vol. 43, No. 2, pp. 101-109, Feb. 2005.

[22] James M. Wilson. "The Next Generation of Wireless LAN Emerges with 802.11n", *Technology@Intel Magazine*, August 2004.

[23] Marvin Kenneth Simon, Mohamed-Slim Alouini, *Digital Communication Over Fading Channels*, Wiley-Interscience, 2005.

[24] Theodore S. Rappaport, *Wireless Communications: Principles and Practice*, Prentice Hall, 2001.

[25] Ahmad R. S. Bahai, Burton R. Saltzberg, and Mustafa Ergen, *Multi-carrier digital communications: Theory and Applications of OFDM*, Springer, 2004.

[26] M.Valkama, M. Renfors, and V. Koivunen, “Advanced Methods for I/Q Imbalance Compensation in Communication Receivers”, in *IEEE Trans. Signal Processing*, Vol. 49, No. 10, pp. 2335-2344, October 2001.

[27] M. Valkama, K. Salminen, and M. Renfors, "Digital I/Q imbalance compensation in low-IF receivers: principles and practice," in *14th International Conference on Digital Signal Processing, (DSP 2002)*, Vol.2, pp. 1179-1182 , July 2002.

[28] L. Anttila, M. Valkama, and M. Renfors, "Gradient-based blind iterative techniques for I/Q imbalance compensation in digital radio receivers," in *IEEE 8th Workshop on Signal Processing Advances in Wireless Communications, (SPAWC 2007)*, pp.1-5, June 2007.

[29] I. Kostanic and W. Mikhael, “Blind source separation technique for the reduction of co-channel interference”, in *IEE Electronics Letters*, Vol. 38, No. 20, pp. 1210-1211, September 2002.

[30] I. Kostanic and W. Mikhael, “Rejection of the Co-Channel Interference Using Non-Coherent Independent Component Analysis Based Receiver”, in *Proc. of the 45th IEEE International Midwest Symposium On Circuits and Systems*, Vol. 2, pp. 621-624, August 2002.

[31] W.Mikhael, and T.Yang, “Optimum Block Adaptive Algorithm for Gradient Based Independent Component Analysis(OBA/ICA) for Time Varying Wireless Channels”, in *Proc. 62nd IEEE Vehicular Technology Conference*, Vol. 4, pp. 2240 – 2243, Sept, 2005.

[32] W.Mikhael, and T.Yang, “A Gradient-Based Optimum Block Adaptation ICA Technique for Interference Suppression in Highly Dynamic Communication

Channels", in *EURASIP Journal on Applied Signal Processing*, Vol. 2006, pp.1-10.

[33] T. Yang, W. Mikhael, "ICA-based Interference Rejection for Diversity Receivers in Non-Stationary Channels", in *IASTED International Conference on Circuits, Signals and Systems (CSS 2004),* Clearwater Florida, November 2004.

[34] R.Ranganathan, W.B Mikhael and T.Yang, "An Optimum Block Adaptive ICA Algorithm with Individual Adaptation for Wireless QAM Receivers in Dynamic Environments", in *The 49th IEEE Midwest Symposium on Circuits and Systems (MWSCAS '06)*, Vol. 1, pp. 146-149, Puerto Rico, August, 2006.

[35] R. Ranganathan and W.B Mikhael, "A Novel Interference Suppression Technique employing Complex Adaptive ICA for Time-Varying Channels in Diversity Wireless QAM Receivers", in *IEEE International Symposium on Circuits and Systems (ISCAS'07)*, pp. 101-104, New Orleans, Louisiana, USA, May, 2007.

[36] R. Ranganathan and W.B Mikhael, "Fast-converging complex adaptive algorithm for diversity wireless receivers in linearly fading channels", in *IEE Electronics Letters*, Vol. 42, Issue 15, pp. 886-887, July 2006.

[37] R. Ranganathan and W.B. Mikhael, "A Comparative Study of Complex Gradient and Fixed-Point ICA algorithms for Interference Suppression in Static and Dynamic Channels", in *Signal Processing*, Vol. 88, Issue 2, pp.399-406, February 2008.

[38] R. Ranganathan, T. Yang and W.B Mikhael, " Separation of Complex Signals with Known Source Distributions in Time-Varying Channels using Optimum Complex Block Adaptive ICA", in *The 50th IEEE Midwest Symposium on*

Circuits and Systems (MWSCAS '07), pp. 361-364, Montreal, Canada, August, 2007.

[39] R. Ranganathan, T. Yang and W. B Mikhael, "Adaptive ICA for Separation of Complex Signals with Known Source Distributions in Time-Varying Channels", in *IET Electronics Letters*, Vol. 43, Issue 15, pp. 838-839, July 2007.

[40] B. Widrow, J. McCool, and M. Ball, "The complex LMS algorithm", in *Proceedings of the IEEE*, Vol. 63, No. 4, pp. 719–720, April 1975.

[41] M. Chakraborty, and H. Sakai, "Convergence analysis of a complex LMS algorithm with tonal reference signals", in *IEEE Transactions on Speech and Audio Processing*, Vol. 13, No. 2, pp. 286–292, March 2005.

[42] R. Assaf, S.E. Assad, and Y. Harkouss, "Adaptive equalization for digital channels RBF neural network", in *European Conference on Wireless Technology*, pp. 347–350, 3–4 October 2005.

[43] W.B Mikhael, and R.Ranganathan, "Complex FIR Block Adaptive digital filtering algorithm with Independent Adaptation of Real and Imaginary Filter Parameters", in *The 51st IEEE Midwest Symposium on Circuits and Systems (MWSCAS '08)*, Knoxville, Tennessee, USA, August 10-13, 2008 (Accepted May, 2008).

[44] W.B Mikhael and R. Ranganathan, "Complex FIR Block Adaptive algorithm employing Optimal Time-Varying Convergence Factors", in *IEEE NEWCAS-TAISA* '08, Montreal, Canada, June 22-25, 2008 (Accepted March, 2008).

[45] R.Ranganathan, and W.B. Mikhael “Complex Adaptive FIR Digital Filtering Algorithm with Time-Varying Independent Convergence Factors”, in *Signal Processing*, Vol. 88, Issue 7, pp. 1889-1893, July 2008.

[46] W.B. Mikhael and R.Ranganathan, “Complex Optimum Block based LMS algorithm with Individual Adaptation of Parameters”, Submitted to *Signal Processing*, September, 2008.

[47] P.Comon, “Independent Component Analysis- a new concept?” in *Signal Processing*, Vol.36, pp. 287-314, 1994.

[48] T. W. Lee, M. Girolami, and T. J. Sejnowski, "Independent component analysis for mixed sub-gaussian and supergaussian sources," in *Neural Computation*, Vol. 11, No. 2, pp. 417-442, 1999.

[49] A.Hyvrinen, and E.Oja, “One-unit learning rules for independent component analysis”, in *Advances in Neural Information Processing Systems*, The MIT Press, Cambridge, Massachusetts, 1997.

[50] A. Hyvarienen, J. Karhunen and E. Oja, *Independent Component Analysis*, John Wiley and Sons, 2001.

[51] Dinh Tuan Pham, "Blind separation of instantaneous mixture of sources via an independent component analysis," in *IEEE Transactions on Signal Processing,* Vol.44, No.11, pp. 2768-2779, Nov 1996.

[52] T. W. Lee, M. S. Lewicki, and T. J. Sejnowski, “ICA mixture models for unsupervised classification of non-gaussian sources and automatic context switching in blind signal separation”, in *IEEE Transactions on Pattern Recognition and Machine Intelligence*, Vol. 22, No. 10, pp. 1-12, 2000.

[53] S.I. Amari, S. C. Douglas, A. Cichocki, and H. H. Yang, "A new learning algorithm for blind signal separation," in *Advances in Neural Information Processing Systems*, Vol. 8, pp. 757--763, 1996.

[54] K. Kiviluoto, and E. Oja, " Independent Component Analysis for parallel financial time-series", in *Proc. International Conf. On Neural Information Processing (ICONIP '98)*, Vol. 2, pp. 895-898, Tokyo Japan, 1998.

[55] J. Porill, J.W. Stone, J. Berwick, J. Mayhew, and P. Coffey, "Analysis of optical imaging data using weak models and ICA", in *Advances in Independent Component Analysis*, pp. 217-233, Springer-Verlag, 2000.

[56] R. Vigario, J. Sarela, V. Jousmiki, M. Hamalainen, and E. Oja, "Independent component approach to the analysis of EEG and MEG recordings," in *IEEE Transactions on Biomedical Engineering* , Vol.47, No.5, pp. 589-593, May 2000.

[57] T. Ristaniemi, and J. Joutsensalo, "Advanced ICA-based receivers for DS-CDMA systems," in *The 11th IEEE International Symposium on Personal, Indoor and Mobile Radio Communications (PIMRC 2000)*, Vol.1, pp.276-281, 2000.

[58] R. Cristescu, T. Ristaniemi, J. Joutsensalo, and J. Karhunen," Blind separation of convolved mixtures for CDMA systems", in *Proc. Tenth European Signal Processing Signal Processing Conference (EUSIPCO '2000)*, pp. 619-622, Tampere, Finland, 2000.

[59] D.L. Donoho, "Nature vs. Math: Interpreting Independent Component Analysis in light of recent work in harmonic analysis", in *Proc. Int. Workshop on Independent Component Analysis and Blind Signal Separation (ICA 2000)*, pp. 459-470, Helsinki, Finland, 2000.

[60] A. Hyvarinen, P.O. Hoyer, and E. Oja, “Image Denoising by Sparse Code Shrinkage”, in *Intelligent Signal Processing*, IEEE Press, 2001.

[61] A. Hyvarinen, “ Fast and robust fixed-point algorithms for independent component analysis”, in *IEEE Transactions on Neural Networks*, Vol. 10, No.3, May 1999.

[62] A. Hyvärinen and E. Oja, “A fast fixed-point algorithm for independent component analysis”, in *Neural Computation*, Vol. 9, No.7, pp. 1483-1492, October 1997.

[63] E. Bingham, and A. Hyvarinen, ‘A Fast Fixed-Point algorithm for independent component analysis of Complex valued signals’, in *International Journal of Neural Systems,* Vol.10, No.1, pp. 1-8, Feb 2000.

[64] E. Bingham, and A Hyvarinen, "ICA of complex valued signals: a fast and robust deflationary algorithm," *Proceedings of the IEEE-INNS-ENNS International Joint Conference on Neural Networks (IJCNN 2000)*, Vol.3, pp. 357-362, 2000.

[65] R.Ranganathan and W.B. Mikhael, “Complex Adaptive ICA algorithm with Individual Adaptation for interference suppression in highly dynamic flat fading wireless environments” Submitted to *EURASIP Journal on Wireless Communications and Networking*.

[66] R.Ranganathan, T.Yang, and W.B. Mikhael, “Optimum Block Adaptive ICA for Separation of Real and Complex Signals With Known Source Distributions in Dynamic Flat Fading Environments”, Submitted to *Journal of Circuits, Systems and Computers (JSCC)*, Feb, 2008.

[67] G.K. Boray and M.D. Srinath, "Conjugate Gradient Techniques for Adaptive Filtering", in *IEEE Transactions. On Circuits and Systems*, Vol. 39, No. 1, pp. 1-10, 1992.

[68] Yousef Saad, *Iterative methods for sparse linear systems*, SIAM, 2003.

[69] J. Erhel, and F. Guyomarc'h, "An augmented Conjugate Gradient method for solving consecutive symmetric positive definite systems", in *SIAM Journal on Matrix Analysis and Applications*, Vol. 21, No. 4, pp. 1279–1299, 2000.

[70] L. Giraud, D. Ruiz, and A. Touhami, "A comparative study of iterative solvers exploiting spectral information for SPD systems", in *SIAM Journal on Scientific Computing*, Vol. 27, No. 5, pp. 1760–1786, 2006.

[71] W.B Mikhael, R. Ranganathan and T.Yang, "Novel Conjugate-Gradient Based Complex Adaptive ICA for Diversity QPSK Receivers in Time-Varying Channel Applications", in *IEEE Radio and Wireless Symposium*, pp. 527-530, Orlando, Florida, Jan 22-24, 2008.

[72] R.Ranganathan, W.B. Mikhael and T.Yang, "Complex Adaptive ICA employing the Conjugate Gradient principle for Signal Separation in Time-Varying Flat Fading Channels", Submitted to *Circuits, Systems & Signal Processing*, August 2008.

[73] R.Ranganathan and W.B Mikhael, "A Novel Digital Beamforming Technique based on Homogeneous Adaptation Employing Time-varying Convergence Factors", *IEEE Radio and Wireless Symposium*, (Accepted, September 2008).

[74] S. Chen, N.N Ahmad, and L. Hanzo, "Adaptive minimum bit-error rate beamforming," in *, IEEE Transactions on Wireless Communications*, Vol.4, No.2, pp. 341-348, March 2005.

[75] J. Li, and P. Stoica, eds, *Robust Adaptive Beamforming*, John Wiley & Sons, New York, NY, 2005.

[76] Seungwon Choi, Jinho Choi, Heung-Jae Im, and Byungcho Choi, "A novel adaptive beamforming algorithm for antenna array CDMA systems with strong interferers," in *IEEE Transactions on Vehicular Technology,* Vol.51, No.5, pp. 808-816, Sep 2002.

[77] M. Budsabathon, Y. Hara, and S. Hara, "Optimum beamforming for pre-FFT OFDM adaptive antenna array," in *IEEE Transactions on Vehicular Technology*, Vol.53, No.4, pp. 945-955, July 2004.

[78] S. Chen, S. Tan, and L. Hanzo, "Adaptive beamforming for binary phase shift keying communication systems". in *Signal Processing*, Vol. 87, No.1, pp. 68-78, 2007.

[79] M. S. Brandstein and D. B.Ward, Eds., *Microphone Arrays: Signal Processing Techniques and Applications*. Berlin: Springer-Verlag, 2001.

[80] J. Benesty, J. Chen, Y. Huang and J. Dmochowski, "On microphone array beamforming from a MIMO acoustic signal processing perspective," in *IEEE Transactions on Audio, Speech and Language Processing*, Vol. 15, No. 3, pp. 1053-1065, March 2007.

[81] R.Ranganathan, and W.B. Mikhael, "Efficient Adaptive Beamforming techniques employing novel complex block adaptive algorithms with optimally and

independently generated convergence factors", Submitted to *IEEE Transactions on Signal Processing*, October 2008.

[82] C. Dubuc, D. Starks, T. Creasy, and Yong Hou, "A MIMO-OFDM Prototype for Next-Generation Wireless WANS," in *IEEE Communications Magazine*, Vol. 42, No.12, pp. 82- 87, Dec. 2004.

[83] G. L. Stuber, J. R. Barry, S. W. Mclaughlin, Y. Li, M. A. Ingram, and T. G. Pratt, "Broadband MIMO-OFDM Wireless Communications," in *Proceedings of The IEEE*, Vol.92, No. 2, pp. 271-294, Feb. 2004.

[84] H. Yang, "A road to Future Broadband Wireless Access: MIMO-OFDM Based Air Interface," in *IEEE Communications Magazine*, Vol.43, No.1, pp.53-60, Jan. 2005.

[85] M. Morelli, A. N. D'Andrea, and U. Mengali, "Frequency Ambiguity Resolution in OFDM Systems," in *IEEE Communications Letters*, Vol. 4, No. 4, pp. 134-136, Apr. 2000.

[86] T. Pollet, M. V. Bladel, and M. Moeneclaey, "BER Sensitivity of OFDM System to Carrier Frequency Offset and Wiener Phase Noise," in *IEEE Transactions on Communications*, Vol. 43, No. 2/3/4, pp. 191-193, Feb/March/April 1995.

[87] J. Armstrong, "Analysis of New and Existing Methods of Reducing Intercarrier Interference Due to Carrier Frequency Offset in OFDM," in *IEEE Transactions on Communications*, Vol. 47, No. 3, pp. 365-369, Mar. 1999.

[88] M. Luise, and R. Reggiannini, "Carrier Frequency Acquisition and Tracking for OFDM Systems," in *IEEE Transactions on Communications*, Vol. 44, No. 11, pp.1185-1191, Nov. 1996.

[89] G. Santella, “A Frequency and Symbol Synchronization System for OFDM Signals: Architecture and Simulation Results,” in *IEEE Transactions on Vehicular Technology*, Vol. 49, No.1, pp. 254-275, Jan. 2000.

[90] B. Chen, and H. Wang, “Blind Estimation of OFDM Carrier Frequency Offset via Oversampling,” in *IEEE Transactions on Signal Processing*, Vol. 52, No. 7, pp. 2047-2057, July 2004.

[91] T. M. Schmidl, and D. C. Cox, “Blind Synchronization for OFDM,” in *IEE Electronics Letters*, Vol.33, No. 2, pp.113-114, Feb. 1997.

[92] H. Liu, and U. Tureli, “A High-Efficiency Carrier Estimator for OFDM Communications,” in *IEEE Communications Letters*, Vol. 2, No. 4, pp. 104-106, Apr. 1998.

[93] Y. Liu, and W. Mikhael, “A Blind Maximum Likelihood Carrier Frequency Offset Correction Approach for OFDM Systems over Multipath Fading Channels,” in *Journal of Circuits, Systems, and Signal Processing*, Vol. 26, No. 1, pp. 43-54, Feb. 2007.

[94] Y. Liu, and W. Mikhael, "Blind carrier frequency offset estimation for OFDM systems based on kurtosis," in *48th Midwest Symposium on Circuits and Systems,* Vol. 1, pp. 127-130, August 2005.

[95] Altera, http://www.altera.com/end-markets/wireless/advanceddsp/beamforming, “Smart Antennas-Beamforming”.

[96] D. P. Bertsekas, *Constrained Optimization and Lagrange Multiplier Methods,* New York: Academic, 1982.

[97] Shun-ichi Amari, Andrzej Cichocki, and H. H. Yang, “A New Learning Algorithm for Blind Signal Separation,” in *Advances in Neural Information Processing Systems*, Vol. 8, pp. 757-763, 1996.

[98] Shun-ichi Amari, “Natural Gradient Works Efficiently in Learning,” in *Neural Computation*, Vol. 10, pp. 251-276, Feb. 1998.

[99] Shun-ichi Amari, T-P. Chen, and Andrzej Cichocki, “Stability Analysis of Learning Algorithms for Blind Source Separation,” in *Neural Networks*, Vol. 10, No. 8, pp. 1345–1351, August 1997.

[100] Lei Wang, Lei, and Rodrigo C. de Lamare, "A Novel Constrained Adaptive Algorithm Using the Conjugate Gradient Method for Smart Antennas," in *41st Asilomar Conference on Signals, Systems and Computers,* pp. 2243-2247, 4-7 Nov. 2007.

[101] V. Kekatos, A.S. Lalos, and K. Berberidis, "Adaptive Conjugate Gradient DFEs for Wideband MIMO Systems Using Galerkin Projections," in *IEEE 66th Vehicular Technology Conference* , pp. 486-490, Sept. 30 -Oct. 3 2007.

[102] D. K. Faddeev, and V. N. Faddeeva, *Computational Methods of Linear Algebra,* San Francisco, CA: Freeman, 1963.

[103] A. A. Jenab, *“*An application of the matrix inversion lemma to nonstationary deconvolution problems,” M.S.E.E. thesis, West Virginia University, Morgantown, 1985.

[104]. R. Ranganathan, T.Yang and W.B Mikhael, “ICA based Intercarrier Interference Mitigation and Multi-user Detection for MIMO-OFDM Systems in Time Variant

Channels", Submitted to *IEEE Wireless Communications and Networking Conference*, September 2008.

[105]. Jonathan Richard Shewchuk, "An Introduction to the Conjugate Gradient Method Without the Agonizing Pain", in http://math.nyu.edu/faculty/greengar/painless-conjugate-gradient.pdf.